In-situ particle acceleration by magnetic reconnection in young stellar objects

INAF

ISTITUTO NAZIONALE DI ASTROFISICA
OSSERVATORIO ASTROFISICO DI ARCETRI

Valentin Brunn

In collaboration with **A. Marcowith, C. Sauty, C. Rab, M. Padovani, D. Galli, F. Pucci**

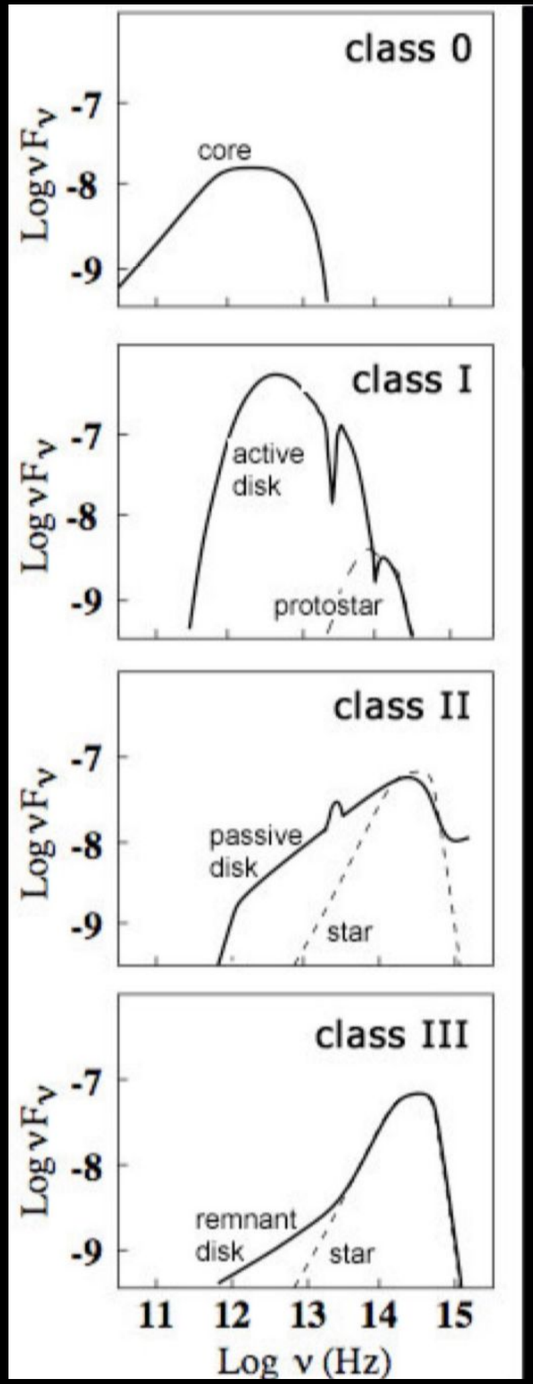

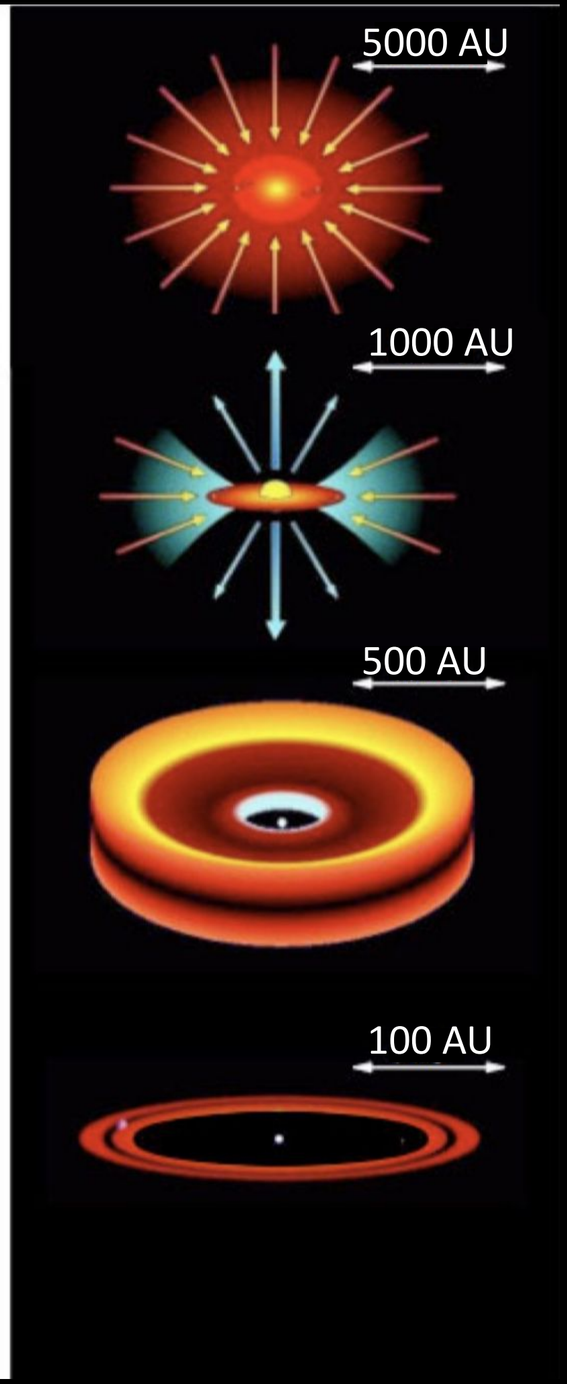

ESA/Webb, NASA, CSA, Ray et al.

ESA/Webb, NASA, CSA

ESA/Webb, NASA & CSA, Tazaki et al.

ALMA (ESO/NAOJ/NRAO)

YOUNG STELLAR OBJECTS

From plasma physics to planets and life

MAIN QUESTIONS

- What drives accretion and outflows?
- How is disk chemistry regulated?
- How are prebiotic molecules formed and delivered?
- How do planets form and evolve?
- What origins the chemical diversity seen by JWST?

ACCRETION PROCESSES

- Matter from disk spirals inward along magnetic field lines
- Shocks heat the gas
- Accretion releases energy

ORIGIN OF CHEMICAL DIVERSITY

- Radial & vertical mixing
- Time variability (flares, bursts)
- Ionization (X-rays, UV, energetic particles)
- Grain evolution & snowlines
- Disk winds & accretion flows

BUILDING BLOCKS OF LIFE

(prebiotic molecules)

H_2O, CO, CO_2, CH_3OH, HCN, NH_3, CH_4, H_2CO, HCOOH, ...

Formed in the disk and delivered to planets

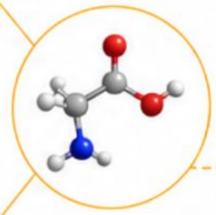

JET & WIND LAUNCHING

- Remove angular momentum
- **Shape disc rings**
- Enrich and shape environment

PLANET FORMATION

- Dust growth → pebbles → planetesimals
- Migration & dynamical evolution
- Composition set by local chemistry and radial transport

SEEN BY JWST

Molecular lines (NIRSpec, MIRI)

- H_2O, CO_2, CO
- HCN, C_2H_2
- **No spectrum looks the same**

SCOPE OF THIS PRESENTATION

Accretion and ejection require efficient **coupling between the gas and the magnetic field.**

The formation of prebiotic molecules, and the chemical diversity observed with JWST, require **rich and evolving disc chemistry.**

All the main questions are related to one fundamental disc property:

the ionisation of the disc.

Ionisation sources for different disc regions

The dominant ionisation mechanism varies with radius and disc structure, shaping the chemical and physical evolution.

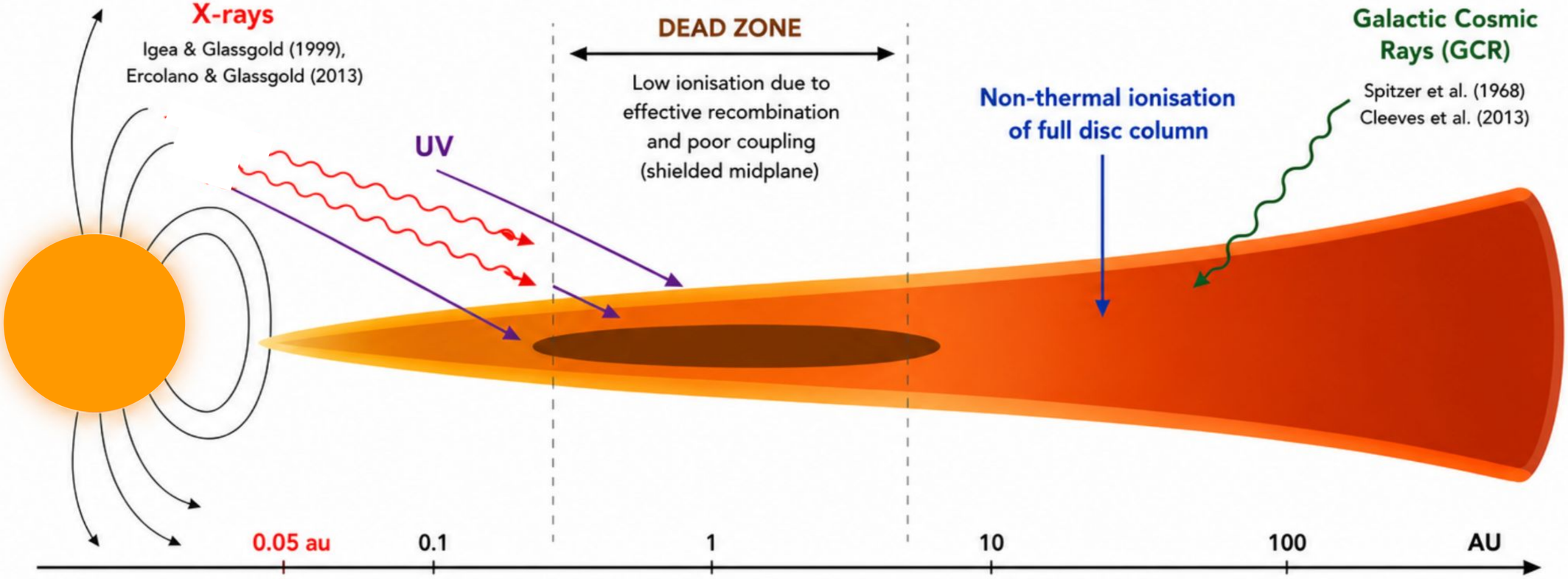

INNER DISC (< 0.05–0.3 au)	DEAD ZONE (~0.1–10 au)	ACTIVE SURFACE LAYERS (~0.1–100 au)	OUTER DISC (> 10–100 au)
Hot, dense, MRI active. Dominated by stellar high-energy radiation and collisional ionisation.	Shielded midplane. Low ionisation, poor coupling, suppressed MRI.	Ionised by stellar radiation and non-thermal processes. MRI can operate.	Low density. Cosmic rays and ambipolar diffusion control ionisation.
Main ionisation: X-rays, UV	**Main ionisation: very weak**	**Main ionisation: UV, X-rays**	**Main ionisation: GCR**

A radial variation of ionisation sources governs the disc's physical state and drives its chemistry.

ALMA observations of ionisation tracers

Ionisation tracer line intensities vs radius

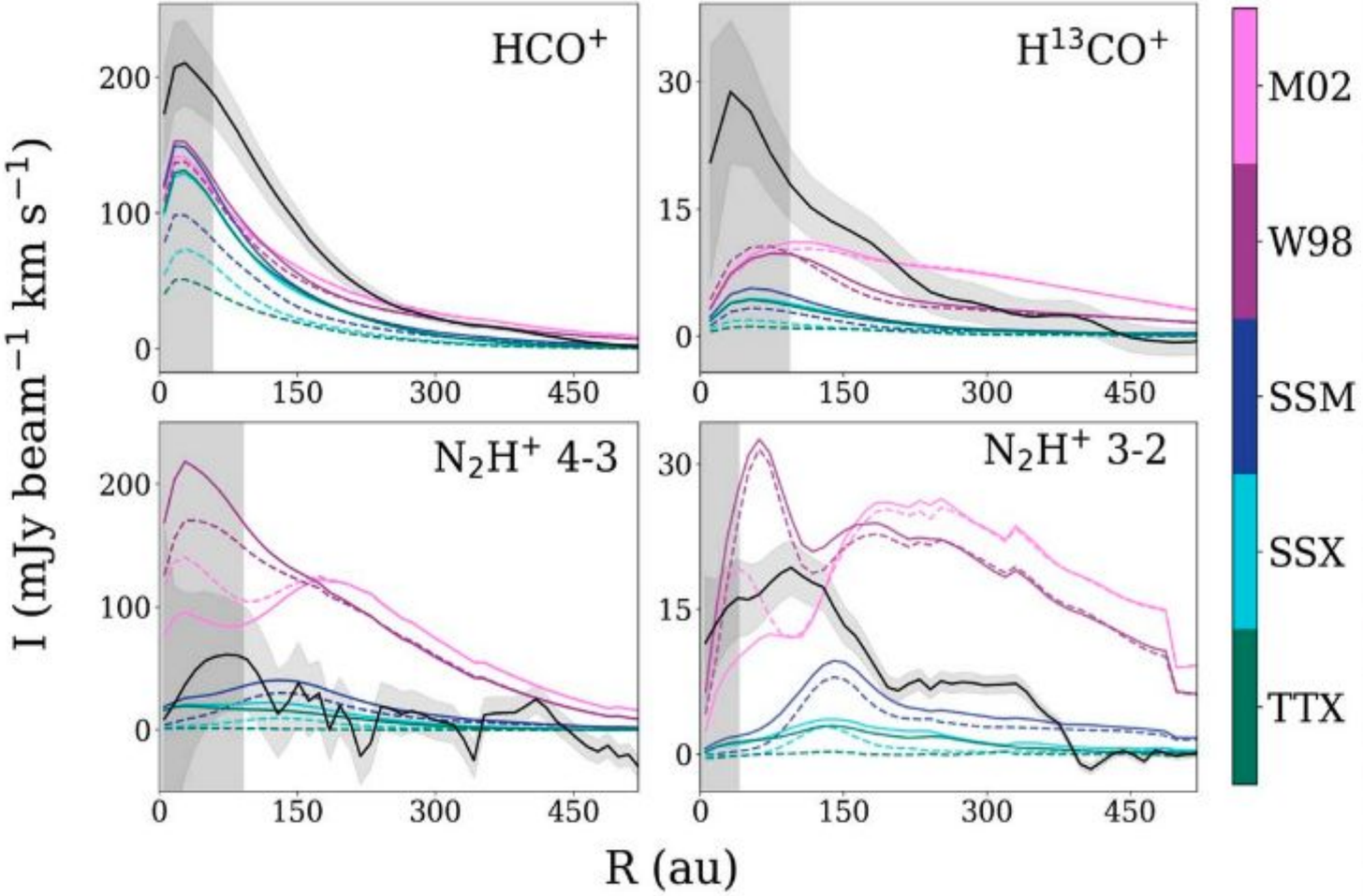

Long et al. (2024)

Models

Colours show the line intensity of ionization tracer assuming different ionisation rate models of X-ray and GCR.

OBSERVATIONS

Black line show observations at large radius models and observation fit but there is a discrepency in the inner 50 AU.

IMPLICATION

Standard protoplanetary disc models need **more ionisation** in the inner disc to fit ALMA observations.

Local EP ionisation sources

Multiple local environments accelerate and ionise energetic particles in young stellar objects

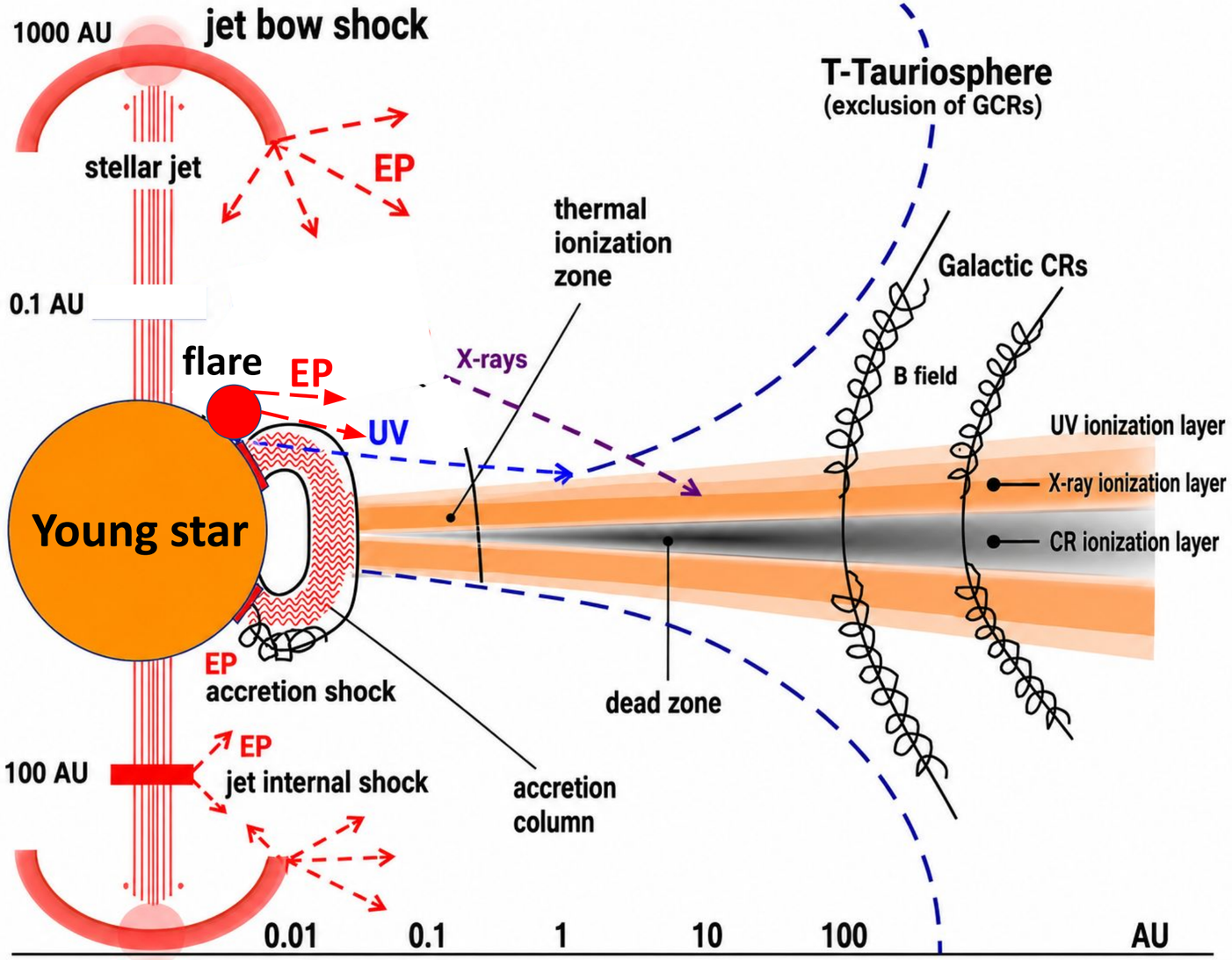

EP ACCELERATION IN JET SHOCKS

- First model of in situ EP acceleration in young stellar object : Padovani et al. 2016.
- Far from the disc: no effect

EP ACCELERATION IN FLARES

- Rodgers-Lee et al. 2017, Rab et al. 2017.
- EP accelerated based on stellar scaling and EP emitted from stellar surface

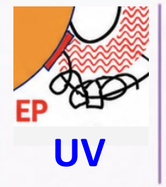

EP ACCELERATION IN ACCRETION SHOCKS

- Padovani et al. 2016, Offner et al. 2019.
- EP accelerated in dense region where they are locally suppressed

IONISATION BY GALACTIC COSMIC RAYS

- GCR attenuated by T-taurosphere (equivalent to the heliosphere)
- Negligible effect on disc ionisation below 100 au
- Cleeves et al. 2013, Padovani et al. 2018

Local EP acceleration is a young field that **has just 10 years.**
It is contributing to the understanding of the physical and chemical properties of planet-forming discs.

Ionisation sources for different disc regions

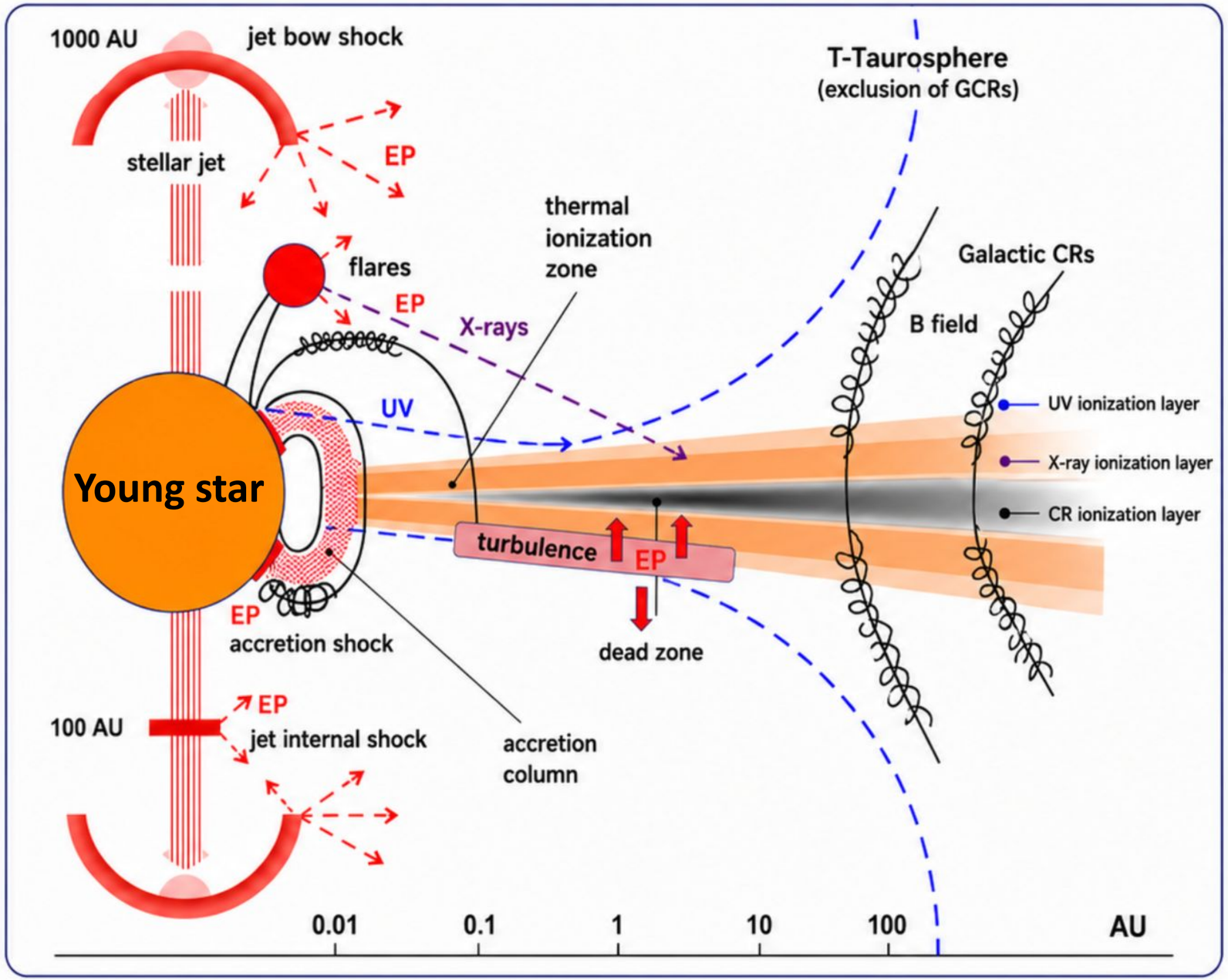

MY CONTRIBUTION

1 EP ACCELERATED IN FLARE WITH MICROPHYSICAL CONSIDERATION

Based on magnetic reconnection, and account for flares with a spatial extent that propagate along magnetic field lines.

2 A SOURCE OF EP NEVER CONSIDERED BEFORE: TURBULENCE-INDUCED MAGNETIC RECONNECTION

A previously unexplored EP source: particle acceleration by turbulence induced magnetic reconnection within the disc.

Particle Acceleration in T Tauri Flares

How to model particles acceleration by magnetic reconnection?

X-ray flares of T Tauri stars

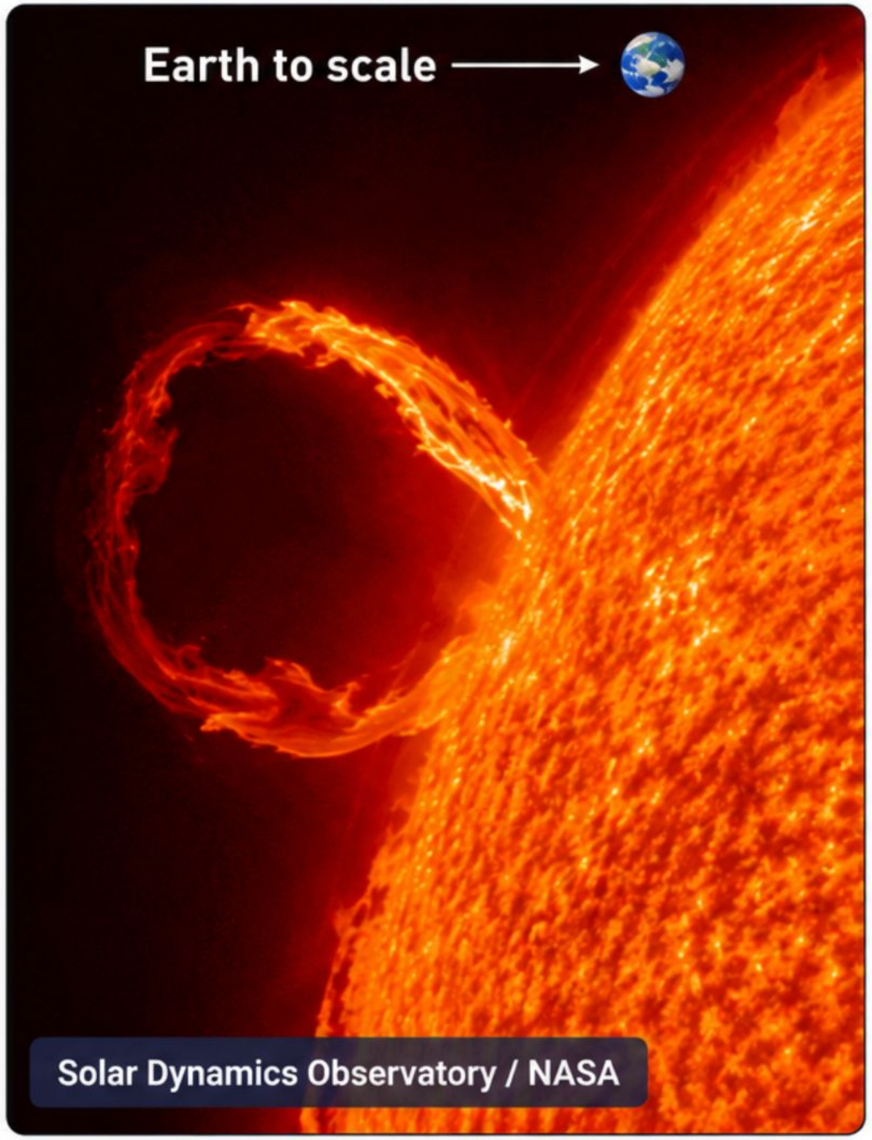

T Tauri flares are observed to be large scale versions of solar flares

3–6 orders of magnitude **more powerful** than the solar Carrington event.

6 orders of magnitude **more frequent**,

2 orders of magnitude **longer**,

2–3 orders of magnitude **larger** X-ray coronal flaring structures than those on the contemporary Sun

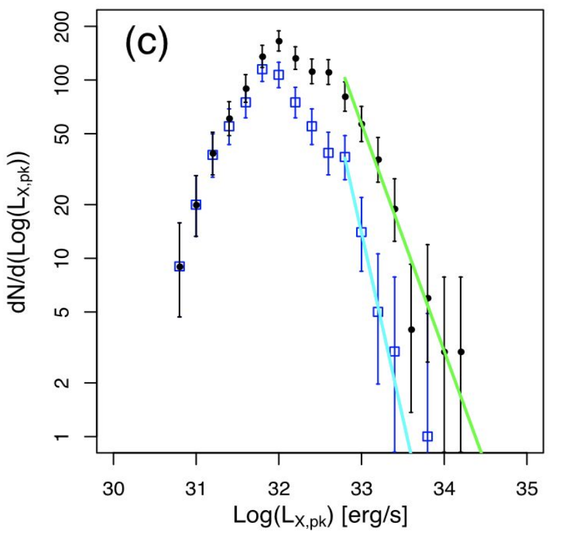

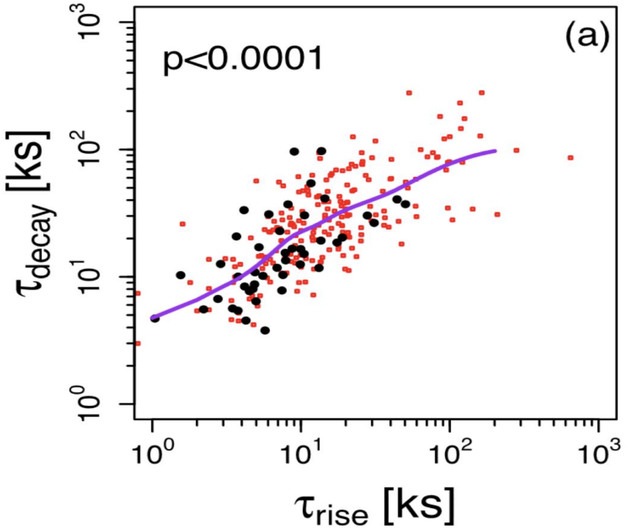

We want to model the energetic particle acceleration by T Tauri flares

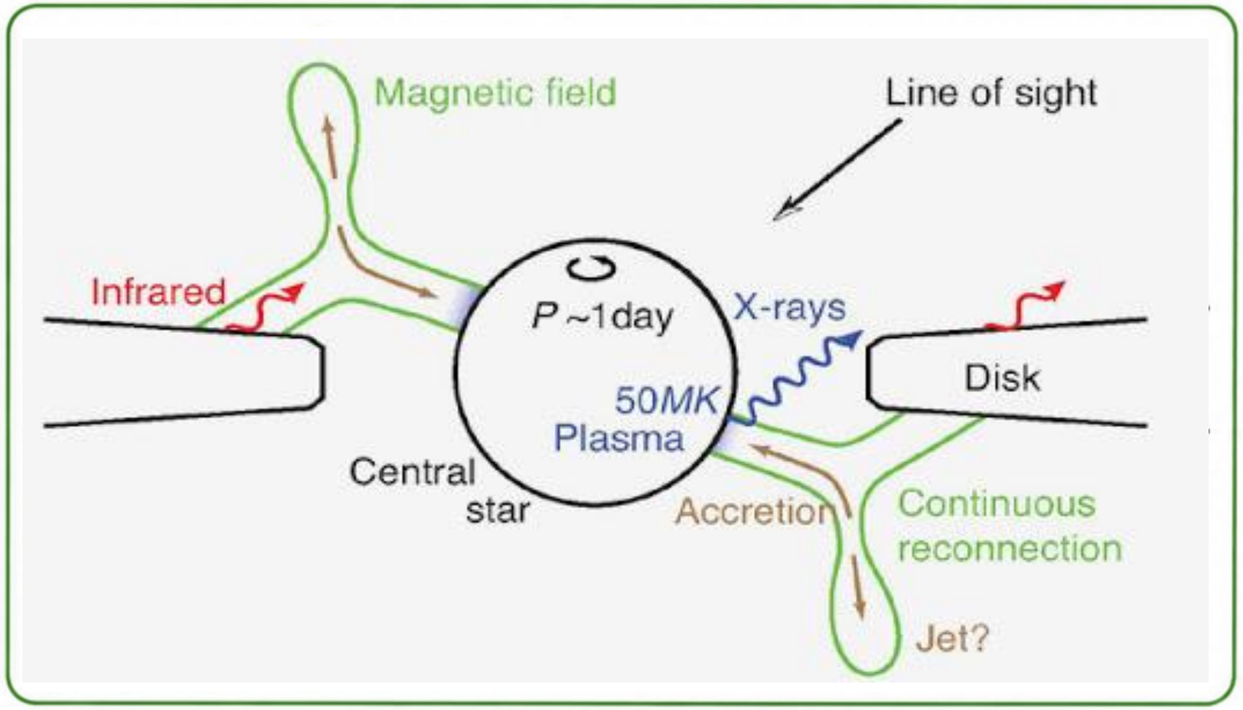

Magnetic Reconnection is expected in the Star–Disc interaction region

The **reconnection regime** determine the **EP acceleration efficiency.**

Zanni and Ferreira (2013)

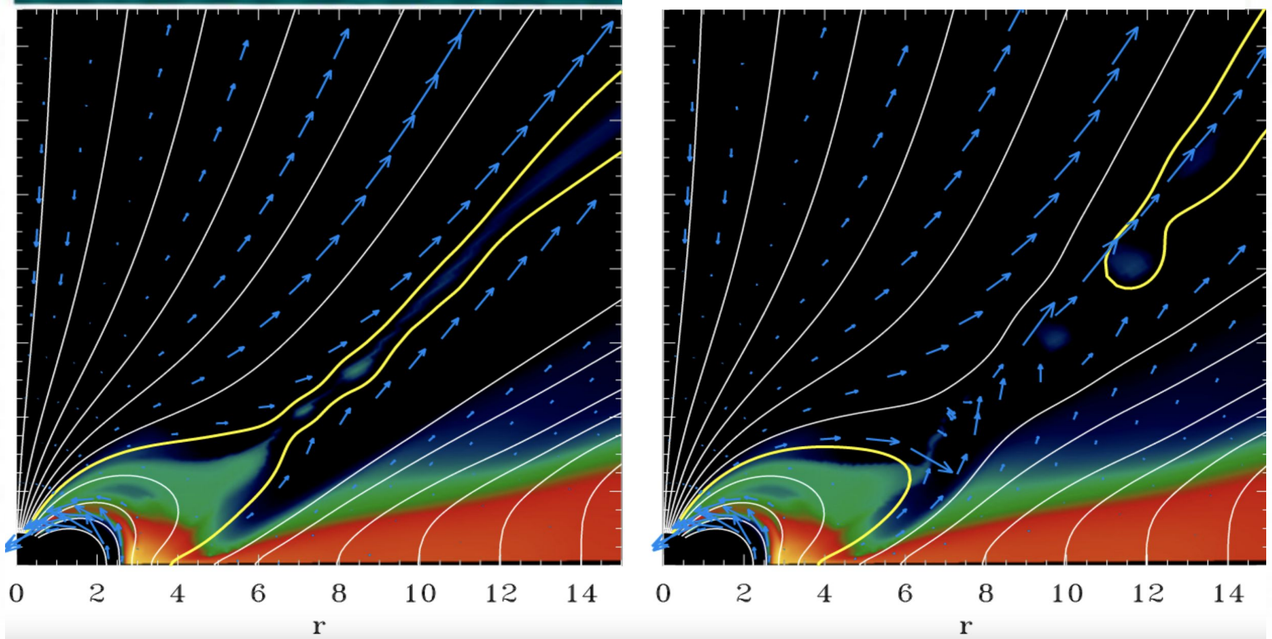

Assuming the plasma properties (T, n_e, L) of T Tauri flares:

Collisional reconnection unstable to plasmoids

Collisional magnetic reconnection unstable to plasmoids

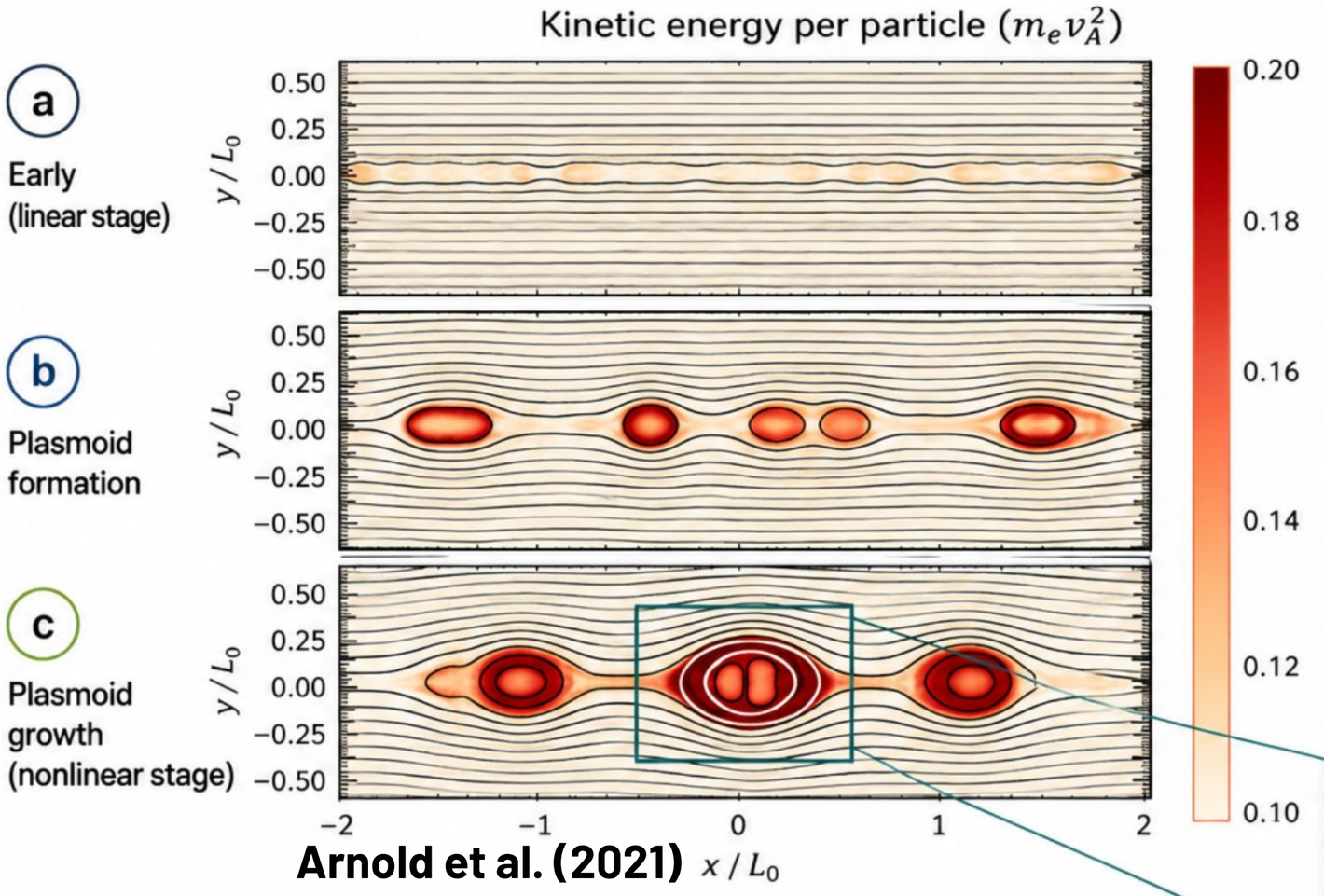

Arnold et al. (2021)

The reconnection regime determine the EP acceleration efficiency.

Acceleration is efficient in plasmoids

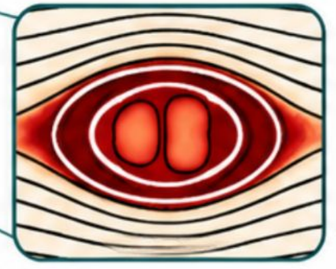

High electric field
(large potential drop)

Particles gain energy
(efficient acceleration)

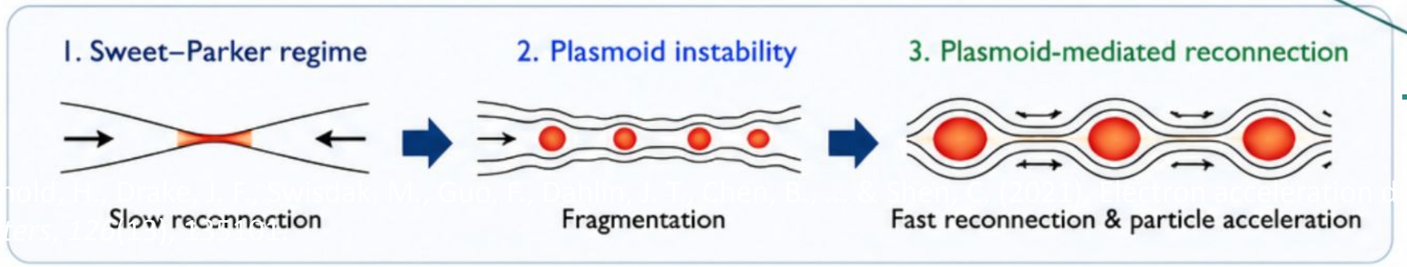

The energy distribution function of electron is a power-law :

$F(E) \propto E^{-\delta}$, $\delta = 3$

The particle fluxes produced by a 10 MK flare

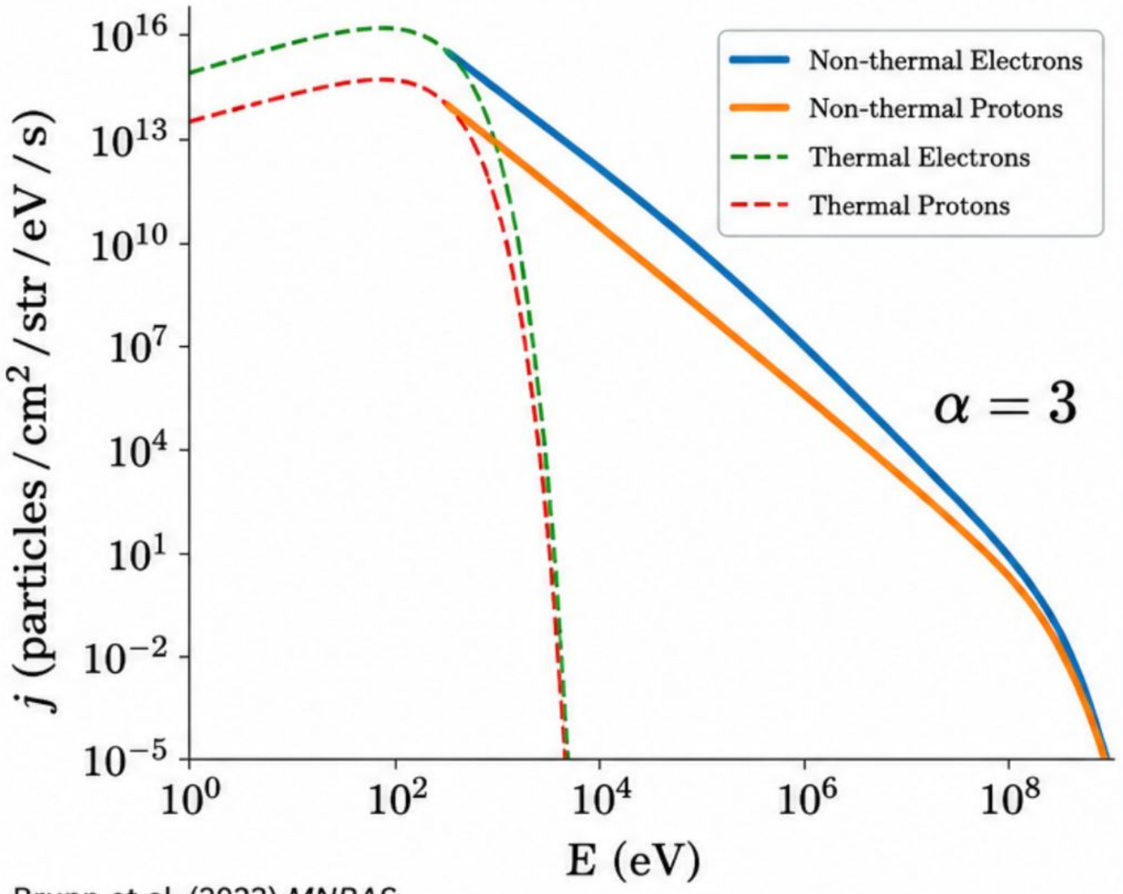

Brunn et al. (2023) *MNRAS*.

1 The power-law shape is based on MHD reconnection simulations.

$$j_0(E) \propto n_e \left(\frac{E}{E_c}\right)^{-\alpha} \exp\left(\frac{E}{E_{max}}\right)$$

- n_e: density normalization
- $\left(\frac{E}{E_c}\right)^{-\alpha}$: power-law with index α
- $\exp\left(\frac{E}{E_{max}}\right)$: exponential cutoff

2 The normalization is fixed by X-ray observations.

X-rays constrain the total non-thermal energy of the flare, which fixes the normalization n_e.

$$[j] = \frac{\text{number of particle}}{\text{energy} \times \text{time} \times \text{area} \times \text{solid angle}}$$

number of particle

Density	Temperature	Maximum energy
$n_e \sim 10^{10} \left(\frac{T}{10^6\,\mathrm{K}}\right) \mathrm{cm}^{-3}$	$T \approx 10^7\,\mathrm{K}$	$E_{\max} = 100\,MeV$

Energetic particles produced by flares ionise the disc

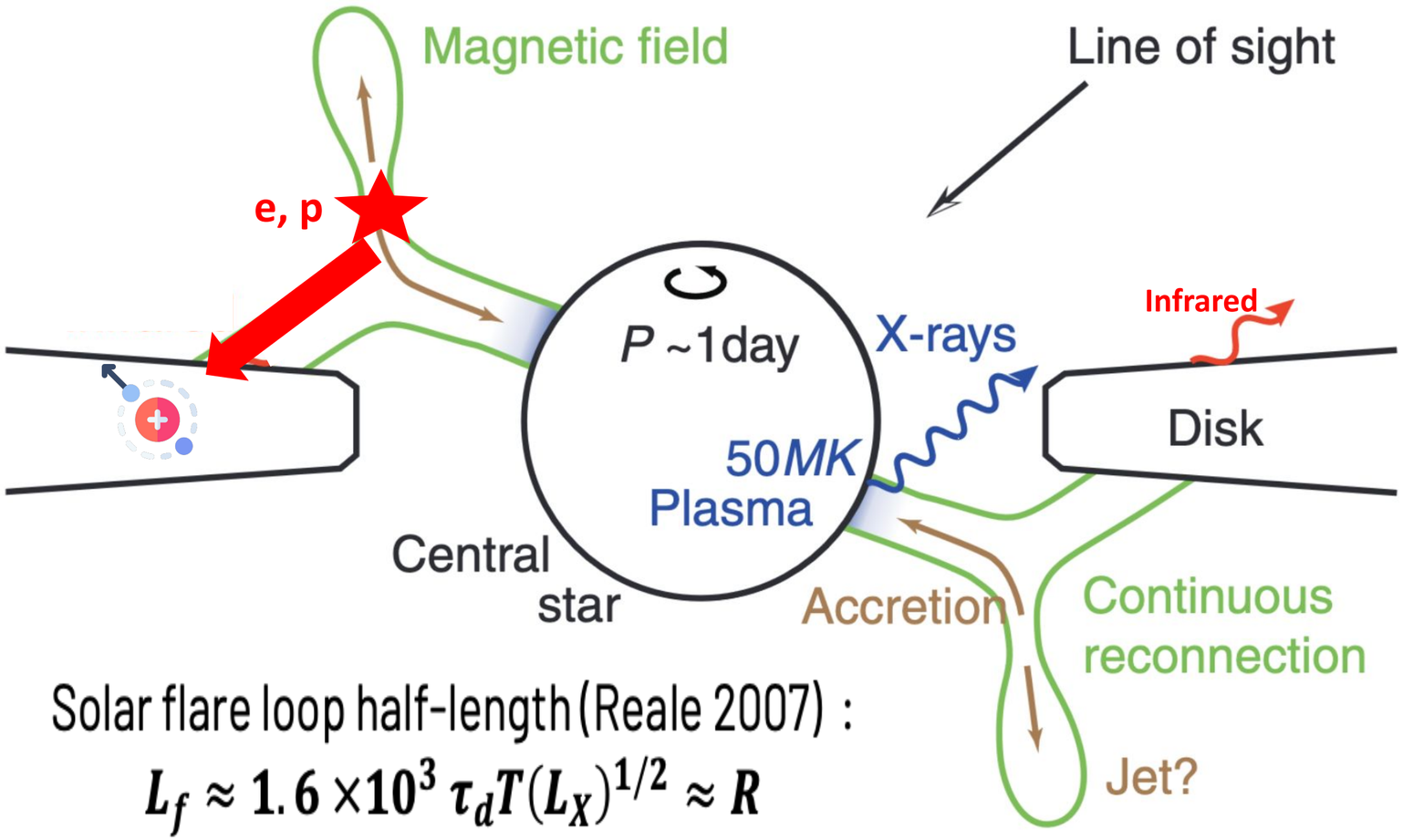

Solar flare loop half-length (Reale 2007) :

$$L_f \approx 1.6 \times 10^3 \, \tau_d T (L_X)^{1/2} \approx R$$

1. Particles are accelerated by magnetic reconnection.
2. They propagate along magnetic field lines.
3. They ionize the disc.

★ : Particle acceleration site

ProDiMo to estimate the chemical abundances of a standard T Tauri disc

Disc structure: total hydrogen number density n_H (cm^{-3})

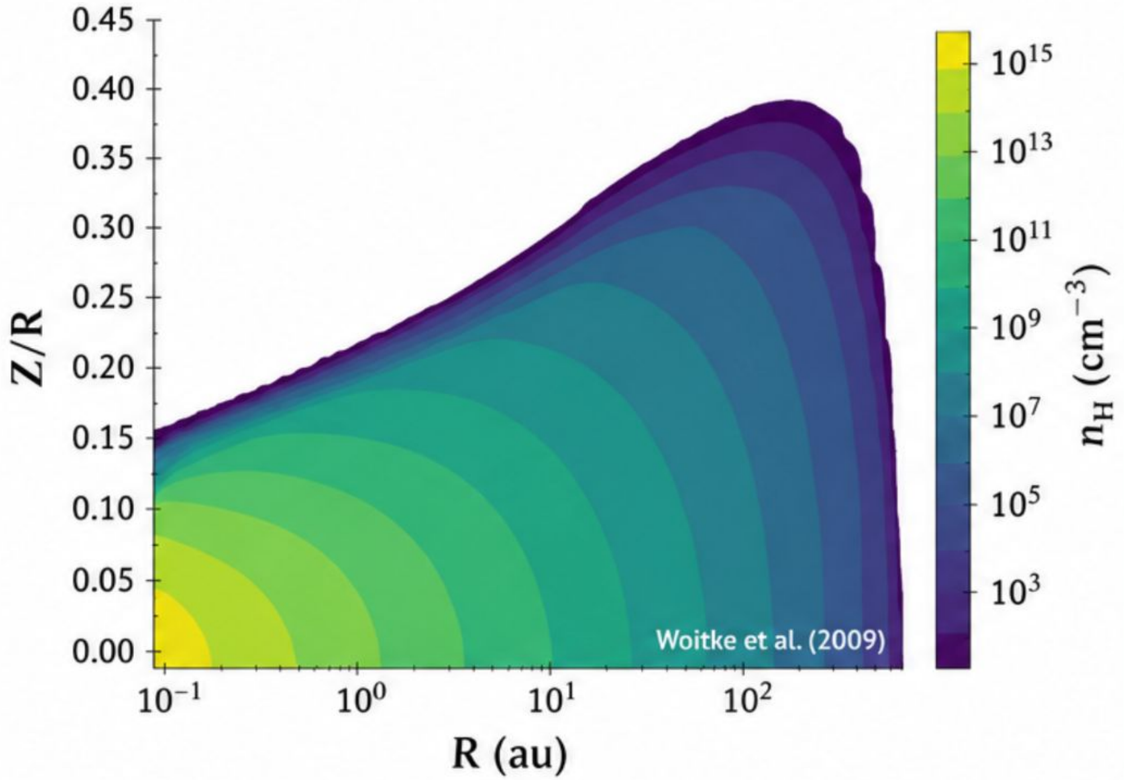

R : radial distance (au) | Z : height above the midplane | n_H : total hydrogen number density

The disc structure sets the physical and chemical environment for our abundance calculations.

1 2D Thermochemical Code : PROtoplanetary DIsc MOdel

(ProDiMo; Woitke et al. 2009)

Computes the thermal balance and chemistry in a 2D disc structure.

2 UV and X-ray radiative transfer

(Kamp et al. 2010, Thi et al. 2011)

Accounts for stellar irradiation and its penetration and attenuation in the disc.

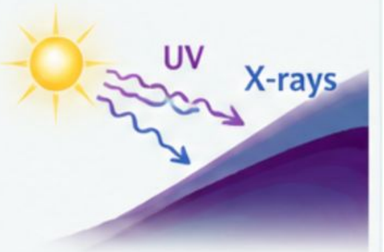

3 Hundreds of chemical species

(Woitke et al. 2016)

Rich chemical network to predict molecular and atomic abundances.

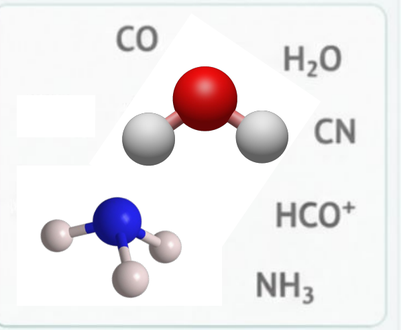

Propagation of EP produced by magnetic reconnection

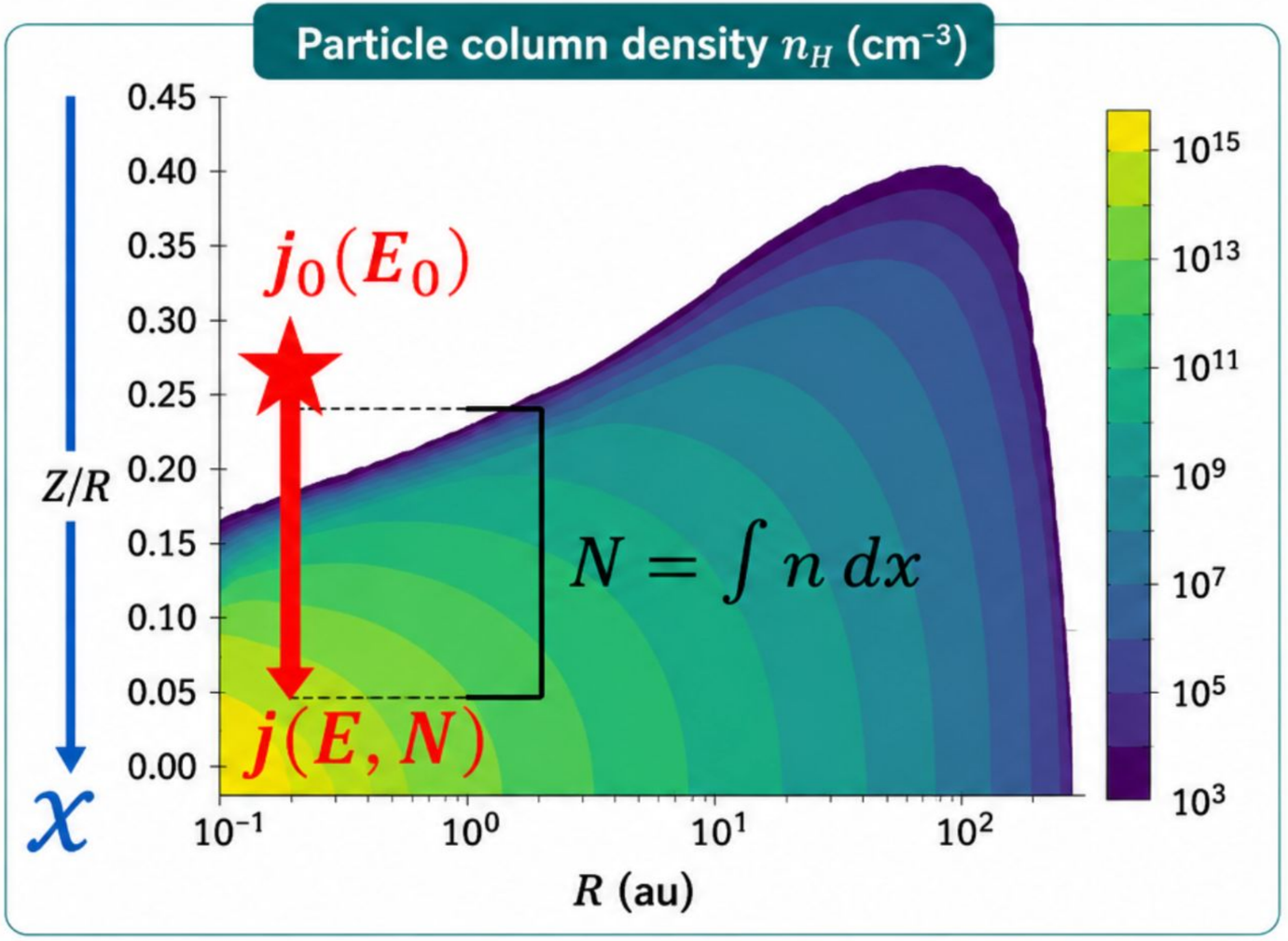

N	: Column density crossed by the particles
E_0	: Initial energy
E	: Energy at column density N
L	: Energy loss function $L(E) = -\frac{dE}{dN}$

Particle flux at column density N

$$j(E, N) = j_0(E_0)\,\frac{L(E_0)}{L(E)}$$

★ **Particle acceleration site**
Particles are injected with initial energy E_0 and flux $j_0(E_0)$.

□ **Column density N**
Total number of particles crossed: $N = \int n\,dx$

↓ **Direction of propagation ($\mathcal{X}$)**
Particles propagate downward along $\mathcal{X}$.

Ionisation rate, the key parameter

IONISATION RATE

$$\zeta(N)\,[s^{-1}] = 2\pi \int j(E,N)\,(1+\phi(E))\,\sigma_{ion}(E)\,dE$$

(Padovani et al. 2009)

$j(E,N)$: propagated particle flux

$\phi(E)$: secondary particles

The **ionization rate** is the number of H_2 **ionisation** per unit time.

Fundamental parameter for chemical and **non-ideal MHD** simulations.

We aim to **compute** the **ionisation rate**.

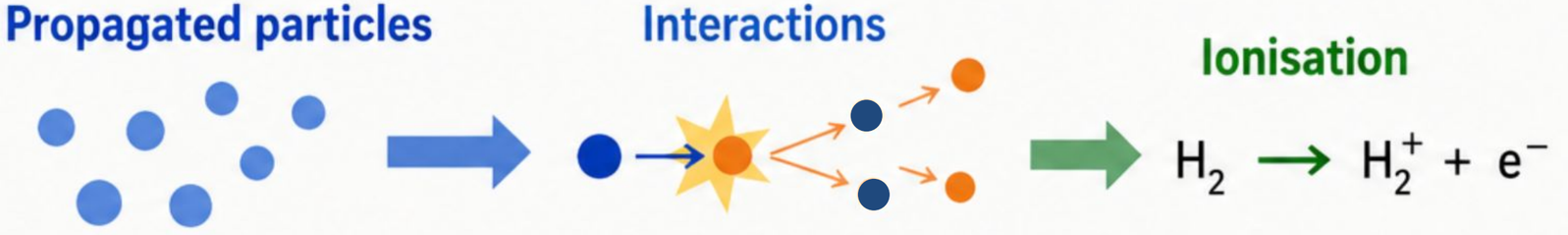

Ionisation rate $\zeta(N)$ $[s^{-1}]$

The ionisation rate produced by a single flare

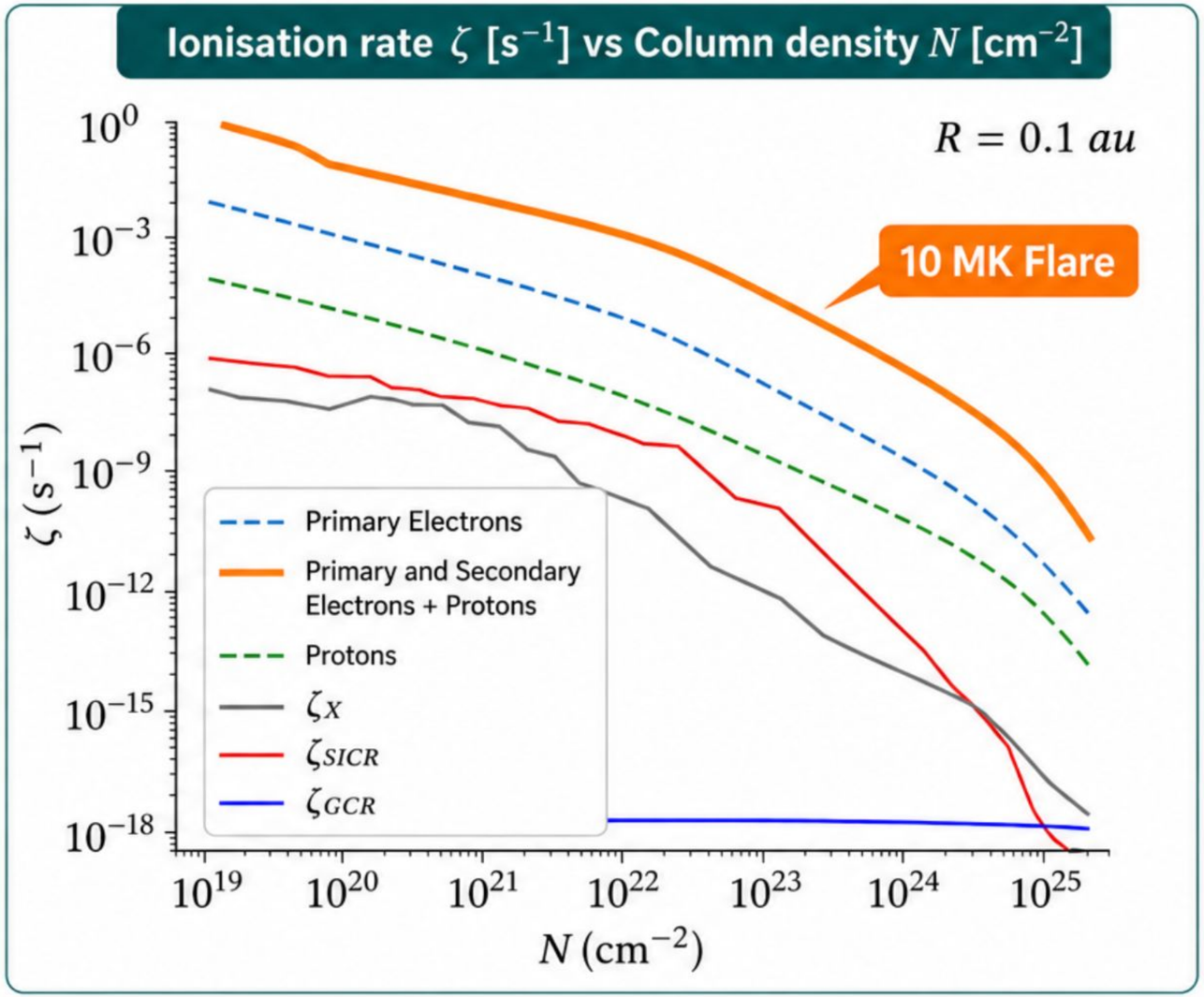

1 **10 MK Flare**

A typical flare temperature

2 **Orders of magnitude higher than other ionisation sources**

Far above standard sources

3 **A promising source of ionisation!**

EP from flare dominate the ionisation at their luminosity peak

Stellar flares are an efficient and promising source of ionisation in T Tauri discs.

Brunn et al. (2023) *MNRAS*

Energetic particles from flares are used as an input in ProDiMo

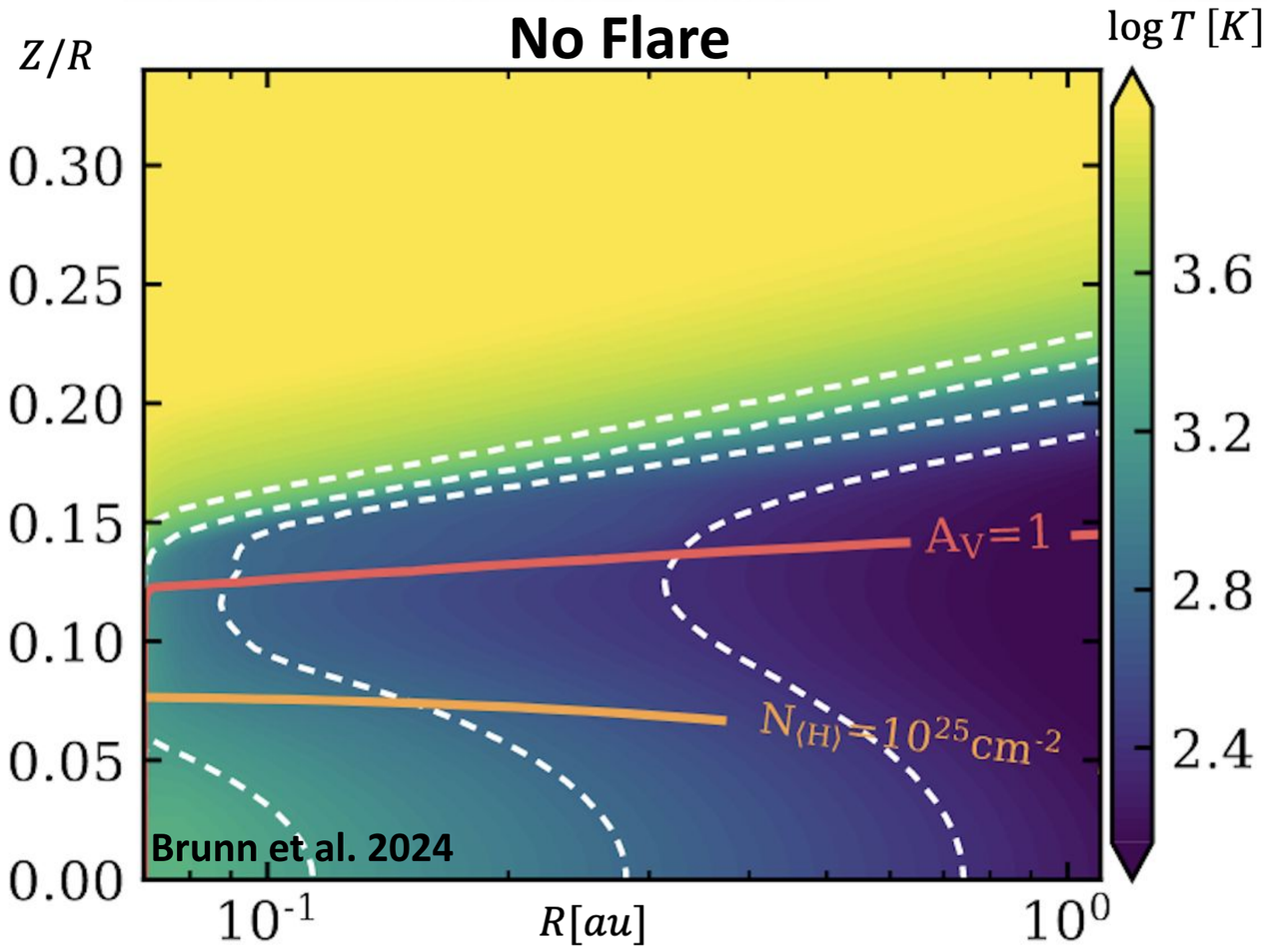

Brunn et al. 2024

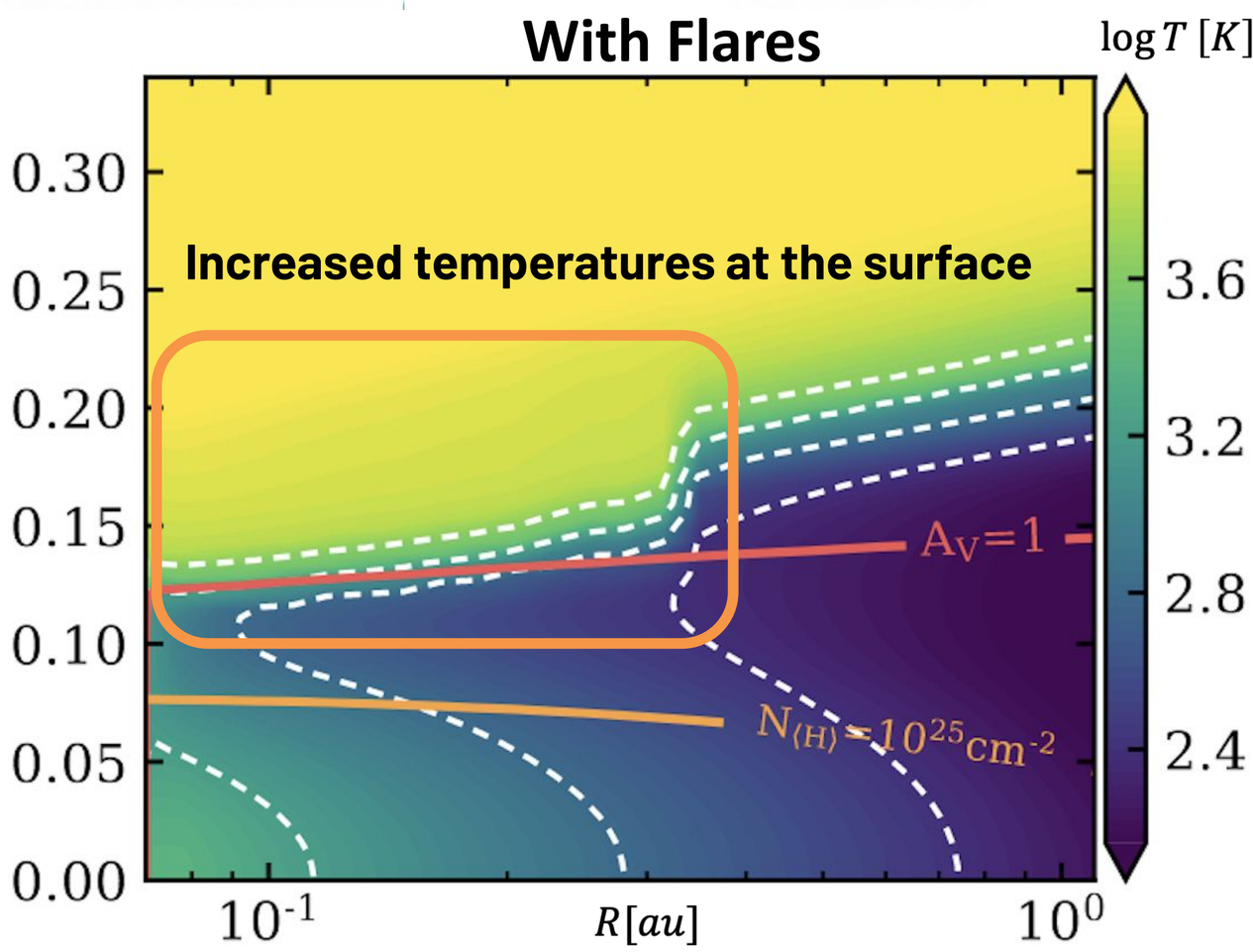

We recompute the thermochemical structure accounting for the additional EP ionization source.

Energetic particles affect the ejection processes in discs

Volumetric eating rate estimated from physical considerations:

$$Q\ (eV\ cm^{-3}\ s^{-1}) = 18\ eV \times n_{H_2} \times \zeta$$

Volumetric eating rate Q vs Radius R

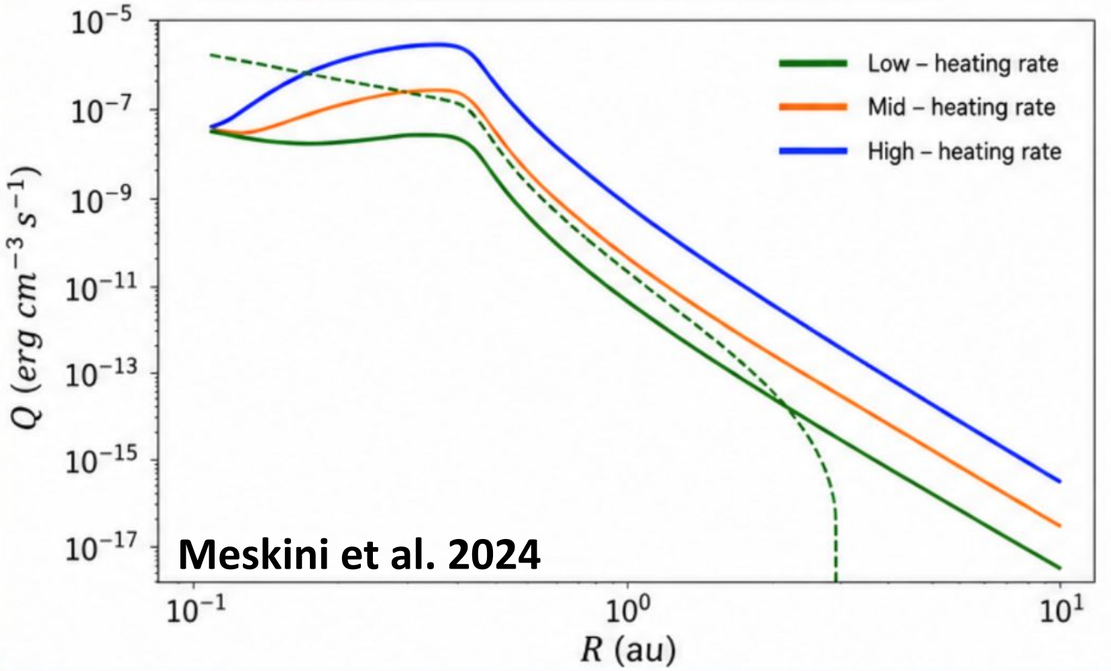

Higher heating rates lead to higher volumetric eating rates, especially in the inner disc regions.

Heating rate distribution in the disc

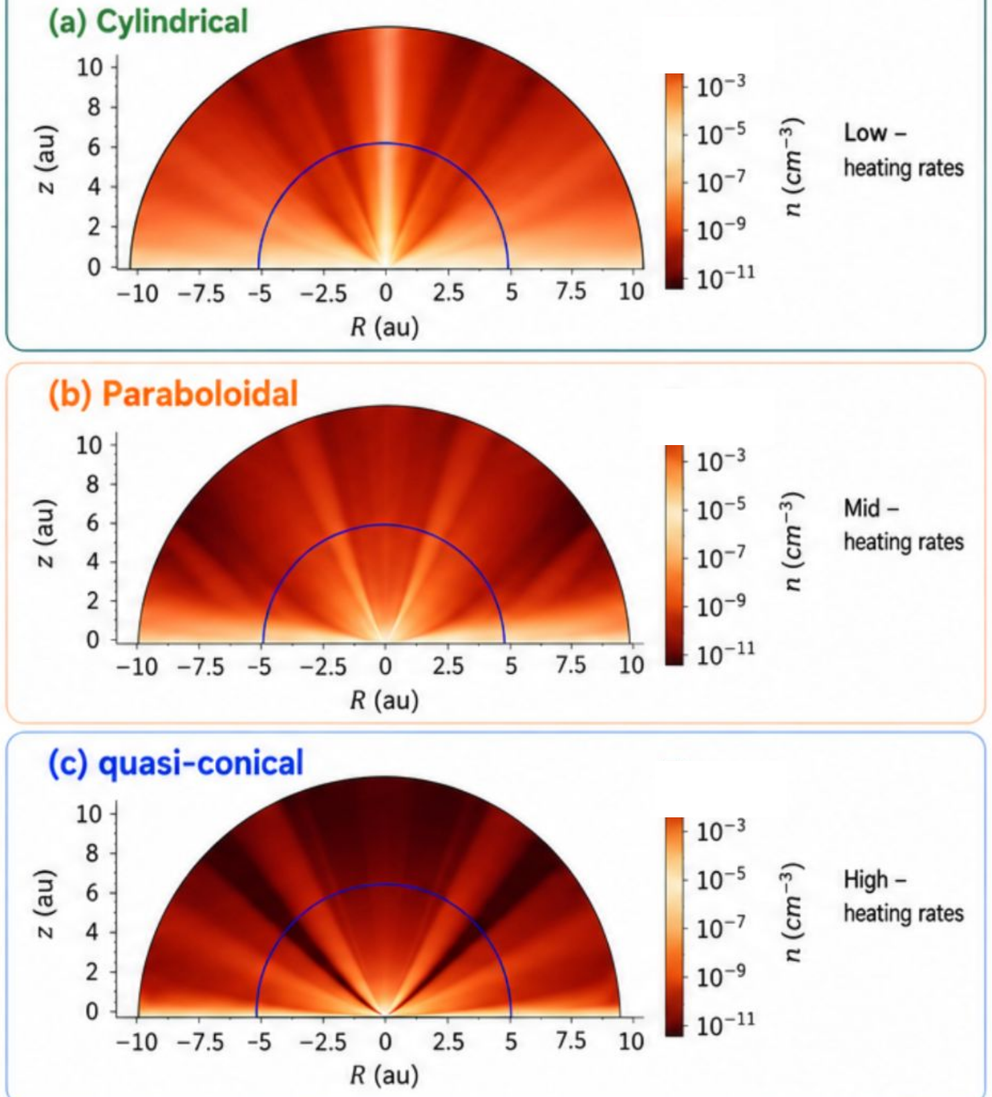

Energetic particles significantly enhance heating and drive efficient ejection in protoplanetary discs.

Energetic particles affect the chemical complexity in discs

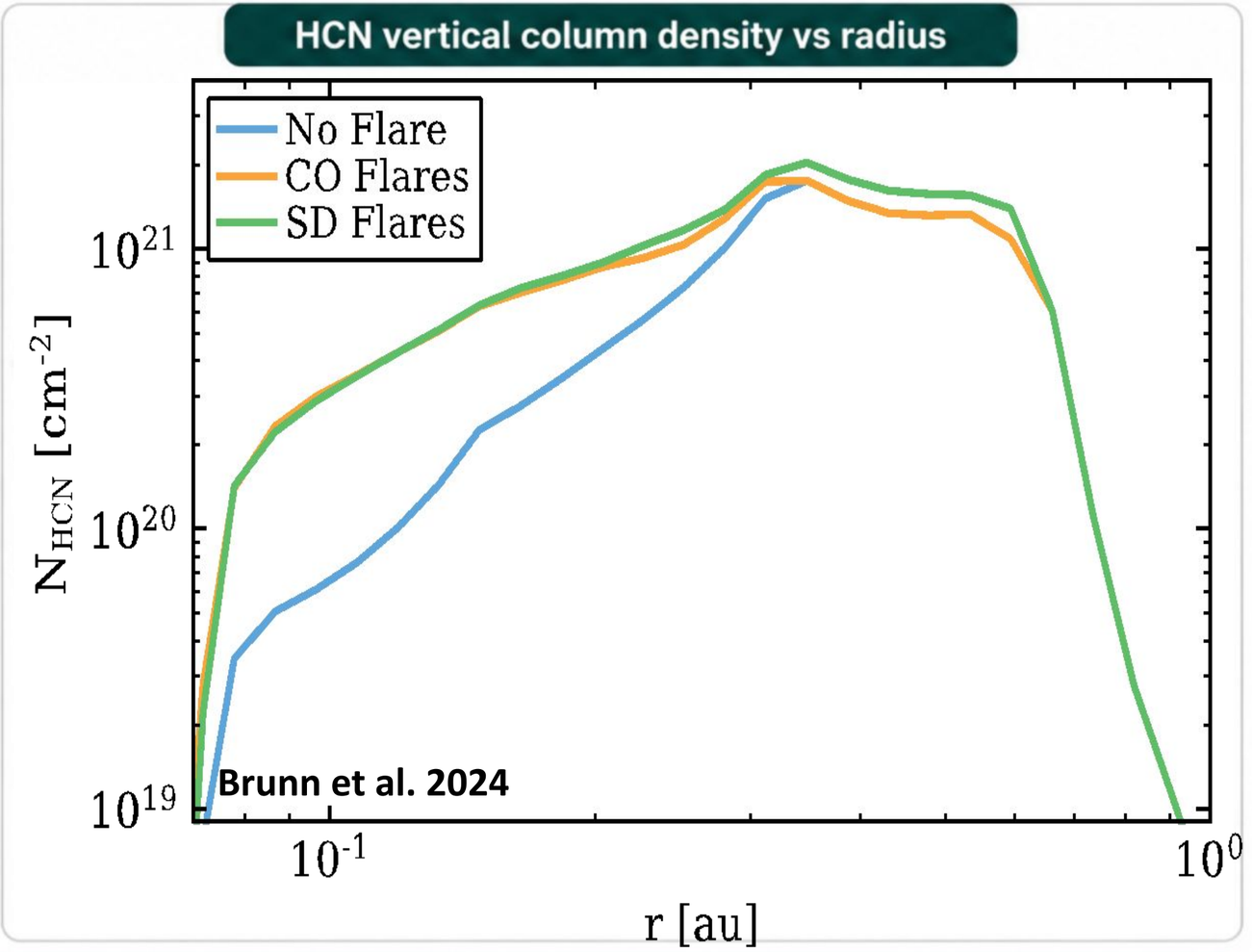

Energetic particles significantly increase HCN column densities across the disc, especially in the inner regions.

1 **HCN is fundamental in prebiotic chemistry**

HCN is a key building block for amino acids, nucleobases, and other complex organic molecules.

2 **EP affect the HCN vertical column density**

Flares (coronal and star–disc) significantly enhance HCN abundances throughout the disc, with the strongest effect in the inner regions.

Energetic particles play a crucial role in driving the chemical complexity of protoplanetary discs.

Energetic particles affect the observational tracers in discs

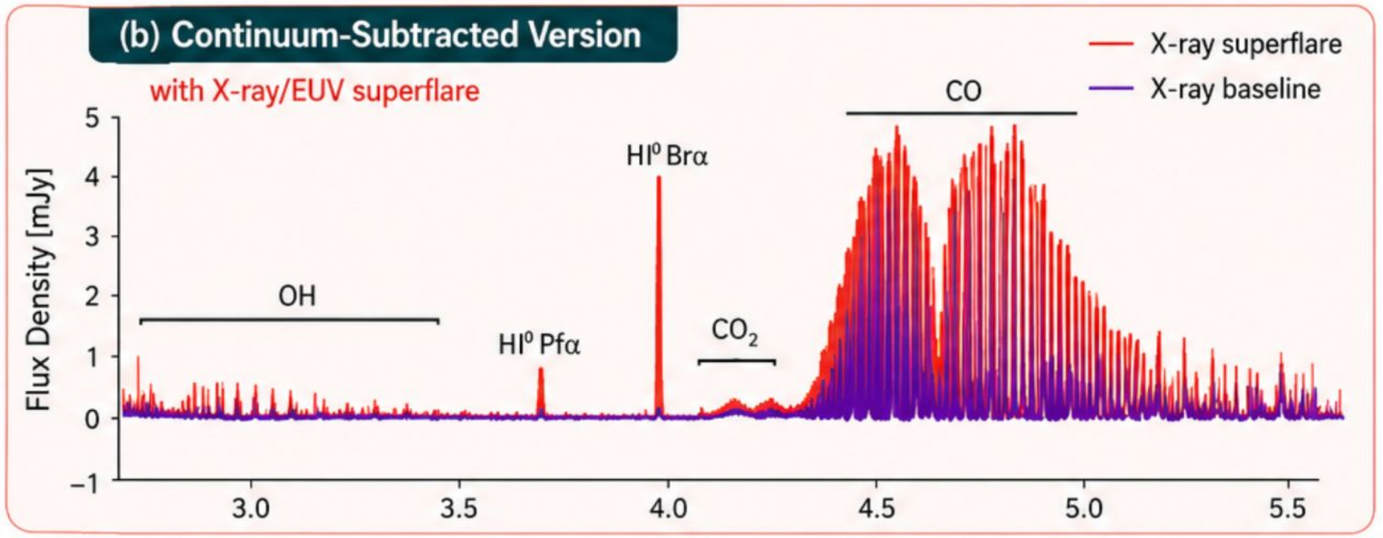

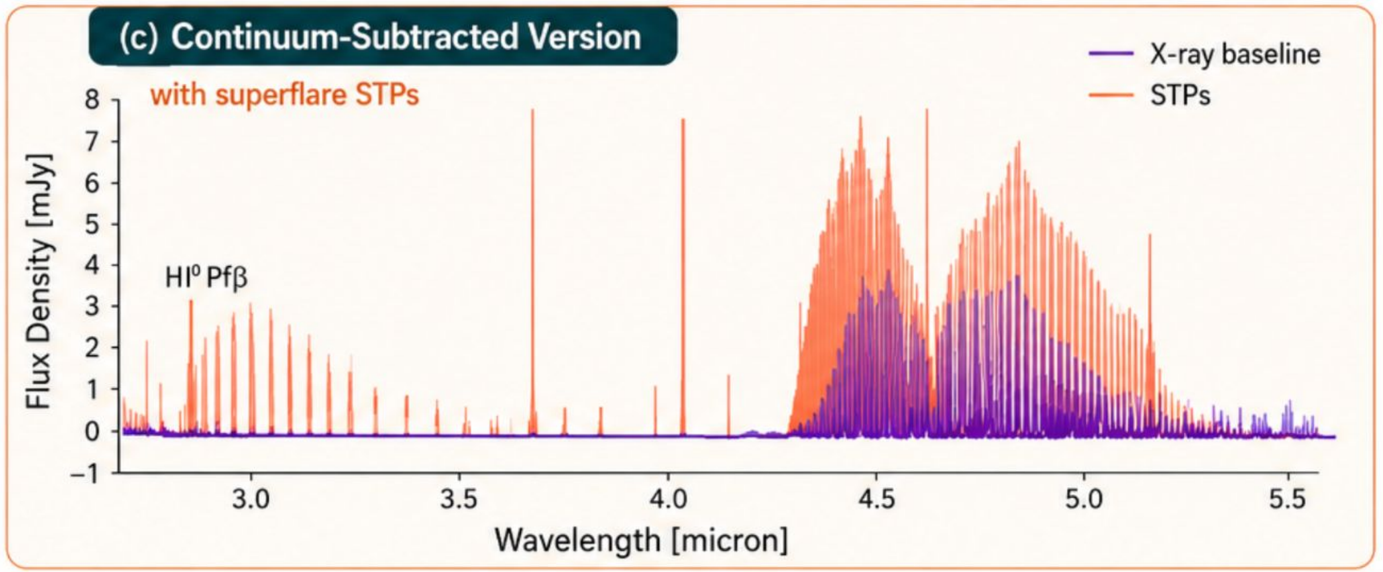

ProDimo predicts strong flare-driven enhancement of key molecular and atomic tracers in protoplanetary discs around an Orion PMS star.

HI: Stronger recombination lines (Brα, Pfα, Pfβ)

OH: Enhanced rovibrational emission

CO_2: Increased molecular emission

CO: Significantly brighter

NIRSpec Synthetic spectra

Flares and energetic particles dramatically boost key spectral tracers, providing powerful diagnostics of disc chemistry and high-energy processing.

Joint Chandra/JWST observation

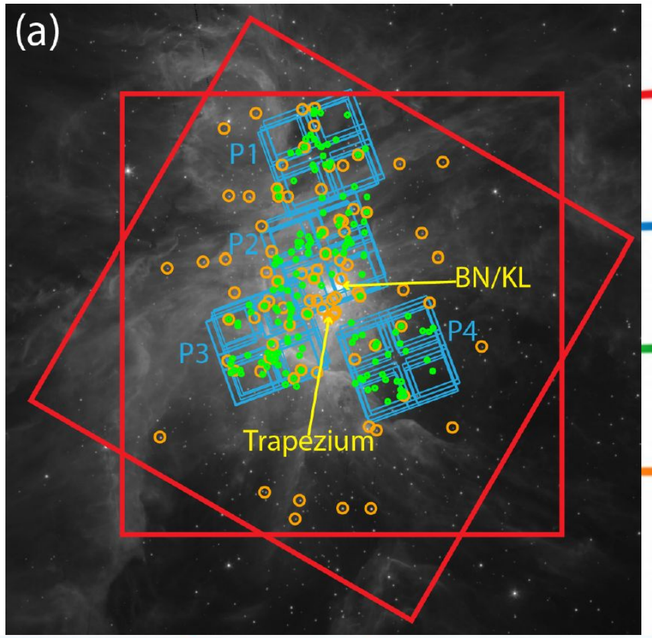

Chandra-ACIS-I field of view (red)

High spatial resolution X-ray imaging of the Orion region.

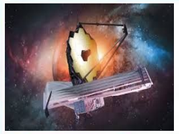

4 JWST NIRSpec MSA pointings (blue)

Near-IR spectroscopy of targeted young stars.

150 disk-bearing stars (green)

Young stellar objects with circumstellar disks.

X-ray super-flaring stars from previous Chandra surveys (orange)

Targets with extreme magnetic activity.

Proposed timeline for Chandra (red) and JWST (blue)

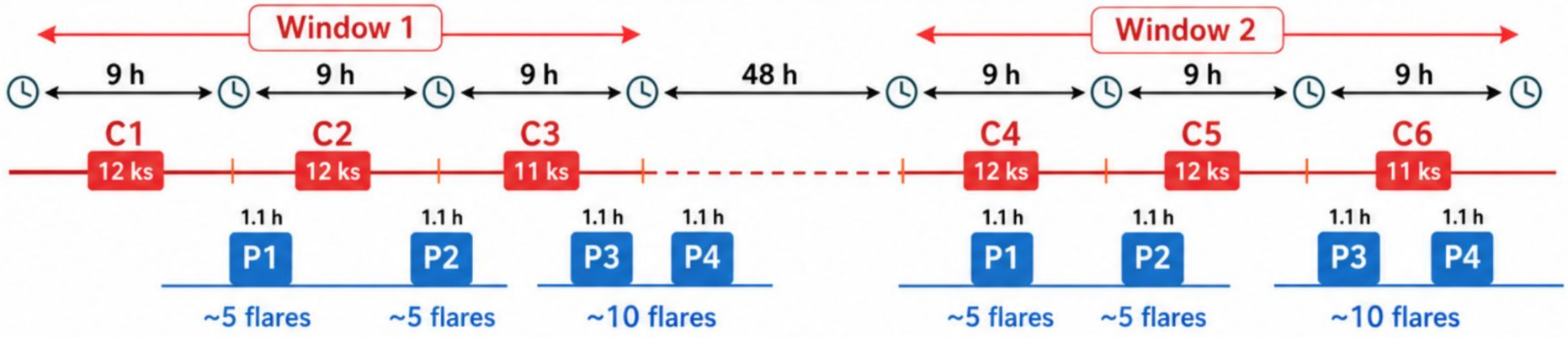

Coordinated Chandra and JWST observations enable us to connect high-energy flares with their impact on the disk environment and protoplanetary evolution.

Particle Acceleration by turbulence induced magnetic reconnection

How to model particles acceleration by magnetic reconnection in turbulence ?

DETERMINE THE EP ACCELERATION

From a stationary disc model and the Xu & Lazarian (2022) reconnection model

1 MRI TURBULENCE MODEL FROM A STATIONARY DISC (provides the turbulent scale and characteristic speeds)

Assume an MRI turbulence model

From a stationary disc model, we obtain:

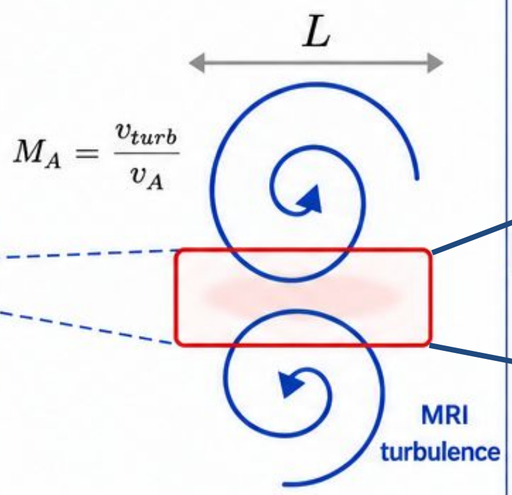

Outputs from the disc model:

L	v_{turb}	v_A
(turbulent scale)	(turbulent velocity)	(Alfvén speed)

These quantities characterize the MRI turbulence in the disc and are used as inputs for the reconnection model.

2 SIZE OF THE RECONNECTION REGION (Xu & Lazarian 2022 model)

The turbulent magnetic reconnection model of Xu & Lazarian (2022) determines the size of the reconnection current sheet.

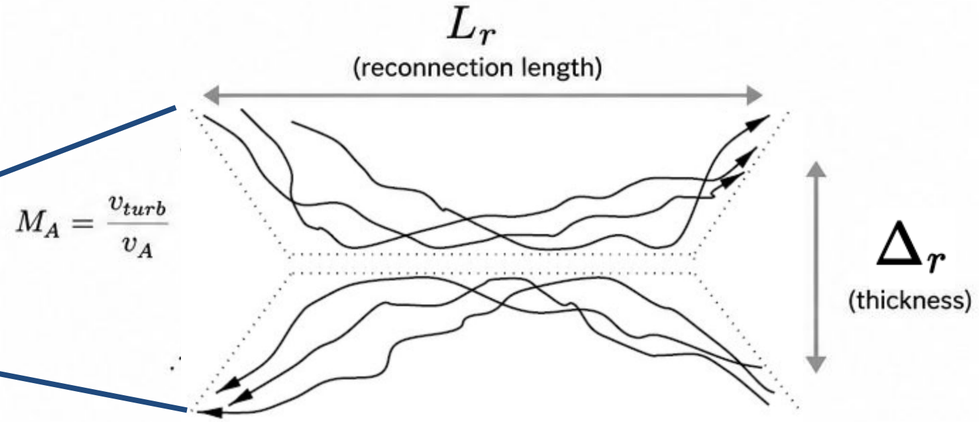

Model prediction: Xu & Lazarian (2022)

$$\Delta r \approx M_A^2 L_r$$

→ Thinner sheet for smaller M_A

We assume that the size of a turbulent eddy L is equal to the reconnection length L_r

IN SUMMARY

1. We assume an MRI turbulence model for a stationary disc.

$L,\ v_{turb},\ v_A$ are determined from the disc model.

$$L = L_r$$

2. The size of the reconnection region is set by the Xu & Lazarian (2022) model:

$$L_r,\ \Delta r \approx M_A^2 L_r$$

with $M_A = v_{turb}/v_A$

Smaller M_A → thinner sheet

FIRST-ORDER FERMI ACCELERATION: $\dot{E} = \alpha_{\rm acc} E$

Particles gain energy by repeatedly scattering between converging flows (Fermi process)

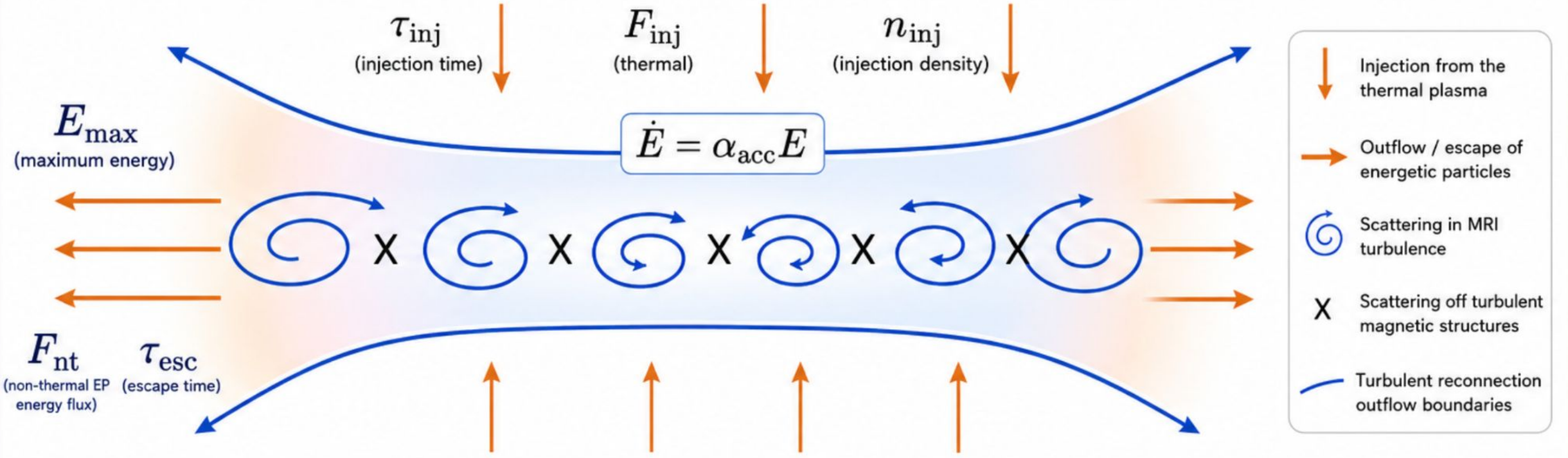

A fraction of the thermal particles from the disc are accelerated to supra-thermal energies by magnetic reconnection

Evolution of the non-thermal EP energy flux $F_{\rm nt}$

$$\frac{\partial F_{\rm nt}}{\partial t} + \frac{\partial}{\partial \epsilon}\left(\dot{E} F_{\rm nt}\right) = \frac{F_{\rm inj}}{\tau_{\rm inj}} - \frac{F_{\rm nt}}{\tau_{\rm esc}} .$$

Time change | Energy change (1st-order Fermi gain) | Injection (thermal supply) | Escape (loss)

(Guo et al. 2014, 2015)

NON-THERMAL EP DISTRIBUTION
IN A TURBULENT RECONNECTION CURRENT SHEET

$$F_{\rm nt}(E) \approx \frac{2\,n_{\rm inj}}{\sqrt{\pi}\,\alpha_{\rm acc}\tau_{\rm inj}} \left(\frac{E}{E_{\rm th}}\right)^{-(1+\alpha_{\rm acc}\tau_{\rm esc})} \Gamma\left(\frac{E}{E_{\rm th}}\exp(-\alpha_{\rm acc}T_{CS})\right)$$

Gamma d'Euler function

1. NORMALISATION

Set by the available accretion energy

$$\dot{U}_{nt} \equiv \int_{E_{inij}}^{E_{max}} F(E)\dot{E}dE = \kappa\,\Gamma_{acc}$$

$$\Gamma_{acc} = \frac{9}{8}\,\rho c_s^2\,\frac{L v_{turb}}{H^2}$$

$$n_{inj} \sim M_A^{-1} n_{th}$$

2. POWER-LAW SHAPE

Set by the turbulent magnetic reconnection parameters

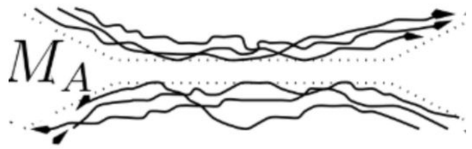

Turbulent magnetic reconnection

From Xu & Lazarian (2022):

$$\frac{1}{\alpha_{acc}\tau_{esc}} = \frac{3}{2}$$

$$\frac{1}{\alpha_{acc}\tau_{inj}} = \frac{3}{2}M_a^2$$

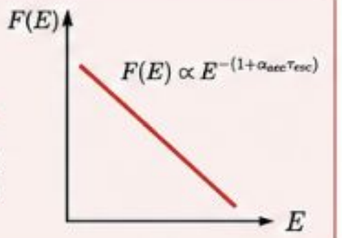

3. MAXIMUM ENERGY (CUTOFF)

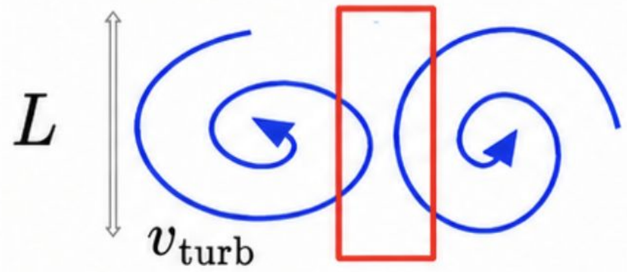

$$T_{\rm CS} = \frac{L}{v_{\rm turb}}$$

$$\Delta = M_A^2 L$$

Cut-off from acceleration time

$$E_{\rm max,CS} = E_{th}\exp\left(\frac{\alpha_{acc}L}{v_{\rm turb}}\right) = E_{th}\exp\left(\frac{2M_A^{-1}}{3}\right)$$

Hillas limit (size/magnetic field)

$$E_{\rm max,H} = eBM_A^2 L$$

$$E_{\rm max} = \min\left(E_{\rm max,CS}, E_{\rm max,H}\right)$$

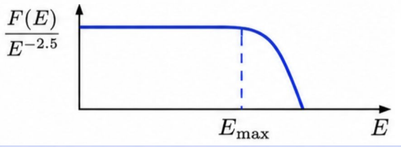

NON-THERMAL EP DISTRIBUTION IN A TURBULENT RECONNECTION CURRENT SHEET

Normalisation
set by the thermal population and the Alfvén Mach number $M_A = v_{\rm turb}/v_A$

$$F_{\rm nt}(E) \sim n_{\rm th} M_A \left(\frac{E}{E_{\rm th}}\right)^{-2.5} \exp\left(-M_A \frac{E}{E_{\rm th}}\right)$$

High-energy cut-off
set by the acceleration efficiency M_A and the thermal energy $E_{\rm th}$

WHERE NON-THERMAL EPs ARE PRODUCED

Radial profile of the total non-thermal EP energy density ($U_{\rm nt}$) relative to the thermal energy density ($U_{\rm th}$).

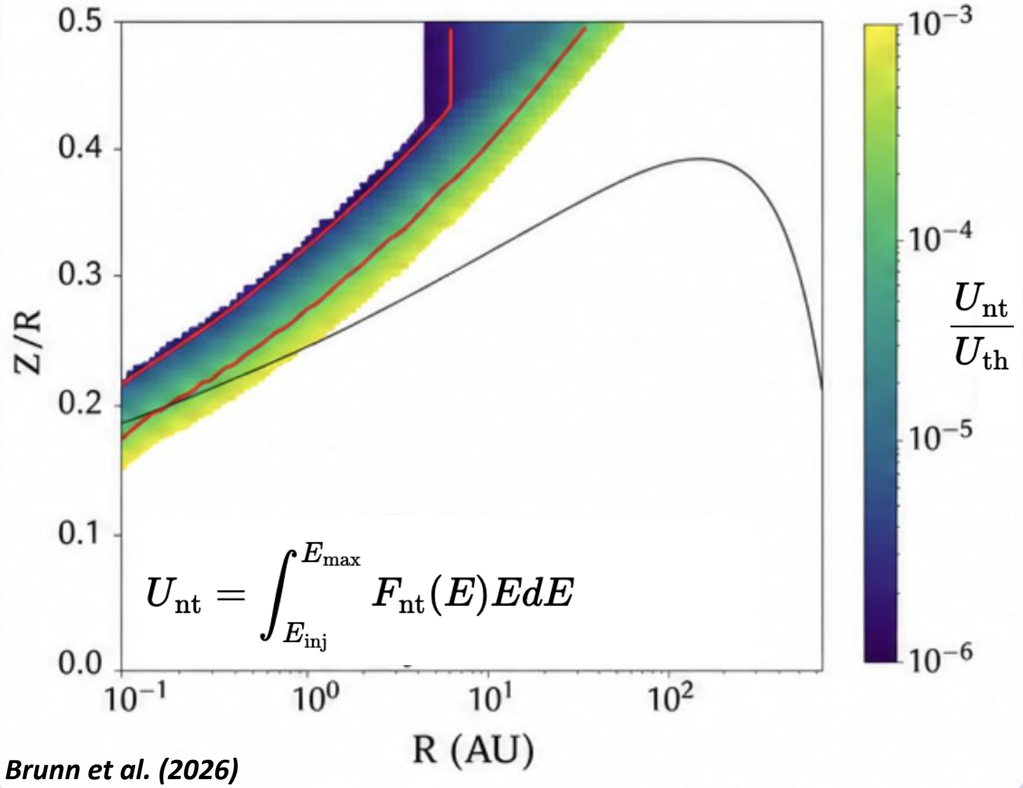

Brunn et al. (2026)

RESULTING NON-THERMAL EP SPECTRA

Energy spectra of non-thermal EPs at different heights (Z/R). Colours indicate height above the mid-plane.

There is an optimal height that maximises the EP energy

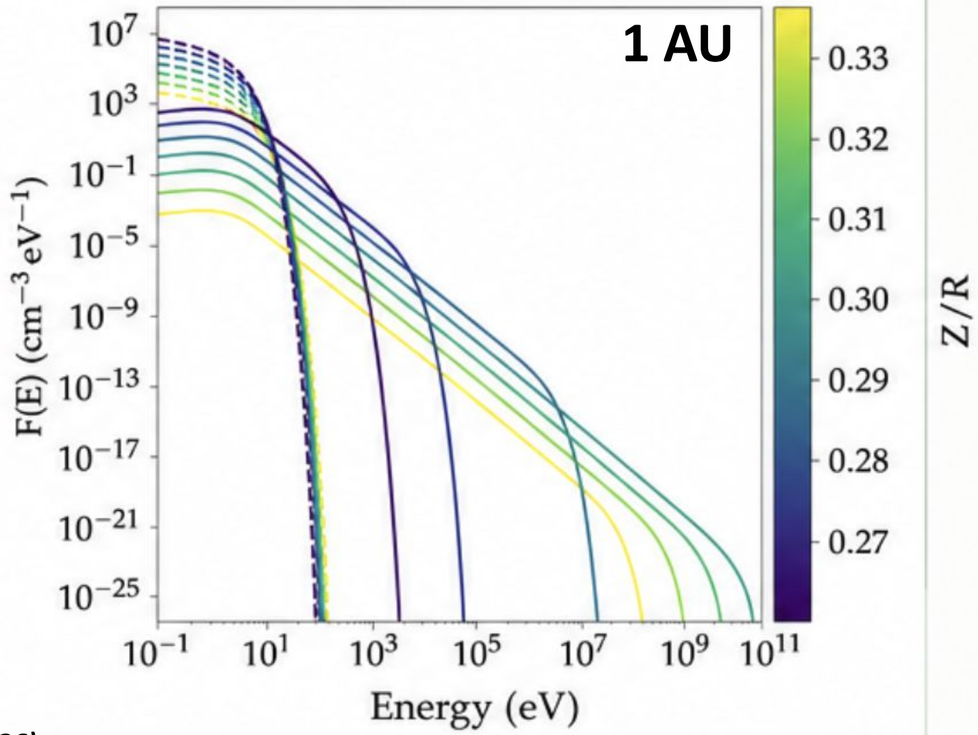

Brunn et al. (2026)

Ionisation by turbulence-induced magnetic reconnection

1. Qualitative picture of the model

Surface acceleration → propagation toward the mid-plane

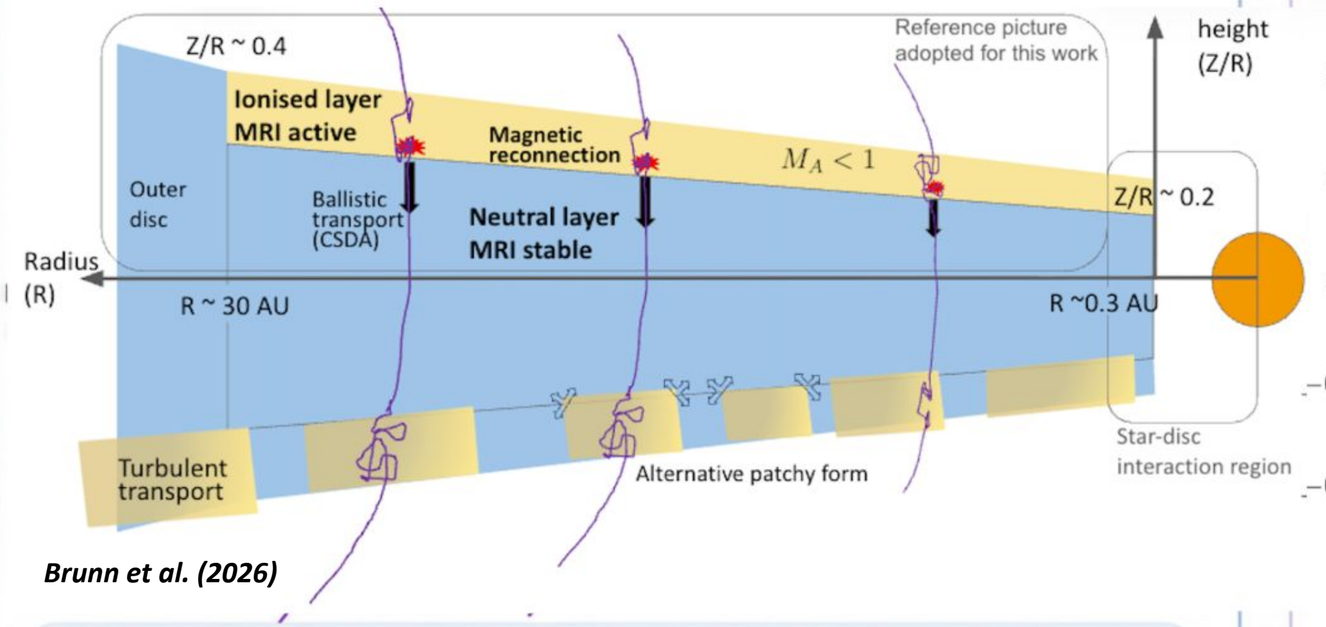

Brunn et al. (2026)

- Magnetic reconnection in the MRI-active surface layers accelerates energetic particles (EPs).
- EP propagate towards the midplane vertically via ballistic transport.
- The intermediate and deep disc layers remain shielded from radiation and are MRI stable.

2. Disc structure from ProDiMo

Top: $n_{\langle H \rangle}$; bottom: M_A

Red contour: efficient EP acceleration, $E > 10$ MeV, where $M_A \lesssim 1$

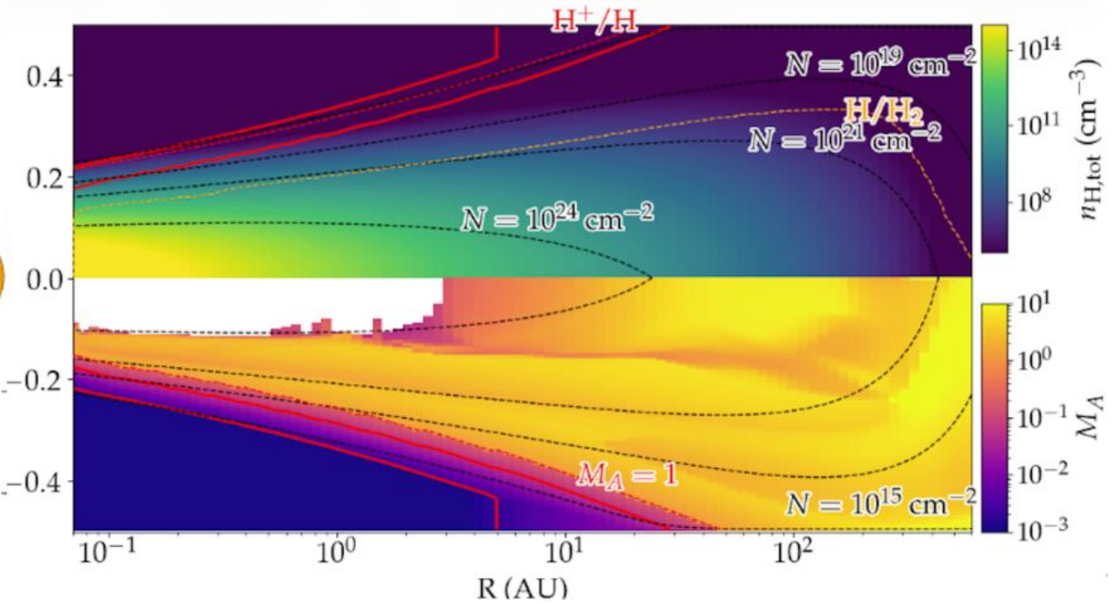

- Red contour shows the region where EPs are efficiently accelerated to high energies ($E > 10$ MeV).
- This corresponds to $M_A \lesssim 1$, where turbulence-driven reconnection is most effective.

Ionisation by turbulence–induced magnetic reconnection

Ionisation rate relative to total rate ζ_{EP}/ζ_{tot}

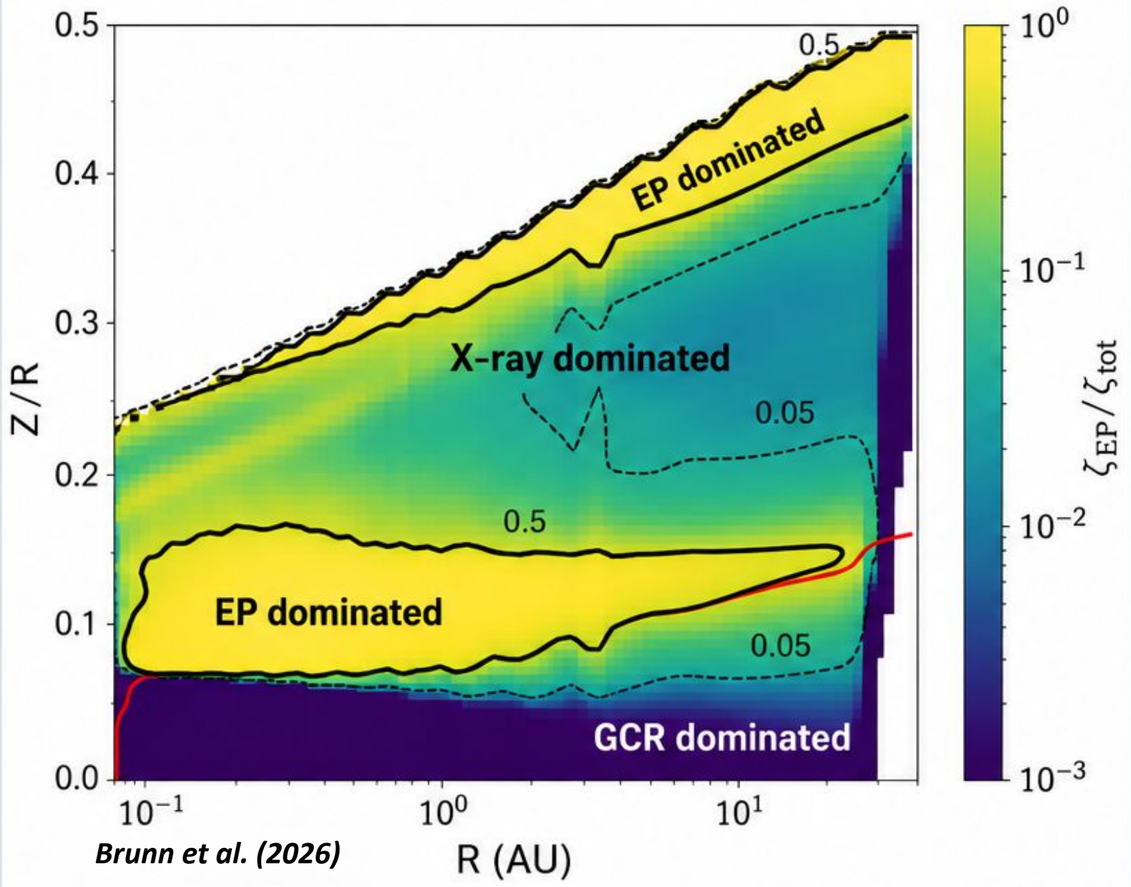

Brunn et al. (2026)

EP contribute more than the sum of all other sources

More than 10% of the sum of all other sources

Increased ionisation rate between 0.3–30 au.

Turbulence–induced magnetic reconnection (EPs) dominates the ionisation in the disc surface and mid-plane over a wide radial range.

The enhancement is strongest between 0.3 and 30 au.

We use this ionisation rate as input in ProDiMo

The radial profile of the ionisation rate from turbulence–induced reconnection is adopted as the input ionisation rate in ProDiMo.

Impact of the additional EP source on disc chemistry

EP ionisation significantly modifies ionisation and molecular abundances in the disc

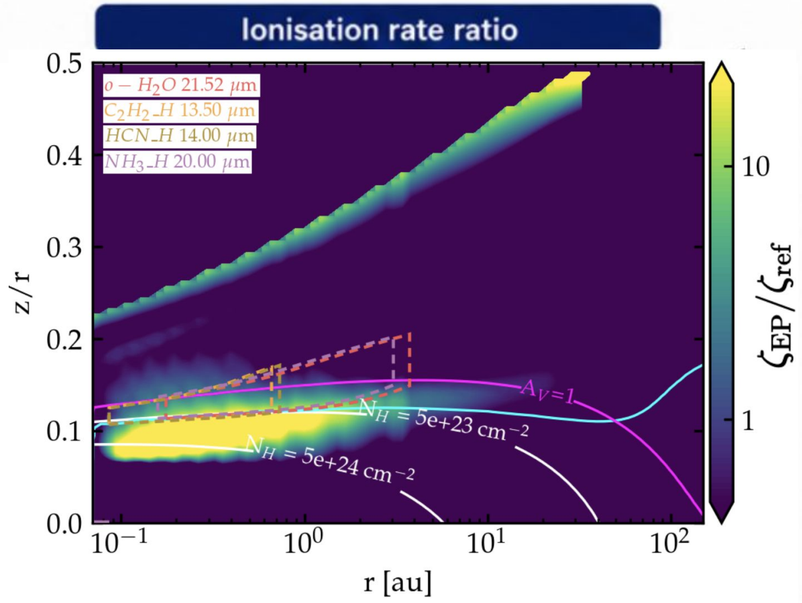

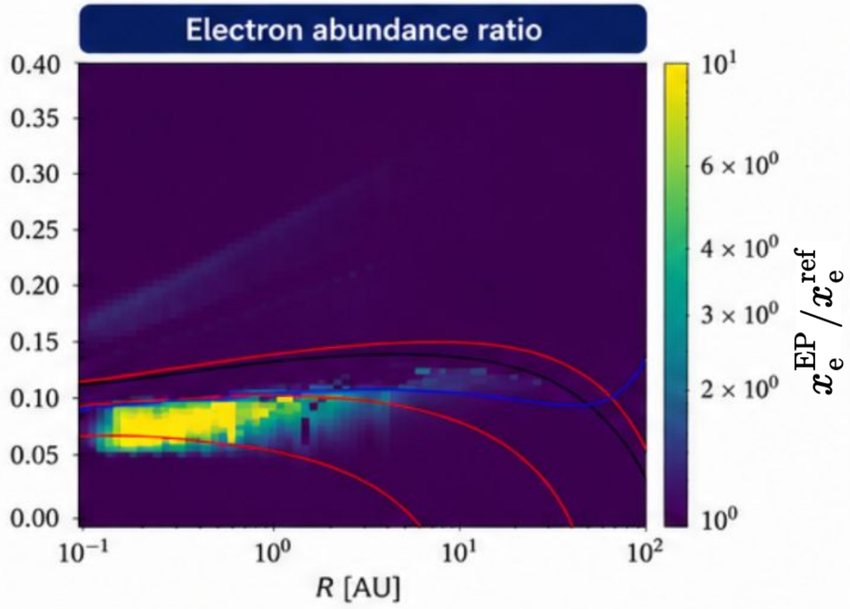

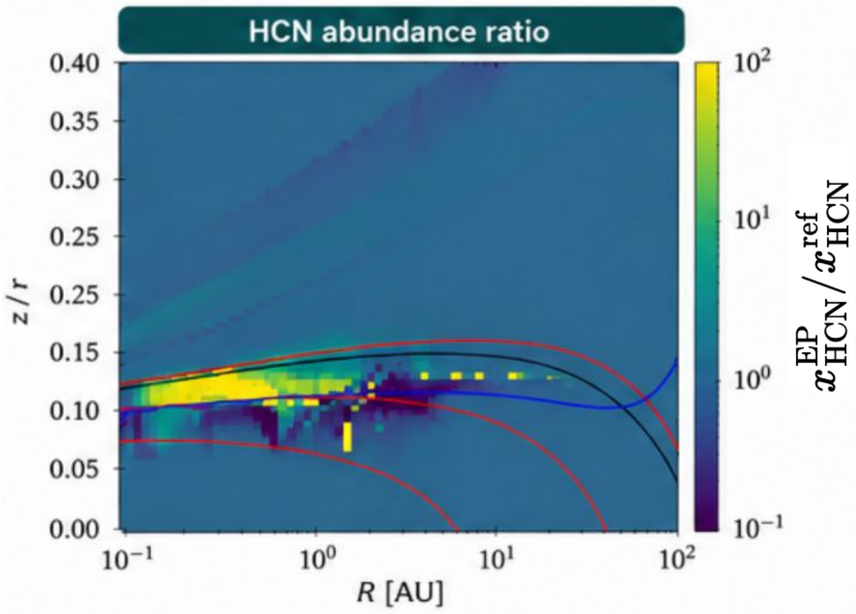

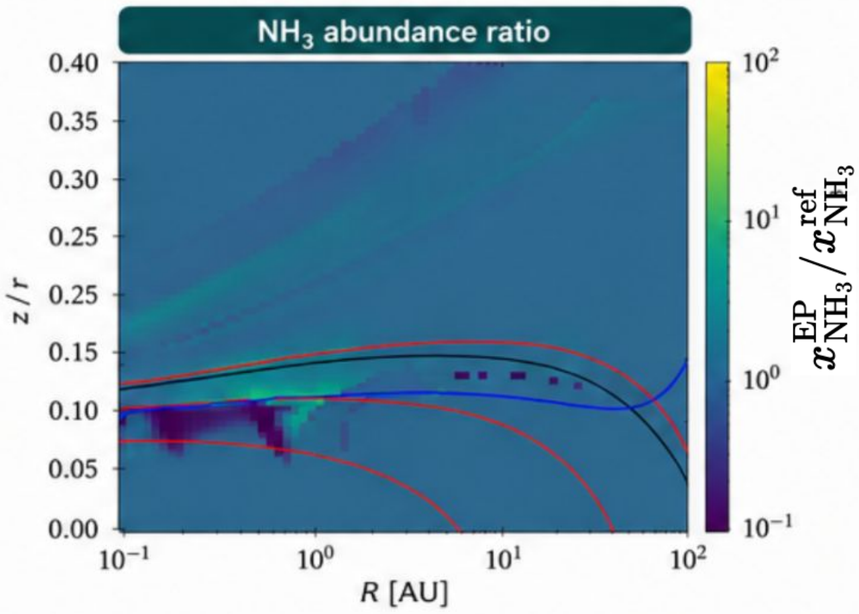

HOW TO READ THESE PANELS

All panels show ratios relative to a reference model without the additional EP source.

CONTOURS AND LINES

- Column density $N_H = 5 \times 10^{22}, 5 \times 10^{23}, 5 \times 10^{24}$ cm^{-2}
- $A_V = 1$ (optical depth to visual extinction)
- UV field $\chi = 1$ (equal to ISM intensity)

KEY IMPACTS OF EP IONISATION

- **Ionisation rate:** increases by up to a factor of 100 in the surface and upper layers.
- **Electron abundance:** increases in regions where $\chi < 1$ (UV-shielded), reducing recombination.
- **HCN abundance:** increases in regions where $\chi > 1$ (strong UV field), enhancing production.
- **NH_3 abundance:** decreases across much of the disc **intermediate layer**

Impact of the additional EP source on synthetic JWST spectra (MIRI)

Energetic particles (EPs) enhance the chemistry of the disc and boost molecular line emission in the mid-IR

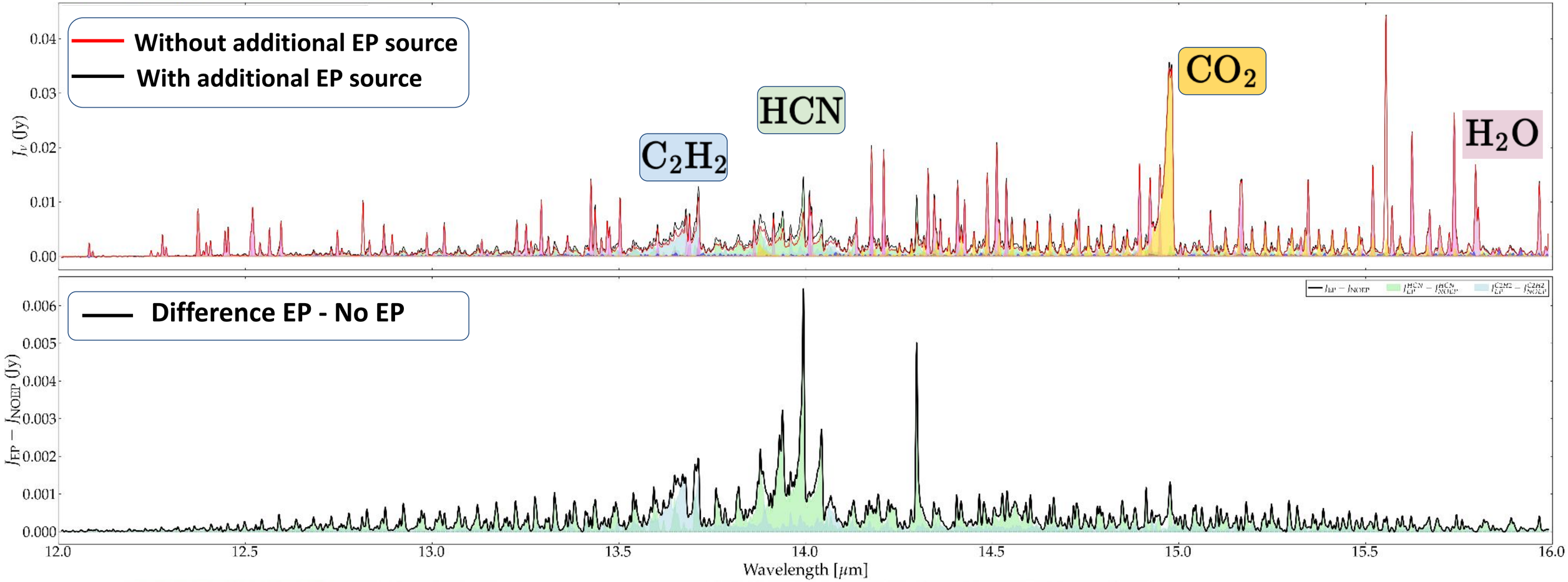

Key takeaways

Stronger lines with EPs
Many molecular lines are significantly brighter when the additional EP source is included.

Largest impact in 13.5–15 μm
The line-rich region (13.5–14.5 μm) and the ~15 μm feature show the strongest enhancements.

Net positive effect
The difference spectrum (EP–NOEP) is positive for most wavelengths, indicating a global increase in line flux.

Direct observational test
These enhancements can be probed with JWST/MIRI, offering a direct way to test EP-driven chemistry.

The additional EP source leaves a strong and measurable imprint on synthetic JWST spectra, revealing the role of energetic particles in shaping disc chemistry and emission.

Impact of the additional EP source on synthetic JWST spectra (MIRI)

The additional energetic particles (EPs) significantly modify the chemical composition of the disc.
Most notably, they **strongly enhance carbon–bearing species**, especially **HCN** and **C_2H_2**.

1. Relative change in line fluxes of key tracers (sum of all lines in the MIRI band) $(F_{EP} - F_{NOEP})/F_{NOEP}$

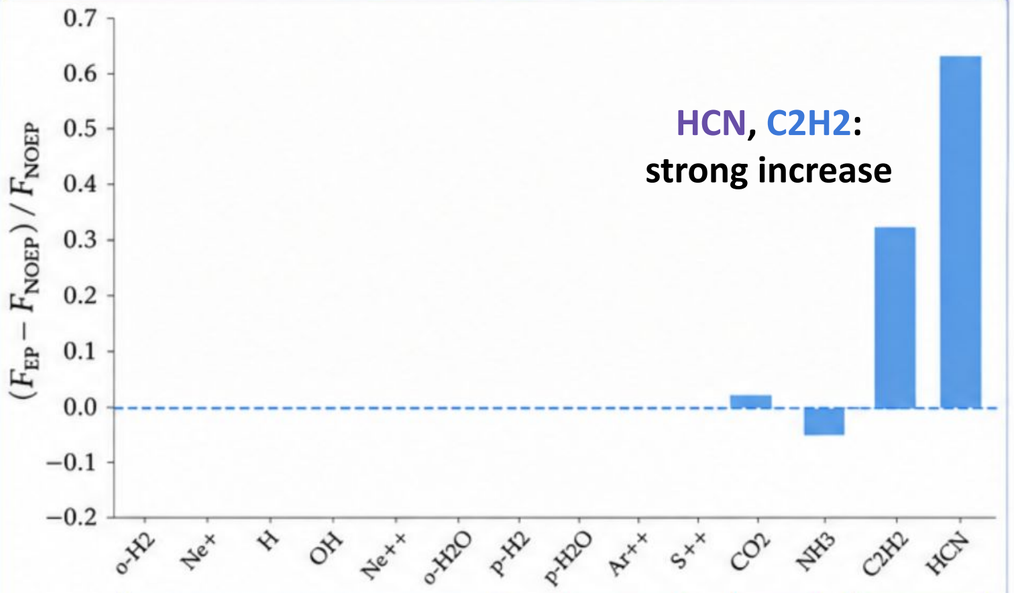

HCN, **C2H2**: **strong increase**

Most species : unaffected

NH3: **decrease**

- Strong enhancements in carbon–bearing species: **HCN** (~+65%) and **C_2H_2** (~+30%),
- Small increase in **CO_2** (~2%) and negligible changes for most other species.
- **NH_3** is decreased (~5%), indicating altered nitrogen chemistry.

2. Line ratios most enhanced by the additional EP source $(R_{EP} - R_{NOEP})/R_{NOEP}$

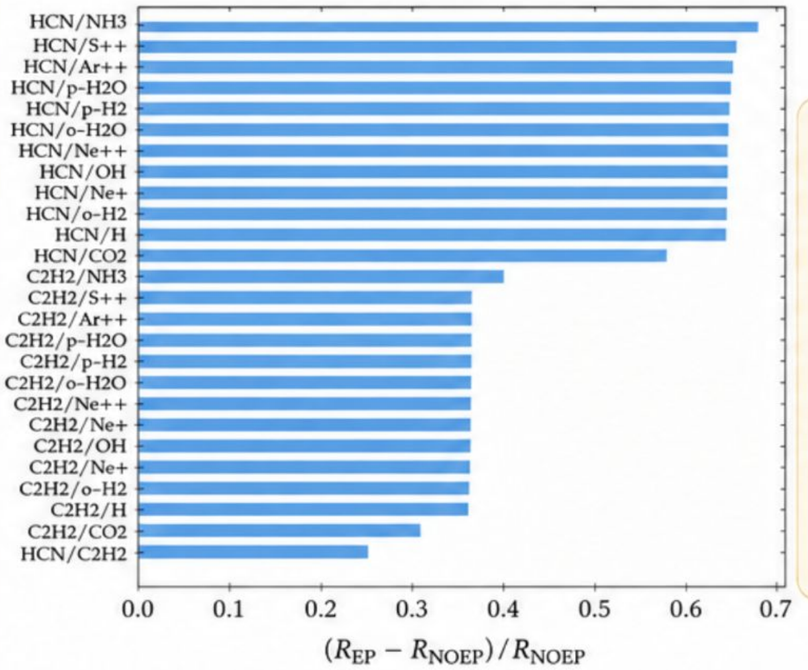

Why use line ratios?

Line ratios are useful because they are less affected than absolute fluxes by source brightness, distance, or calibration uncertainties.

→ **They provide robust diagnostics of the underlying chemistry.**

- Line ratios involving **HCN** show the strongest enhancements (up to ~0.65).
- **C_2H_2**-related ratios are also significantly increased (up to ~0.35).
- These changes reflect a global enhancement of carbon chemistry in the EP-irradiated disc.

Key takeaway

The additional EP source drives a strong enhancement of carbon-bearing species, particularly **HCN** and **C_2H_2**, while leaving most other species unchanged.
Line ratios provide the most reliable diagnostics to detect and quantify EP-driven non-thermal ionisation in discs.

In situ EP acceleration by magnetic reconnection in young stellar objects

Two EP acceleration regimes operate in the disc and leave complementary JWST observational signatures

From flares to turbulence: EPs are key drivers of the disc chemistry revealed by JWST.

INNER DISC
(0.05 – 0.3 au)

EPs from flares
bursting & intermittent

- Strong but sporadic EP injections
- Magnetic reconnection in stellar/inner-disc flares

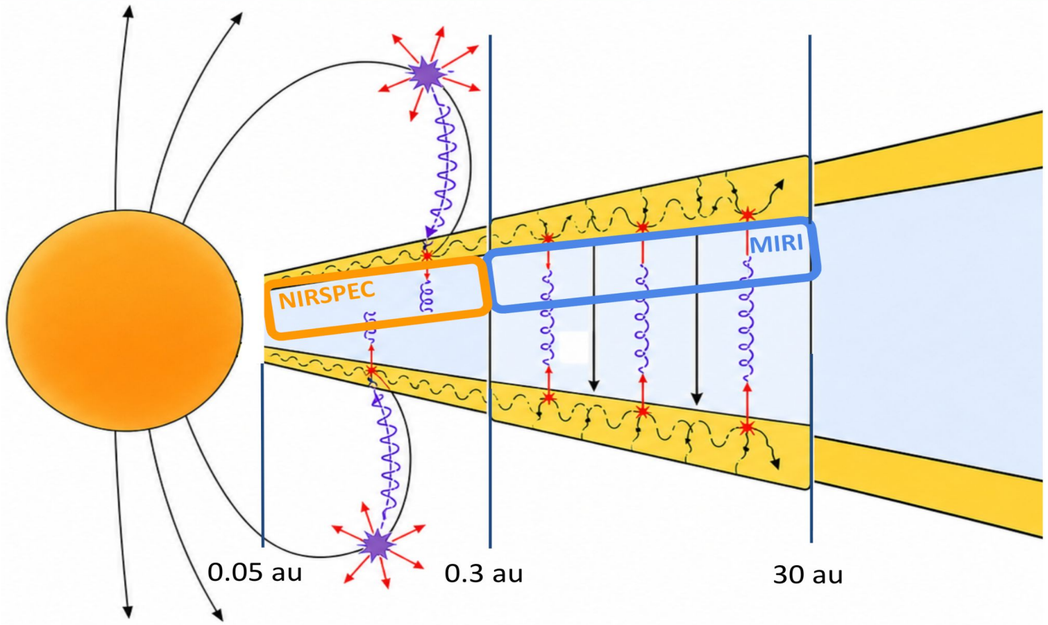

INTERMEDIATE DISC
(0.3 – 30 au)

EPs from turbulence
continuous & steady

- Weaker but continuous EP acceleration
- Turbulence-induced magnetic reconnection

OBSERVATIONAL CONSEQUENCES WITH JWST

INNER DISC: JWST / NIRSpec
(near-IR, 0.6 – 5 μm)

- Sensitive to strong, time-variable enhancement of key tracers
- Tracers: CO, OH, HI

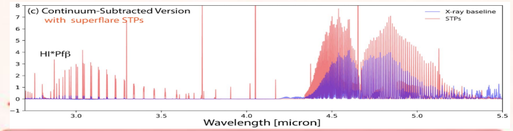

Bursting EPs → variable chemical emission

Two regimes complement each other in space and time

INTERMEDIATE DISC: JWST / MIRI
(mid-IR, 5 – 28 μm)

- Traces sustained enhancement of molecular emission
- Tracers: HCN, C_2H_2

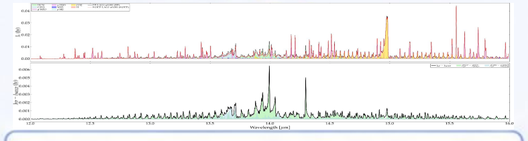

Continuous EPs → steady chemical emission

OVERALL IMPACT

In situ EP acceleration by magnetic reconnection operates across the disc with complementary regimes.

Together, they leave a clear, multi-wavelength chemical imprint detectable with JWST.

Flare-driven EPs dominate the inner disc (0.05–0.3 au) and shape the JWST / NIRSpec signatures (CO, OH, HI).
Turbulence-driven EPs dominate the intermediate disc (0.3–30 au) and shape the JWST / MIRI signatures (HCN, C_2H_2).

Locally accelerated EPs must be considered and further studied for a better description of protoplanetary discs

Monte Carlo Analysis to account for temporal effects from YSO observations

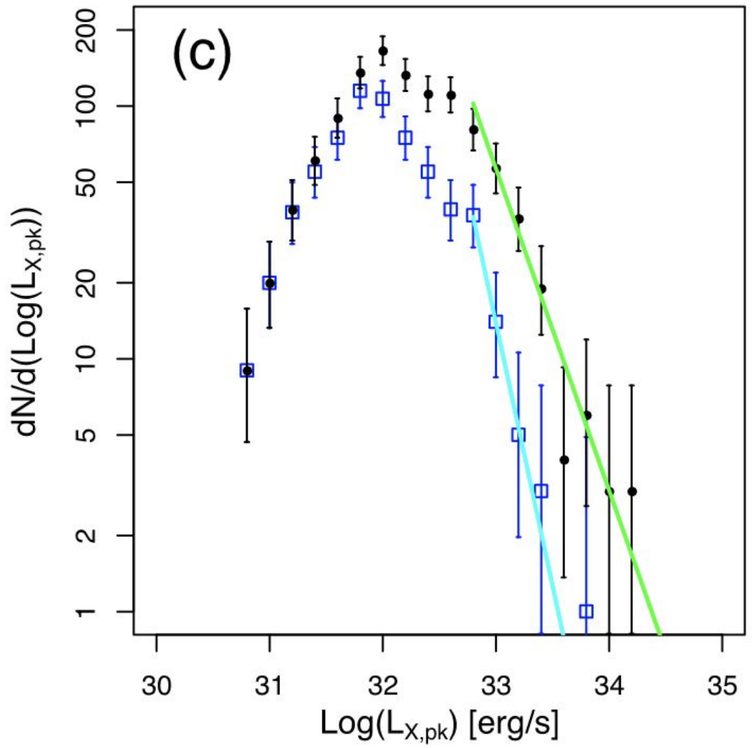

Getman et al. (2021)

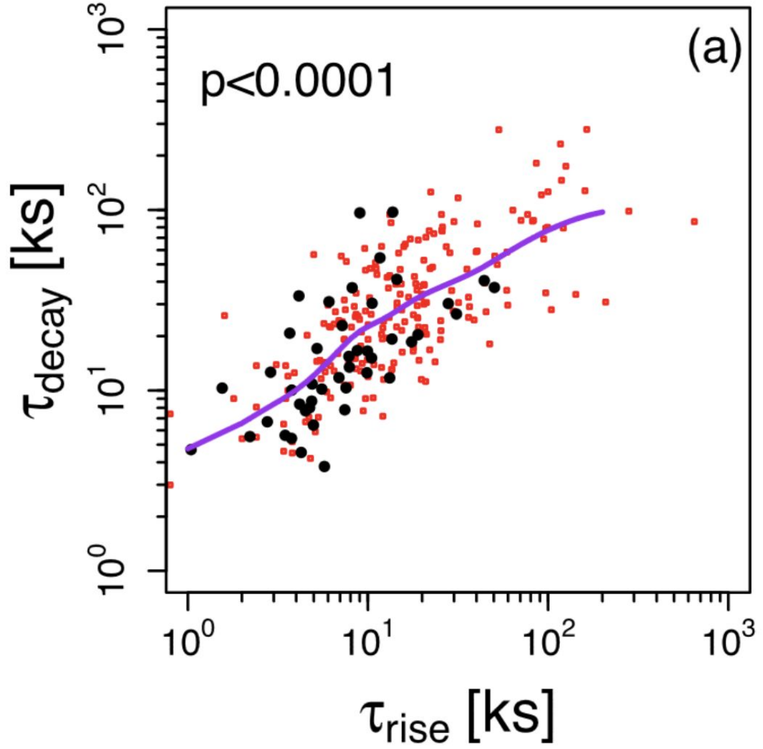

Getman et al. (2021)

- **Luminosity distribution.**
- **Frequency distribution.**
- **Duration distribution.**

Perspectives

Short term perspectives:

- **Extend our propagation model to high column density, accounting for diffusion**
- **Develop a model of turbulent reconnection that could occur farther in the disc**
- **Work on the effects on chemistry and production of the synthetic JWST spectra**

Perspectives

Short term perspectives:

- Extend our propagation model at high column density, accounting for diffusion
- Work on the effects on chemistry and production of the synthetic JWST spectra
- Develop a model of turbulent reconnection that could occur farther in the disc

Middle term perspectives:

- Study the effects of EP propagating in winds and jets
- Estimate the production of radioactive isotopologues in discs, important for planetesimals geology

Normalising the supra-thermal particle energy distribution

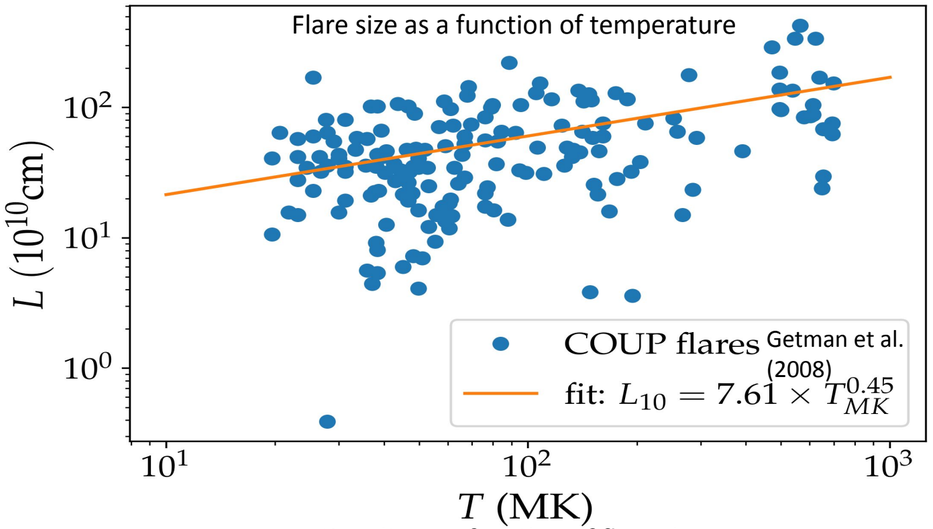

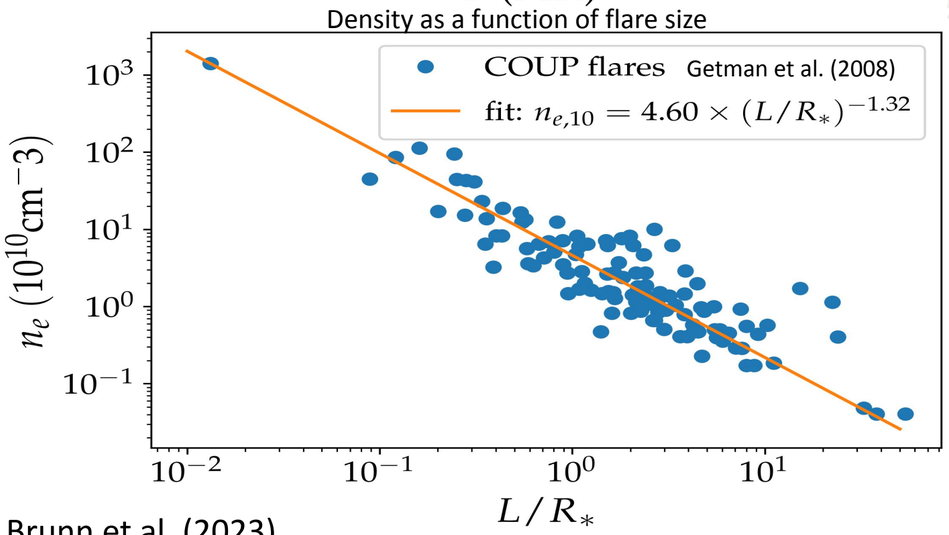

Brunn et al. (2023)

- **We assume that the X-ray emission is bremsstrahlung radiation.**
- **The electron density at the flare location is correlated to the flare temperature,**

$$n_e = 20.5 \times 10^{10} \left(\frac{T}{1MK}\right)^{-0.69} \ cm^{-3}.$$

Energetic particles affect the accretion processes in discs

$$\dot{M}_{acc} \sim 10^{-8} \left(\frac{\alpha(T, n_e, n_n)}{0.01}\right) \left(\frac{R}{10\ au}\right)^{1/2} \left(\frac{M_*}{M_\odot}\right)^{1/2} \left(\frac{\mathrm{N}}{10^{24}\ cm^{-2}}\right) M_\odot\ yr^{-1}$$

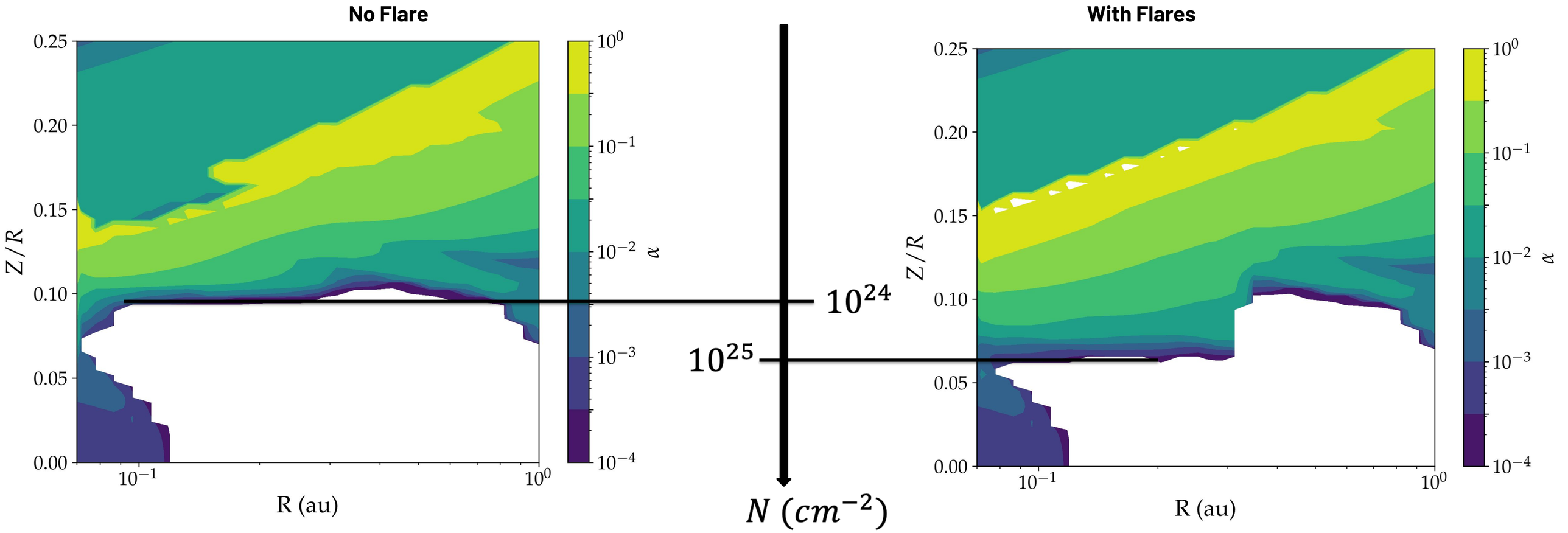

Accounting for flares reduces the size of the dead-zone in the inner disc

Energetic particles affect the accretion processes in discs

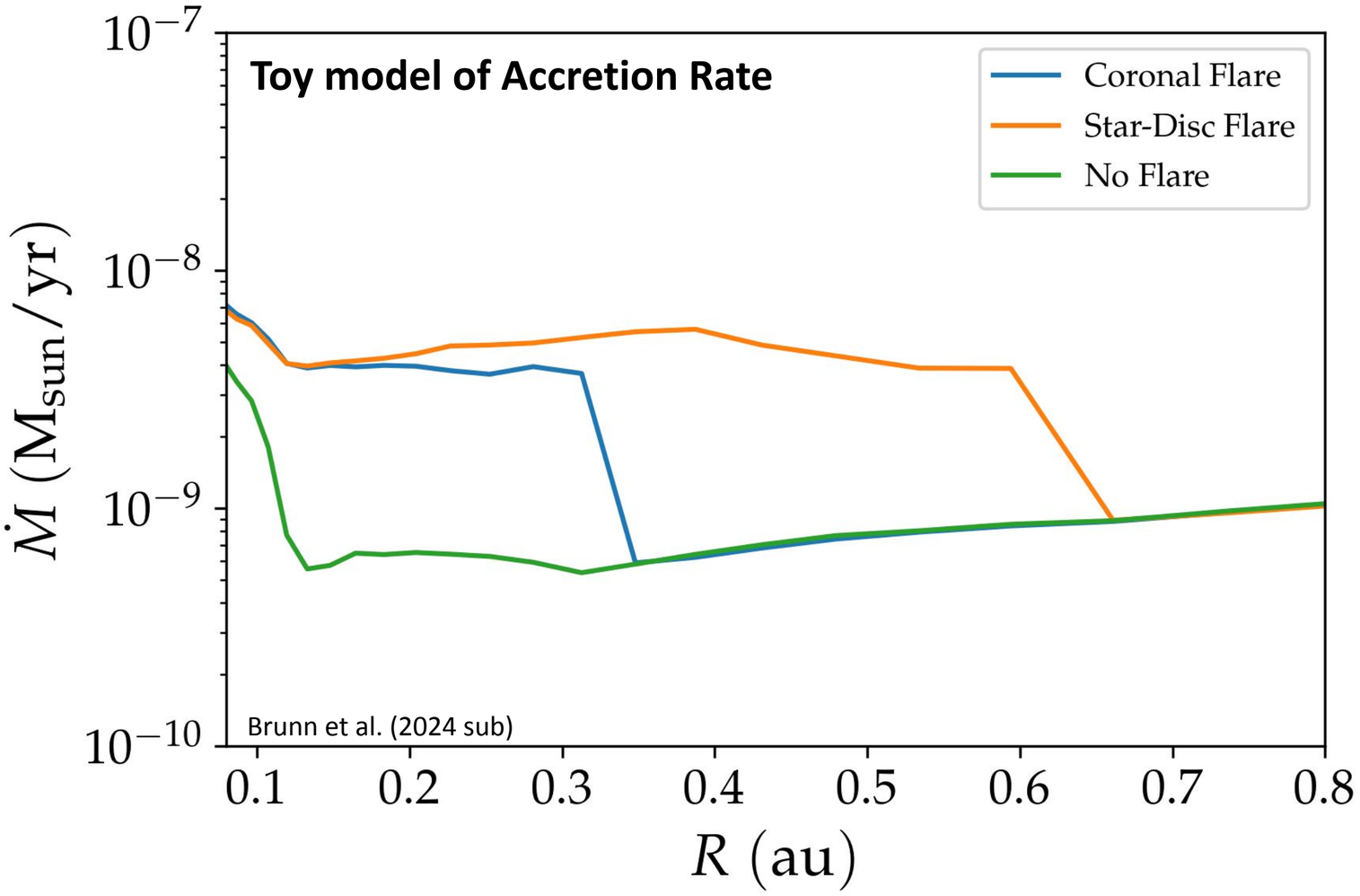

- Accounting for flares reduce the dead-zone size in the inner disc.
- The reduction of the dead zone size leads to an increase of the accretion rate.

The Energy Loss Function

$$L(E) = -\frac{dE}{dN}$$

dE: infinitesimal energy loss

dN: infinitesimal column density crossed by the parti

- L is determined theoretically or in laboratory experiments.
- Solving this equation gives the relation between E_0, E and N.
- L depends on the particle considered (e, p) and the medium targeted $(\mathrm{H}^+, H, H_2, He)$.

The Electron energy loss functions

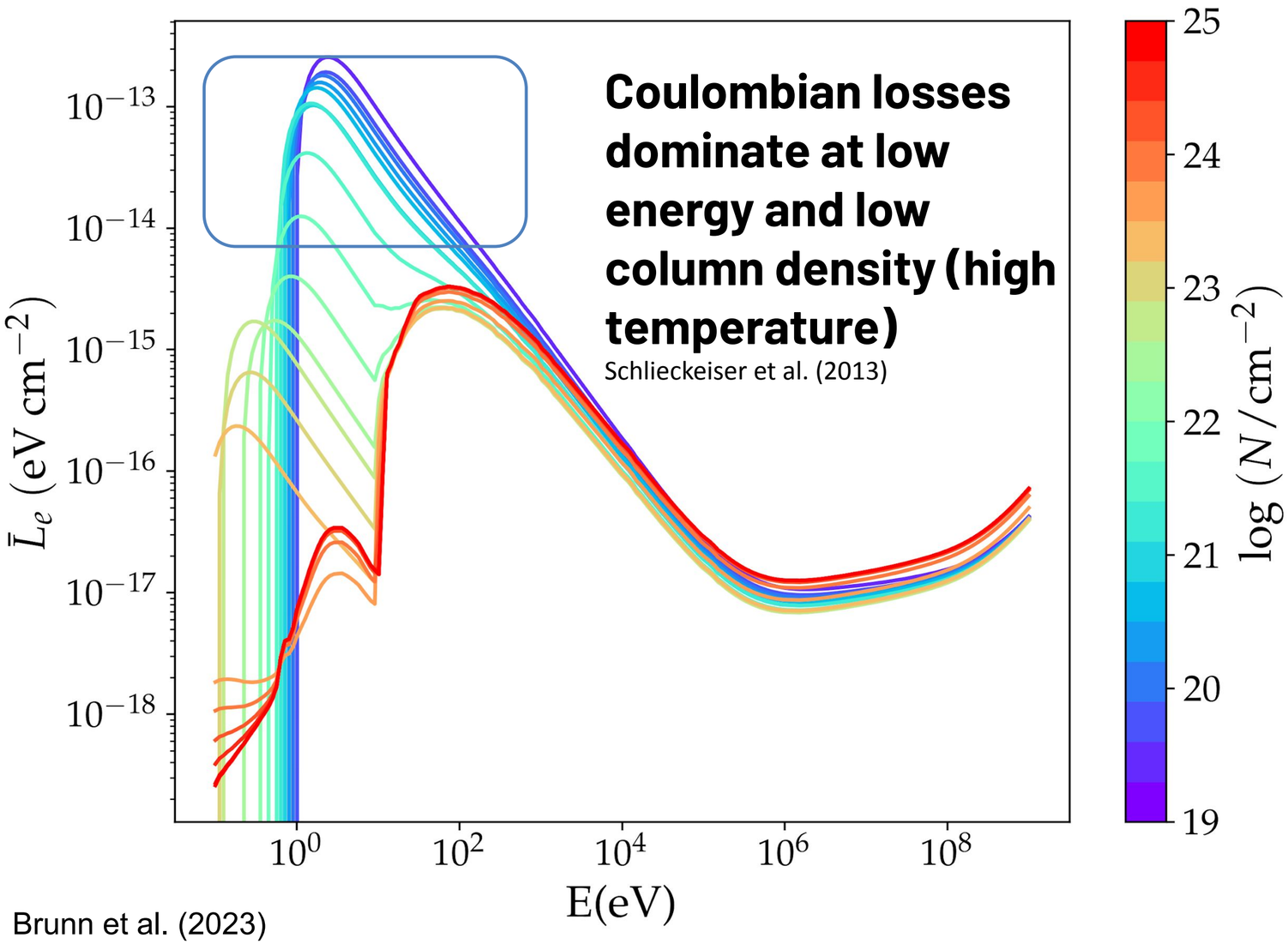

Brunn et al. (2023)

Schlickeiser, R. (2013). *Cosmic ray astrophysics*. Springer Science & Business Media.

The Electron energy loss functions

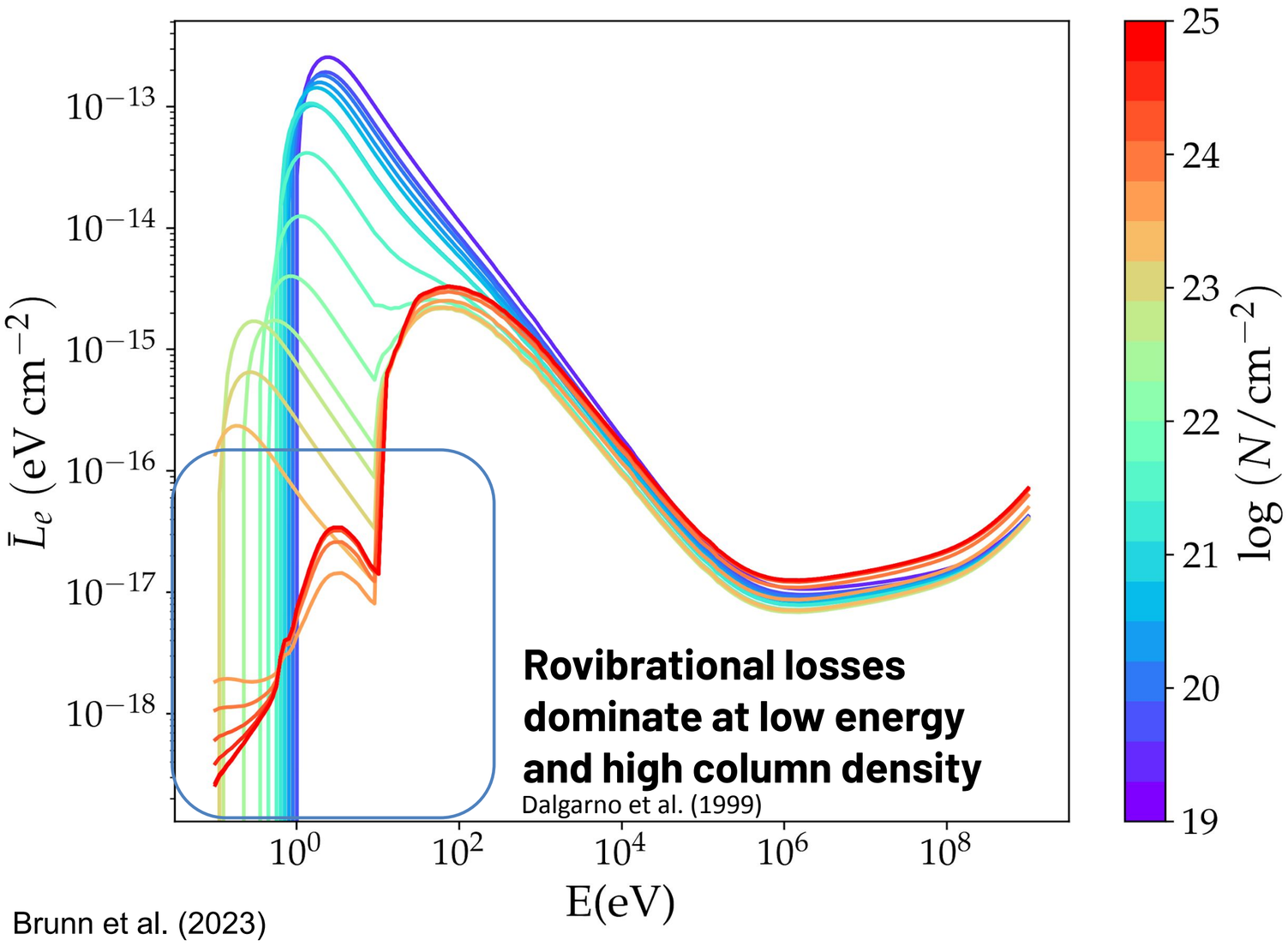

Brunn et al. (2023)

Schlickeiser, R. (2013). *Cosmic ray astrophysics*. Springer Science & Business Media.

Dalgarno, A., Yan, M., & Liu, W. (1999). Electron energy deposition in a gas mixture of atomic and molecular hydrogen and helium. *The Astrophysical Journal Supplement Series*, *125*(1), 237.

The Electron energy loss functions

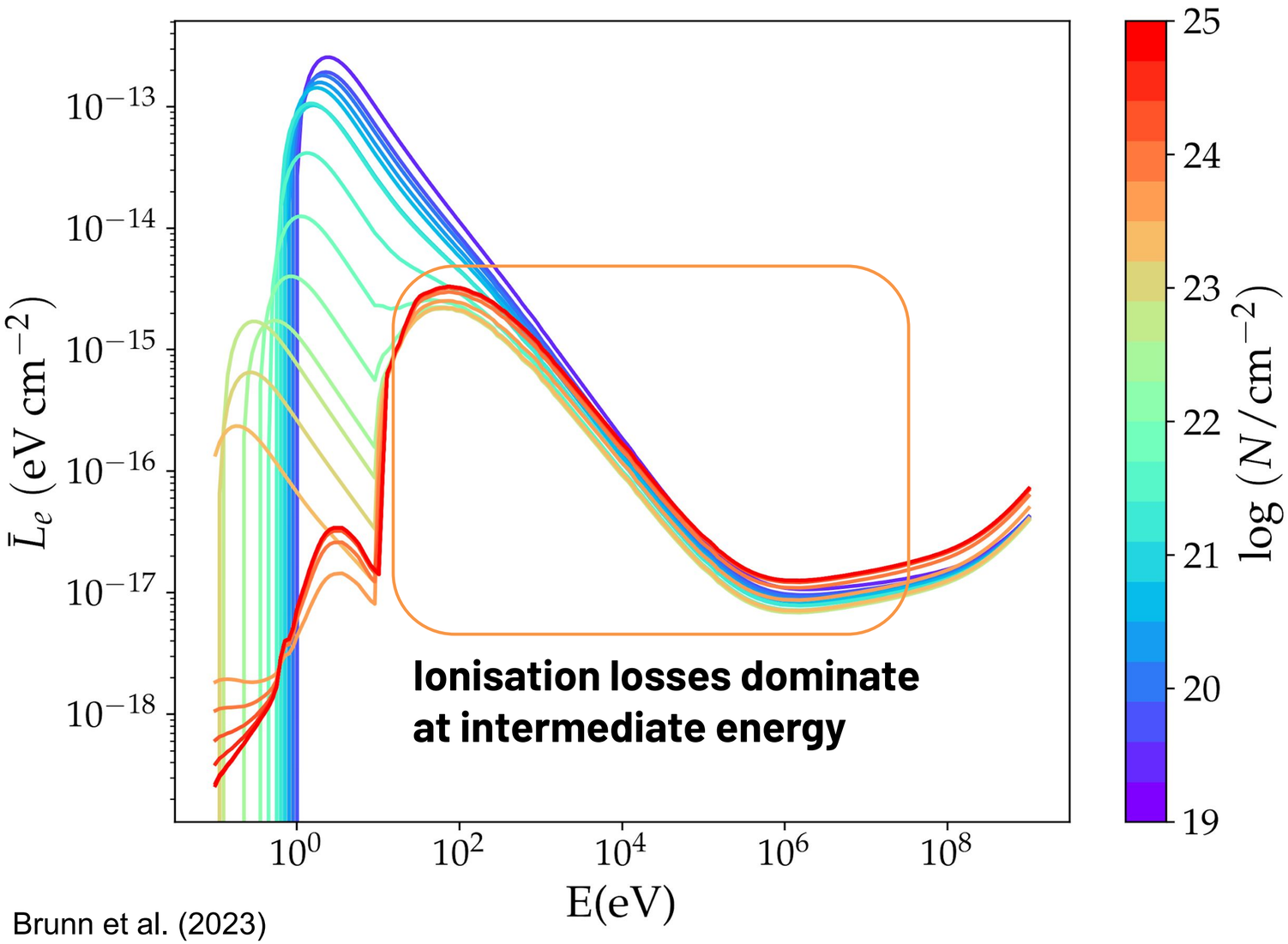

Brunn et al. (2023)

Schlickeiser, R. (2013). *Cosmic ray astrophysics*. Springer Science & Business Media.

Dalgarno, A., Yan, M., & Liu, W. (1999). Electron energy deposition in a gas mixture of atomic and molecular hydrogen and helium. *The Astrophysical Journal Supplement Series*, *125*(1), 237.

The Electron energy loss functions

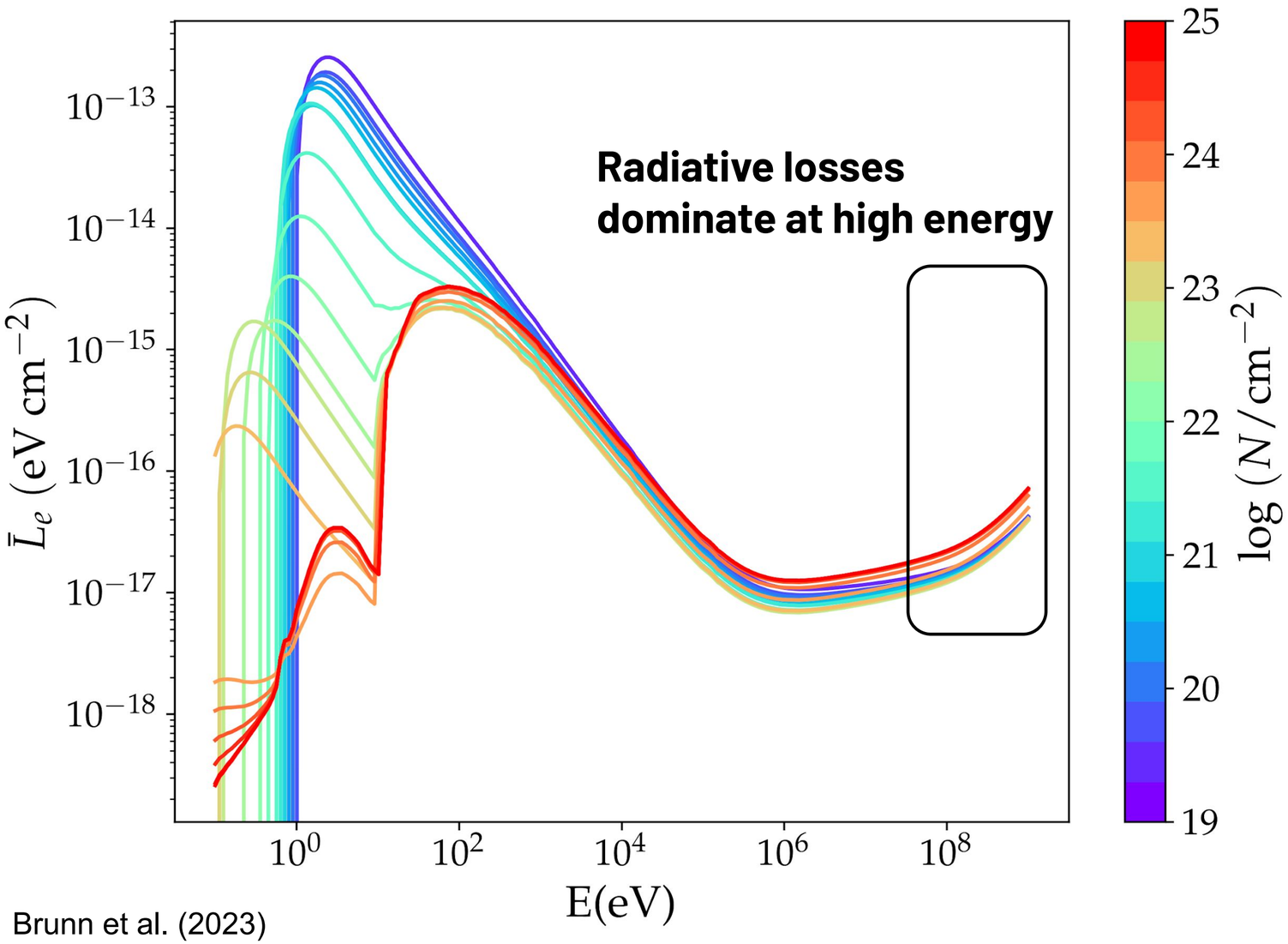

Brunn et al. (2023)

Schlickeiser, R. (2013). *Cosmic ray astrophysics*. Springer Science & Business Media.

Dalgarno, A., Yan, M., & Liu, W. (1999). Electron energy deposition in a gas mixture of atomic and molecular hydrogen and helium. *The Astrophysical Journal Supplement Series*, *125*(1), 237.

Ionisation rate

$$\zeta(N) = 2\pi \int \boldsymbol{j(E,N)}\big(1 + \phi(E)\big)\sigma_{ion}(E)dE$$

$$\boldsymbol{j(E,N)} = j_0(E_0)\frac{L(E_0,0)}{L(E,N)} \quad \textbf{(CSDA)}$$

Injection model
(magnetic reconnection)

Disc Model

$j(E,N)$:
propagated flux

N: effective column density

σ_{ion}: ionisation cross section

L: loss fuction

ϕ: secondary electrons

Padovani et al. 2009

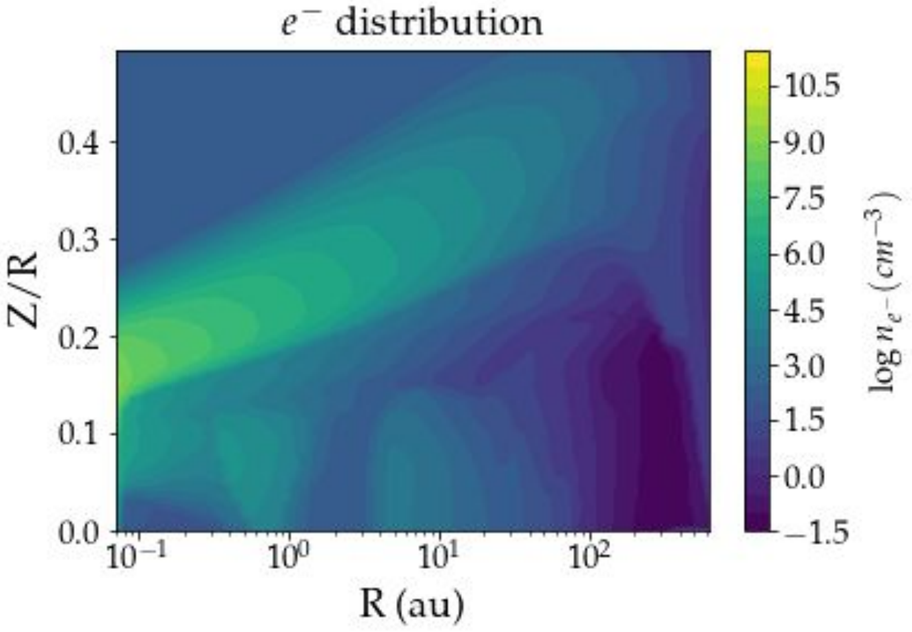

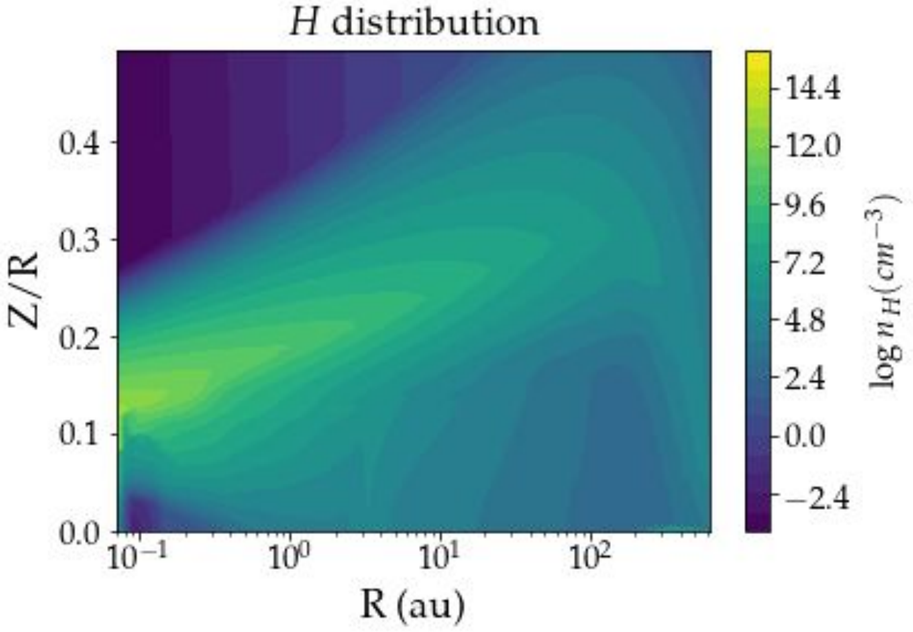

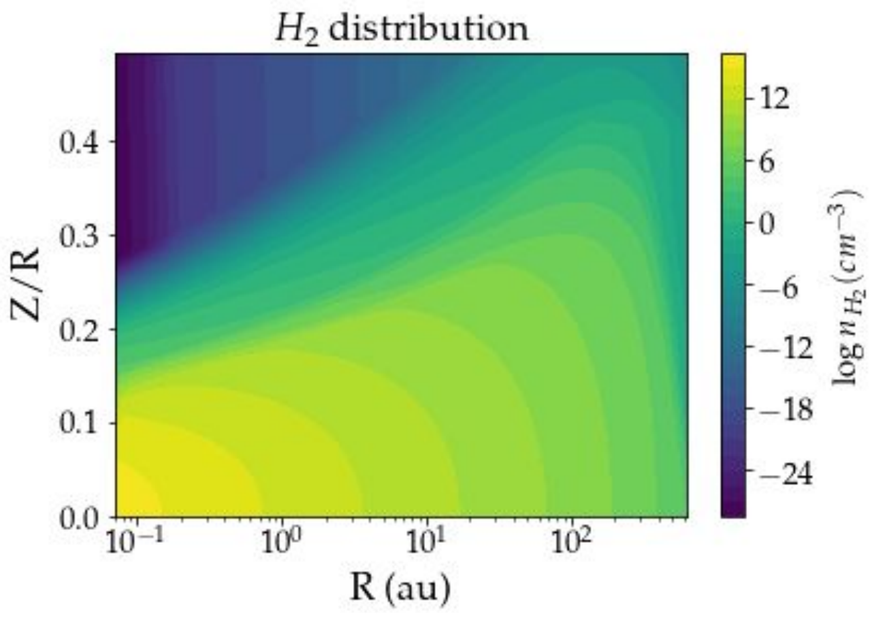

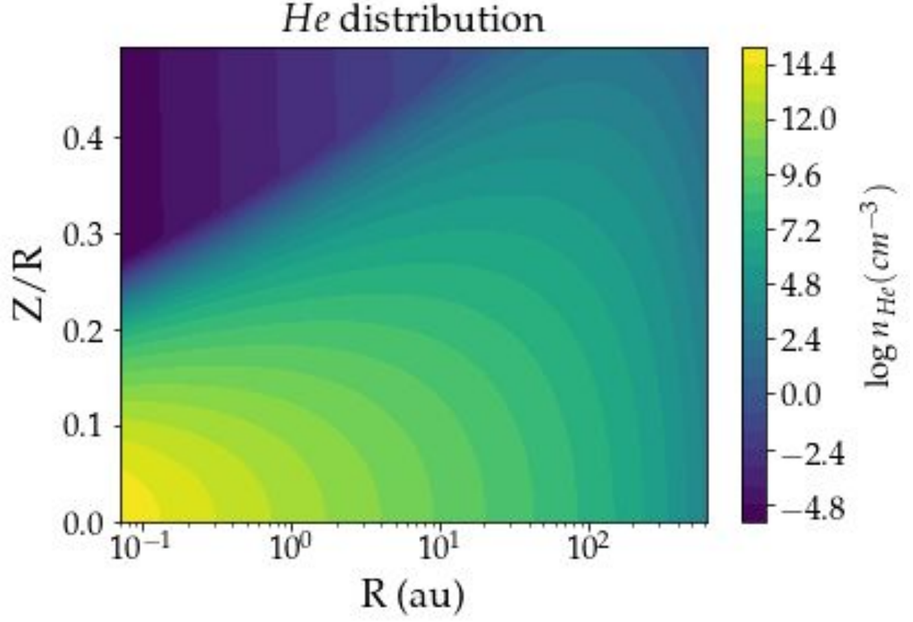

Composition:
$\boldsymbol{H^+}$, **H**, $\mathbf{H_2}$
and **He**

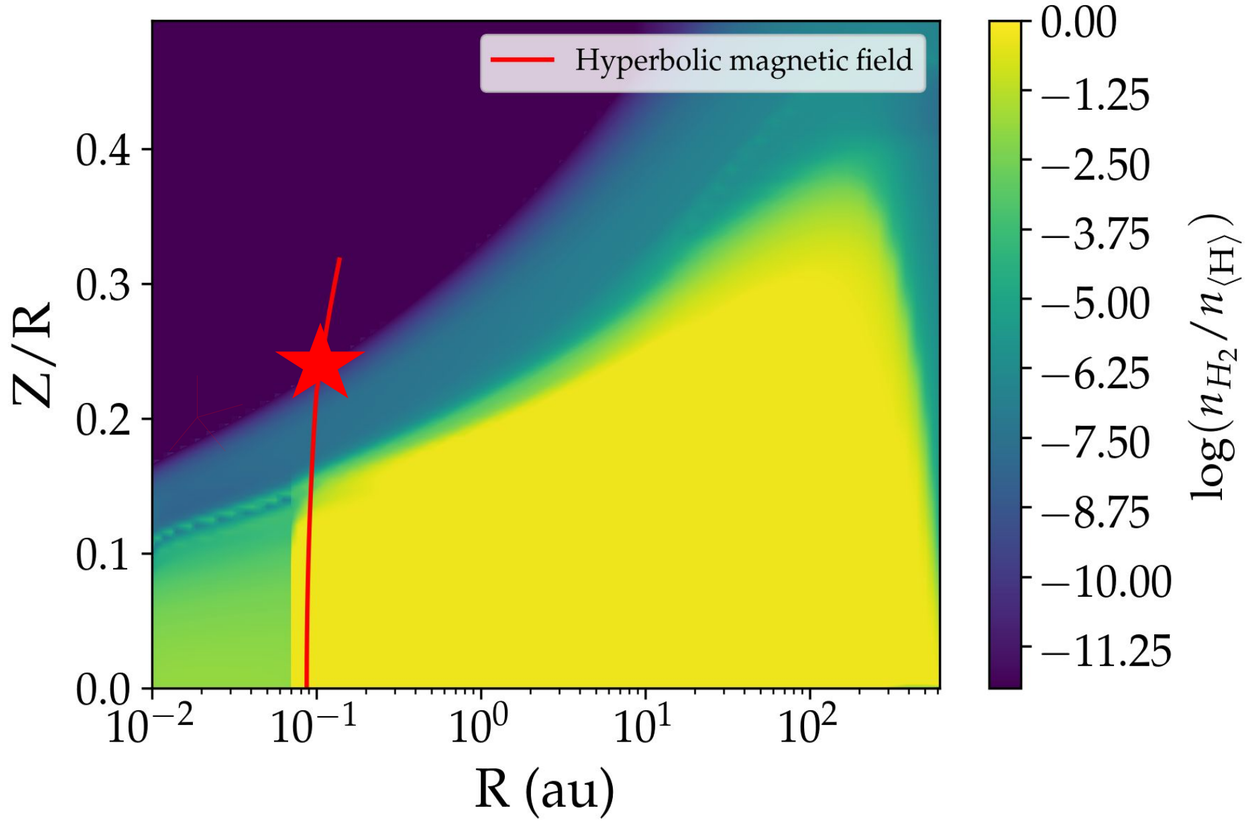

★ : Position of particle penetration site

Particles penetrate **above** the disc and **propagates along** the MF lines

Magnetic Configurations

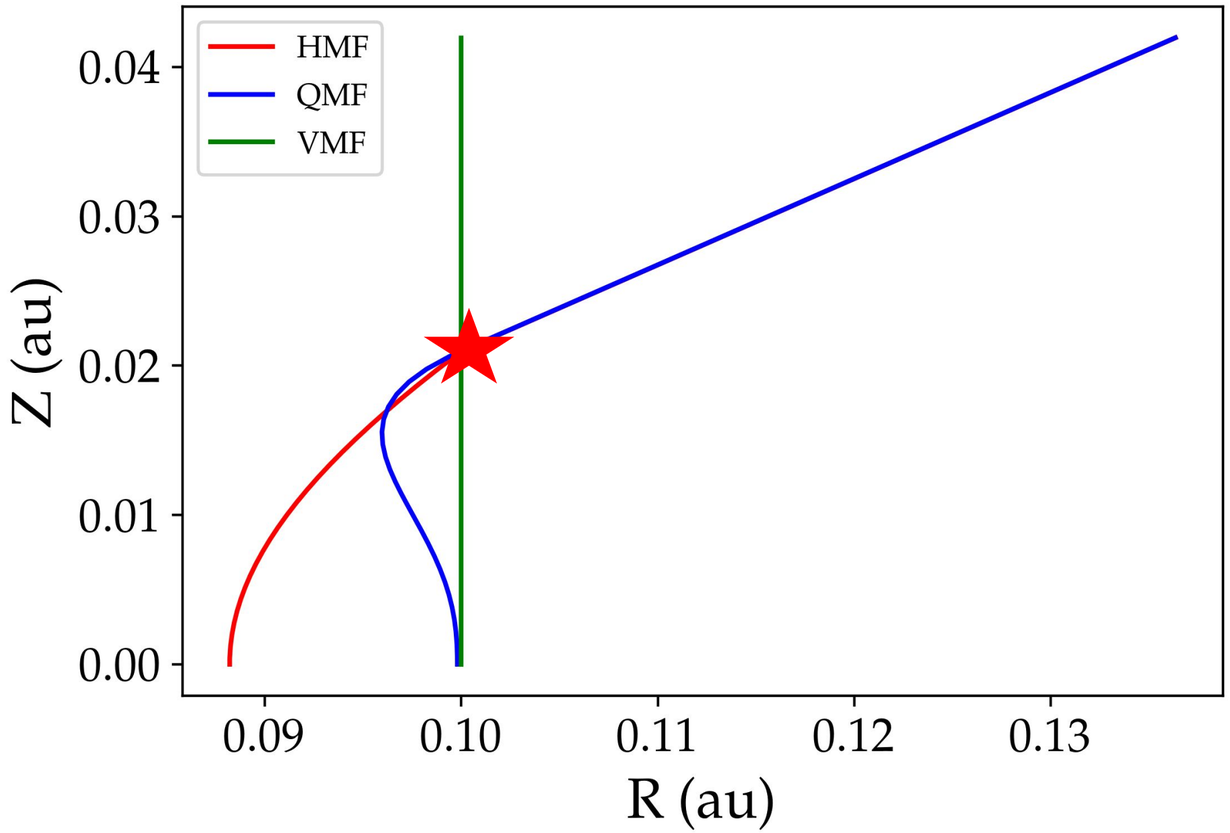

★ : Flare position

Vertical : Reference

Hyperbolic : Standard disc

Quartic : Differential accretion in the disc

Toroidal Magnetic Configurations

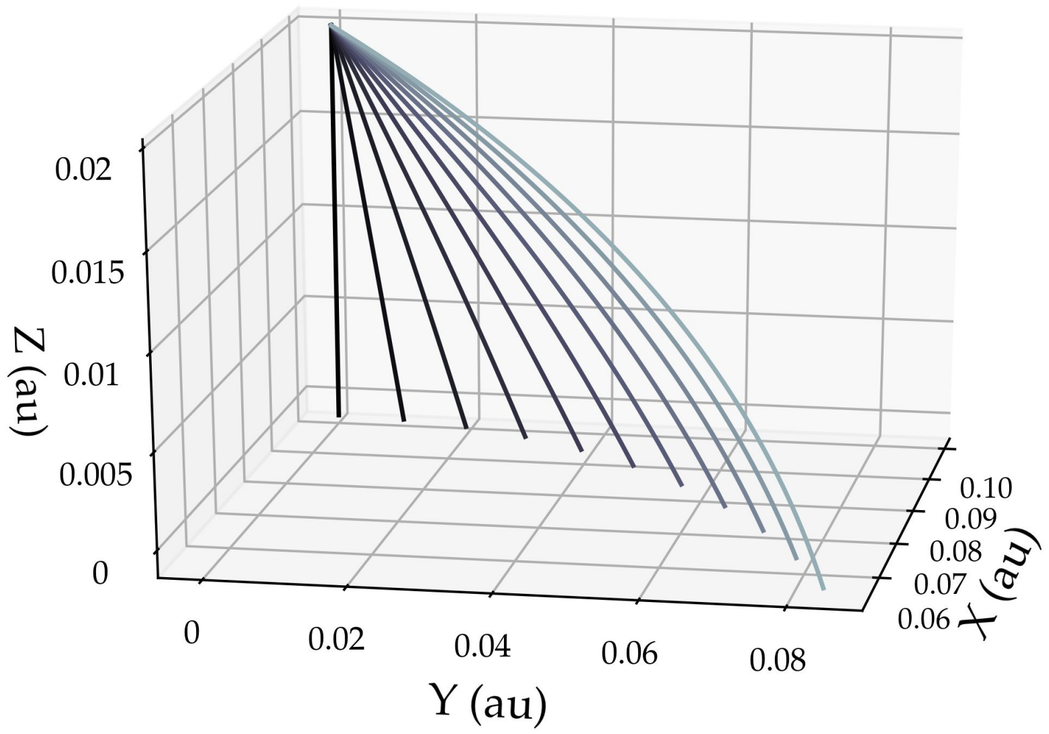

Particles explore **different** column densities for each configuration

Flare size as a function of temperature

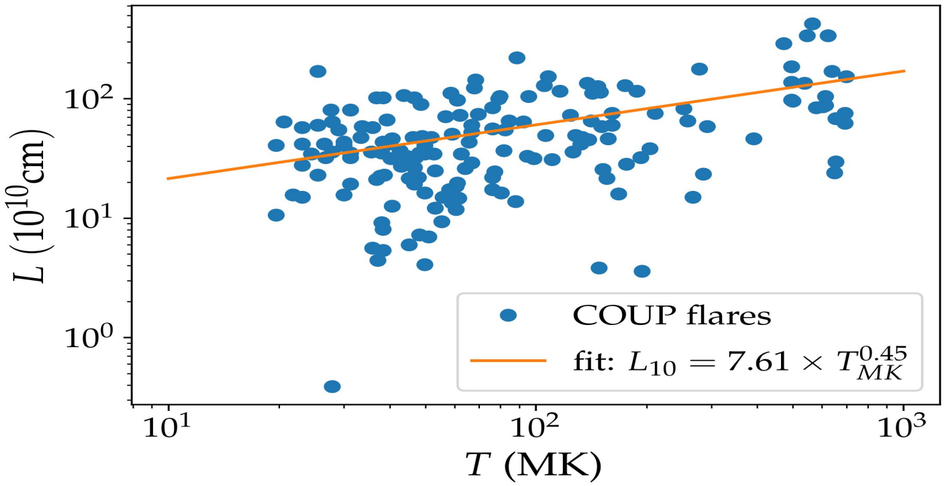

Density as a function of flare size

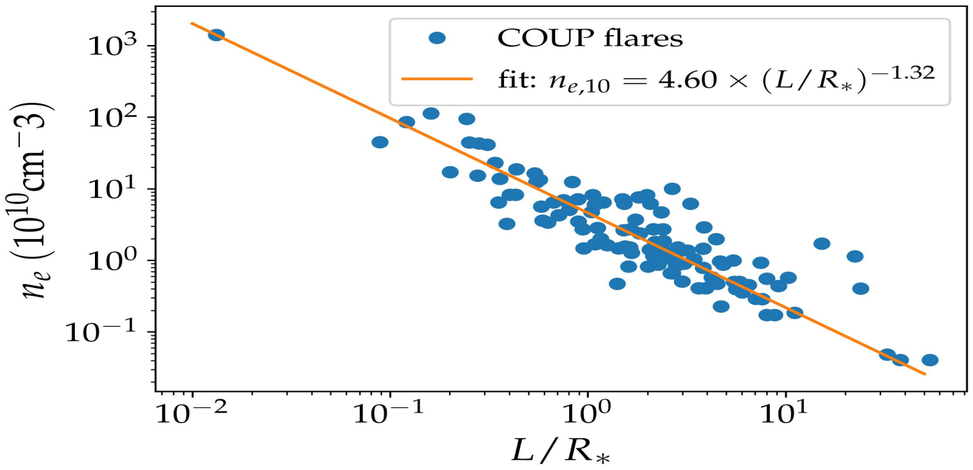

Getman, K. et al. (2008) *The Astrophysical Journal*.

Bremsstrahlung **Luminosity** (erg/s)

$$L_X = 1.4 \times 10^{26} L_{10}(T)^3 n_{e,10}(T)^2 T_6^{1/2} g_B$$

L_{10} : size of the flare over 10^{10}cm
$n_{e,10}$: electron density over $10^{10}\mathrm{cm}^{-3}$
T_6 : temperature over 10^6K
g_B: Bolometric Gaunt factor

Disk model no X-rays from the flare

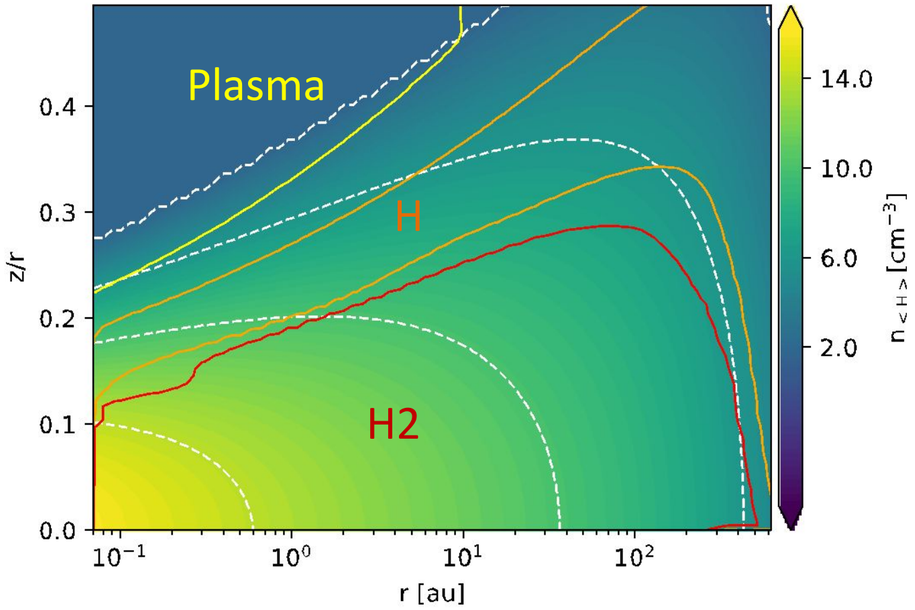

Disk model for 1MK flare

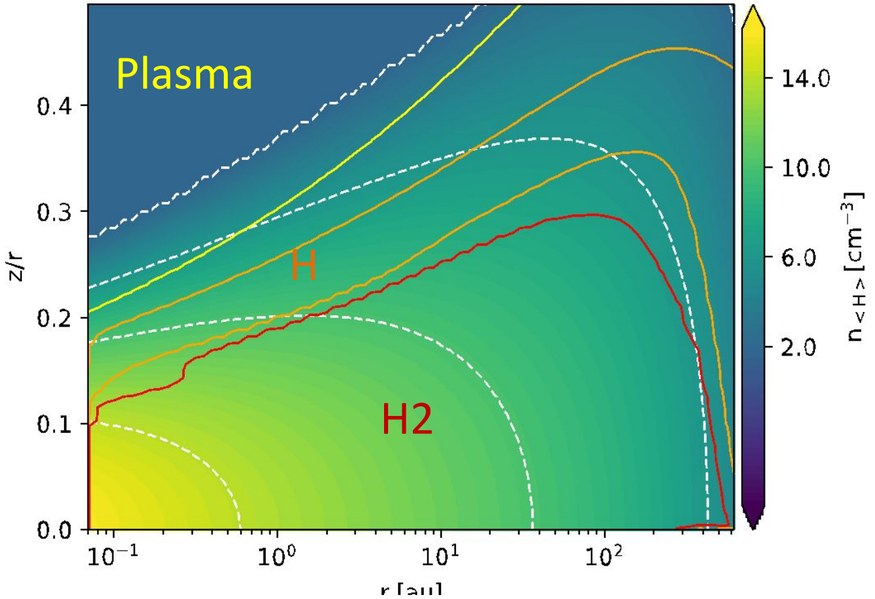

Disk model for 10MK flare

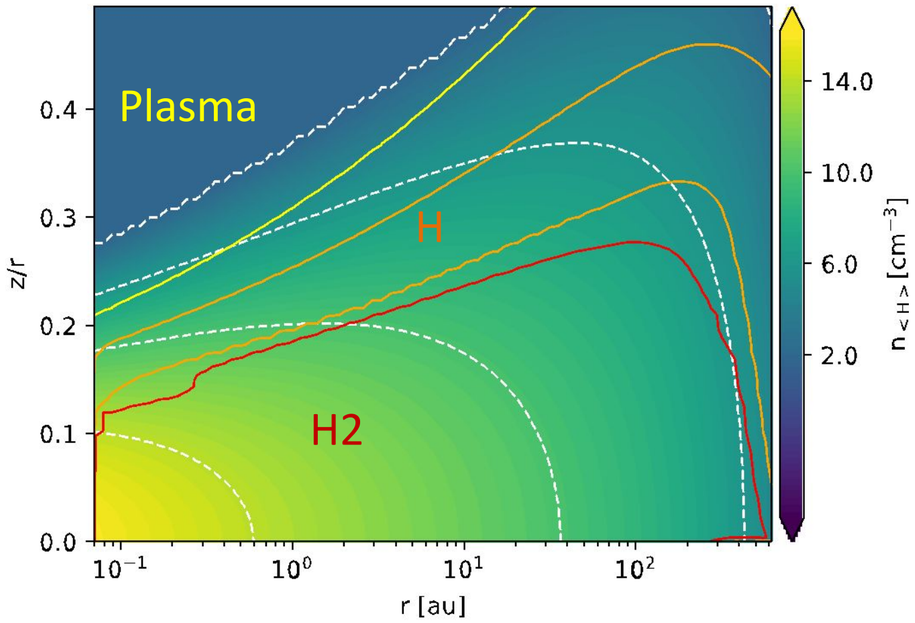

Disk model for 100MK flare

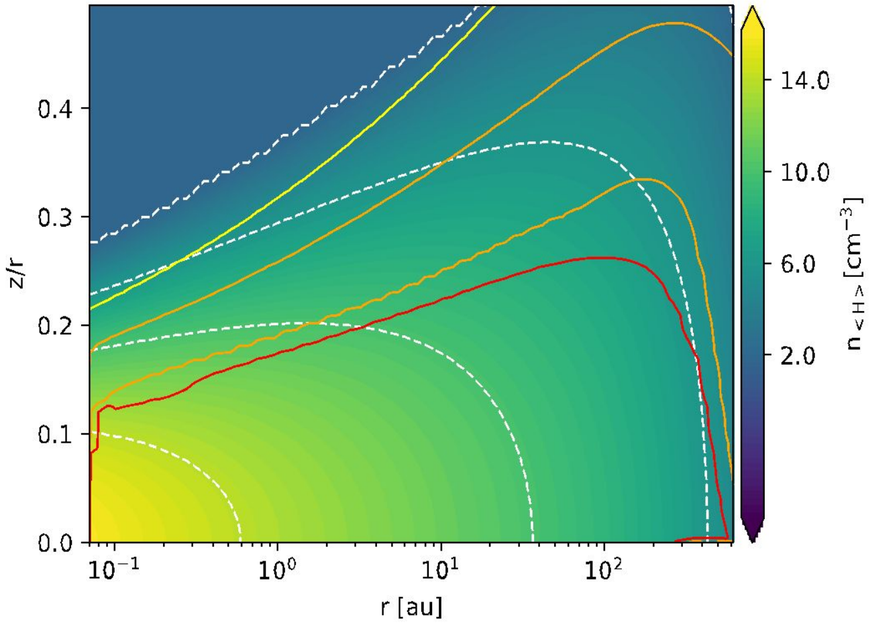

ProDiMo solutions **considering** the **X-ray** emission of the flare

ProDiMo computes the chemical structure of the disc for different flare temperatures

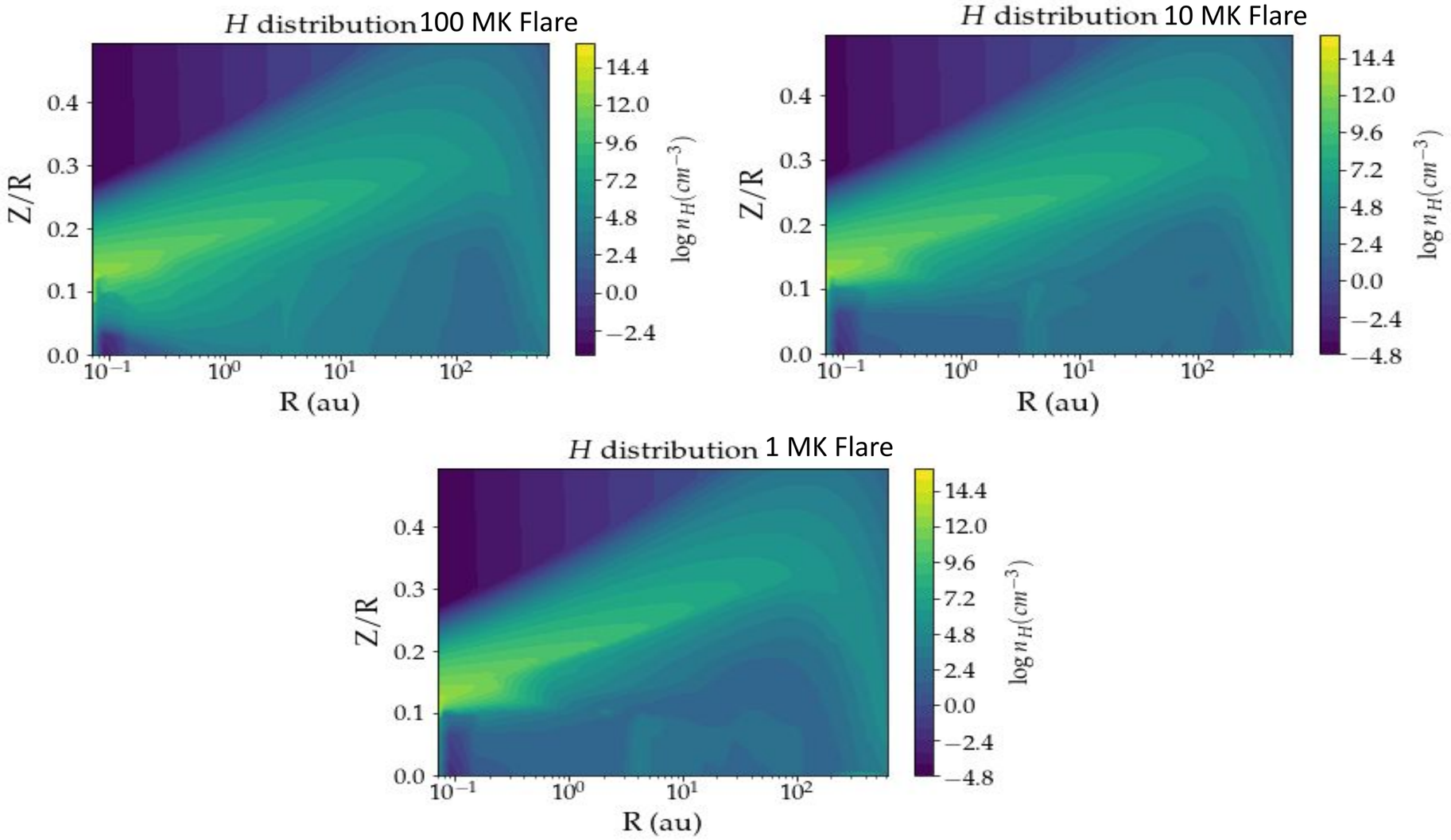

Atomic hydrogen is present **deeper** in the disc for hot flares with **strong X-ray** emission

Particle Injection

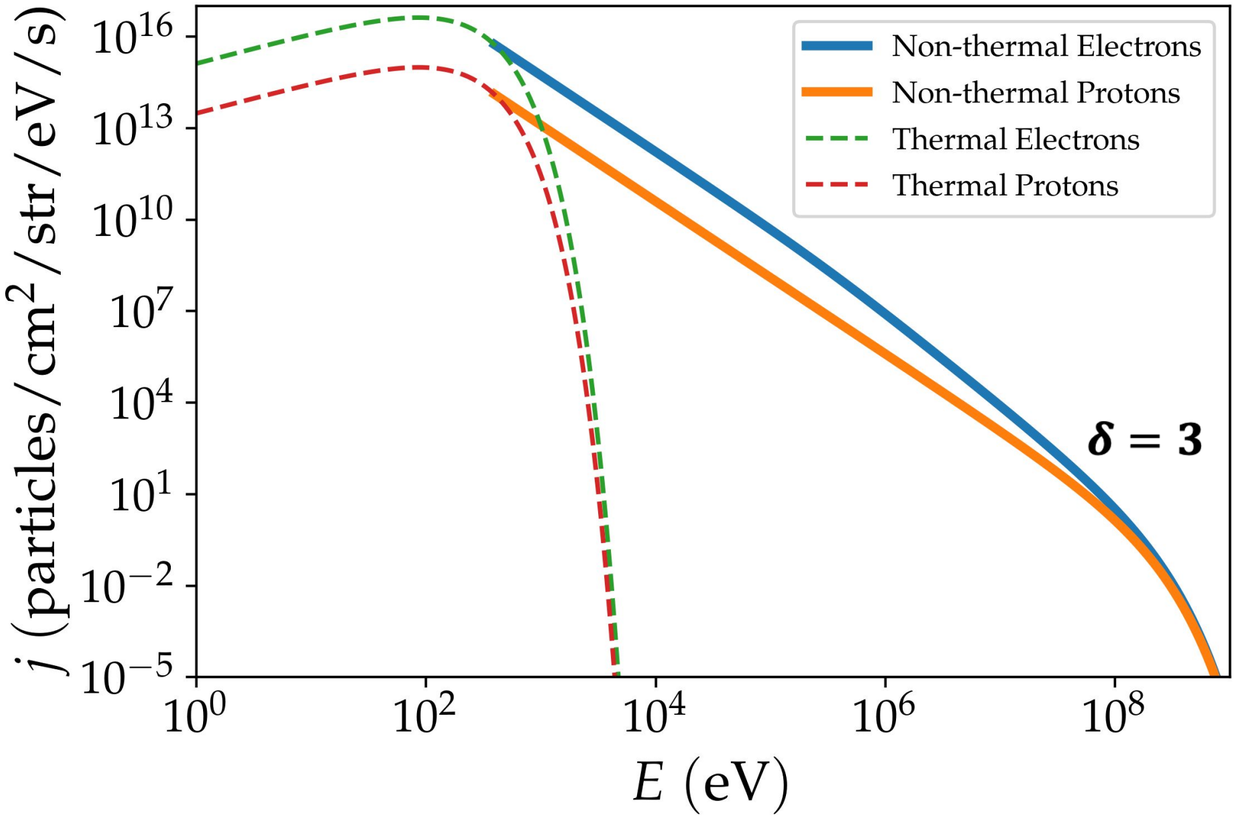

Power law spectrum as in **solar flares**

$$j_0(E) \sim \beta(E) n_e E^{-\delta} e^{-\overline{10}}$$

n_e: non thermal electron density

δ: Power law index

$$j \sim E^{-\delta}$$

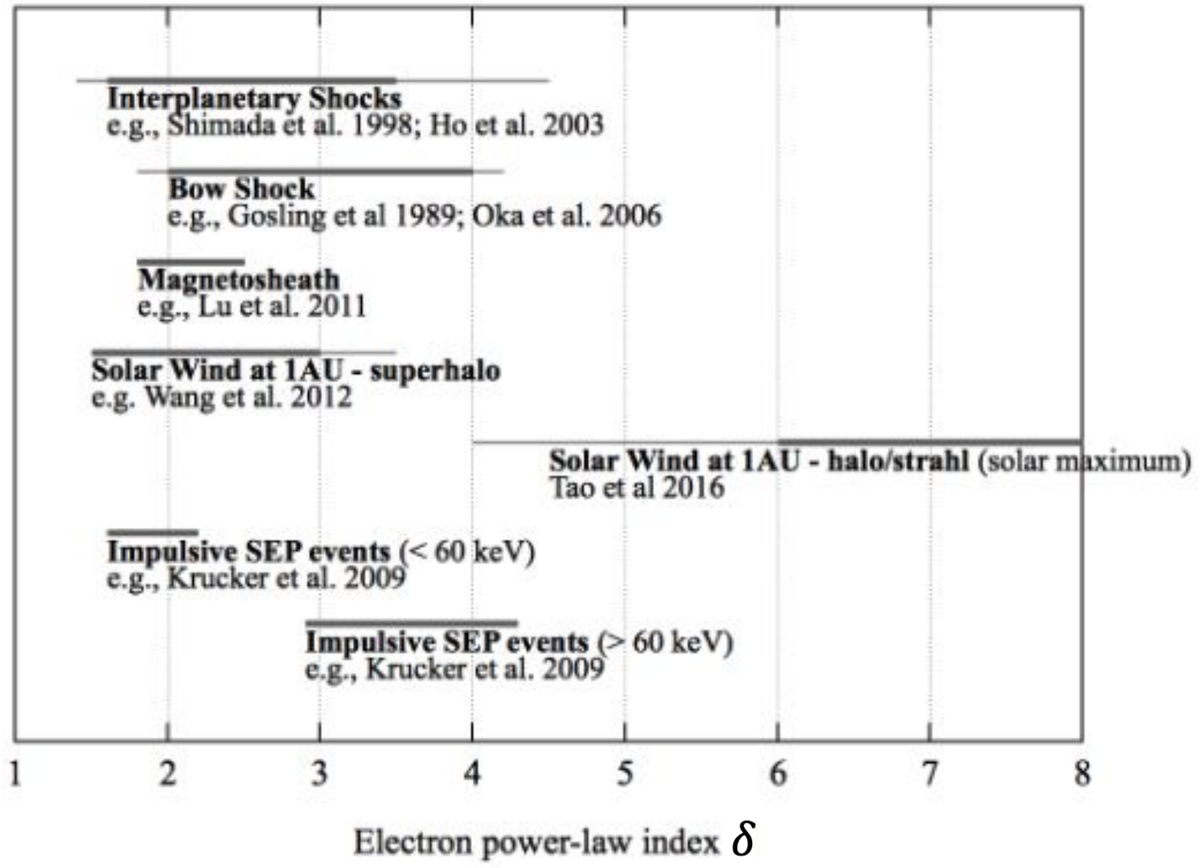

Wide range of value for the power-law index :

$$\mathbf{3 < \delta < 8}$$

Oka, M et al. (2018). *Space Science Reviews*.

$$p = A_p + B_p \tanh\left(C_p \beta\right), \qquad \beta < 0.1$$

$$A_p = 1.8 + \frac{0.7}{\sqrt{\sigma}},\ B_p = 3.7\sigma^{-0.19},\ C_p = 23.4\,\sigma^{0.26}$$

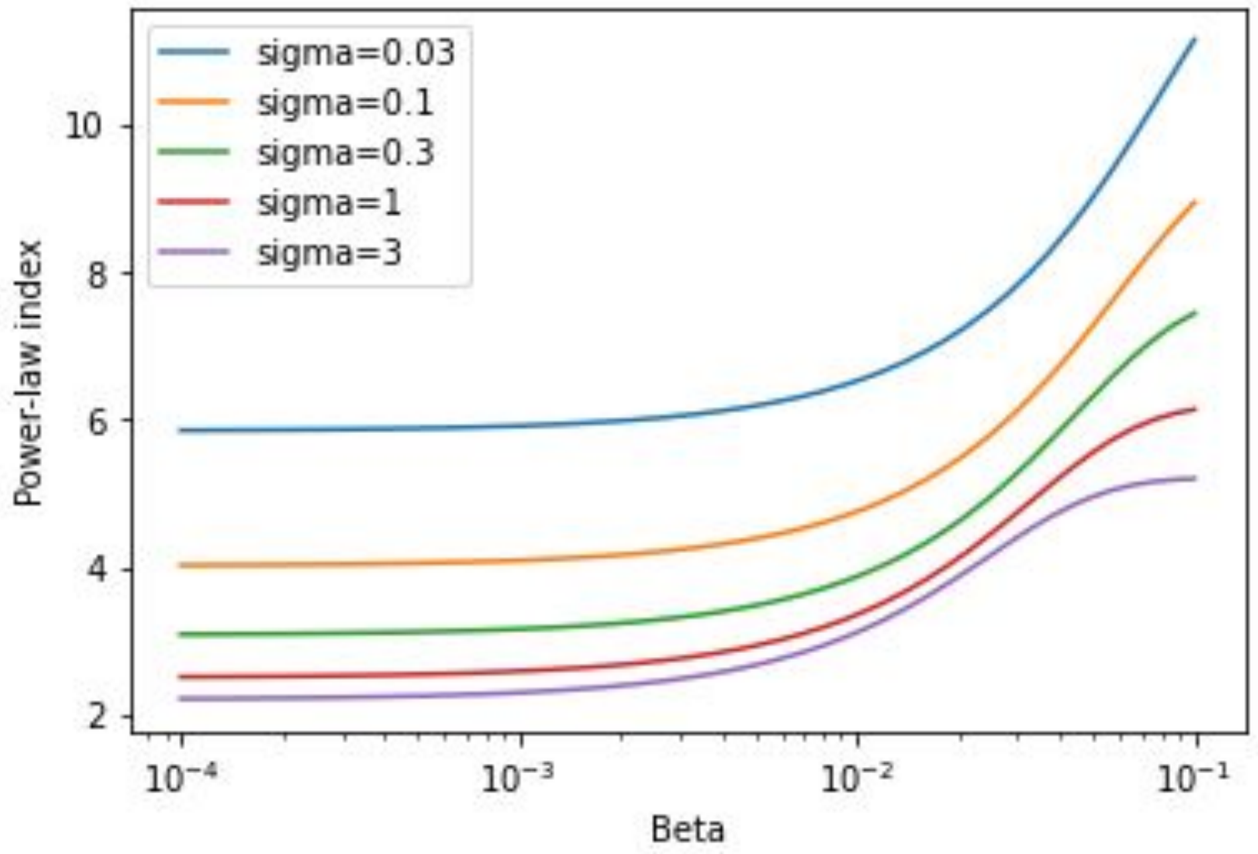

Ball, D., Sironi, L., & Özel, F. (2018). *The Astrophysical Journal*.

Parametric expression of the power-law index from **simulation** depending on :

$$\beta_i = \frac{8\pi n_i k_B T_i}{B_0^2} \quad \text{and}$$

$$\sigma = \frac{B_0^2}{4\pi n_i m_i c^2}. \quad \text{i=e,p}$$

$$\delta = A_p(\sigma) + B_p(\sigma)\tanh\left(C_p\beta\right), \beta < 0.1$$

Parametric expression of the power-law index from **simulation** depending on :

$$\beta_i = \frac{8\pi n_i k_B T_i}{B_0^2}$$ and

$$\sigma = \frac{B_0^2}{4\pi n_i m_i c^2}.$$ i=e,p

Ball, D., Sironi, L., & Özel, F. (2018). *The Astrophysical Journal*.

Toroidal Magnetic Configurations

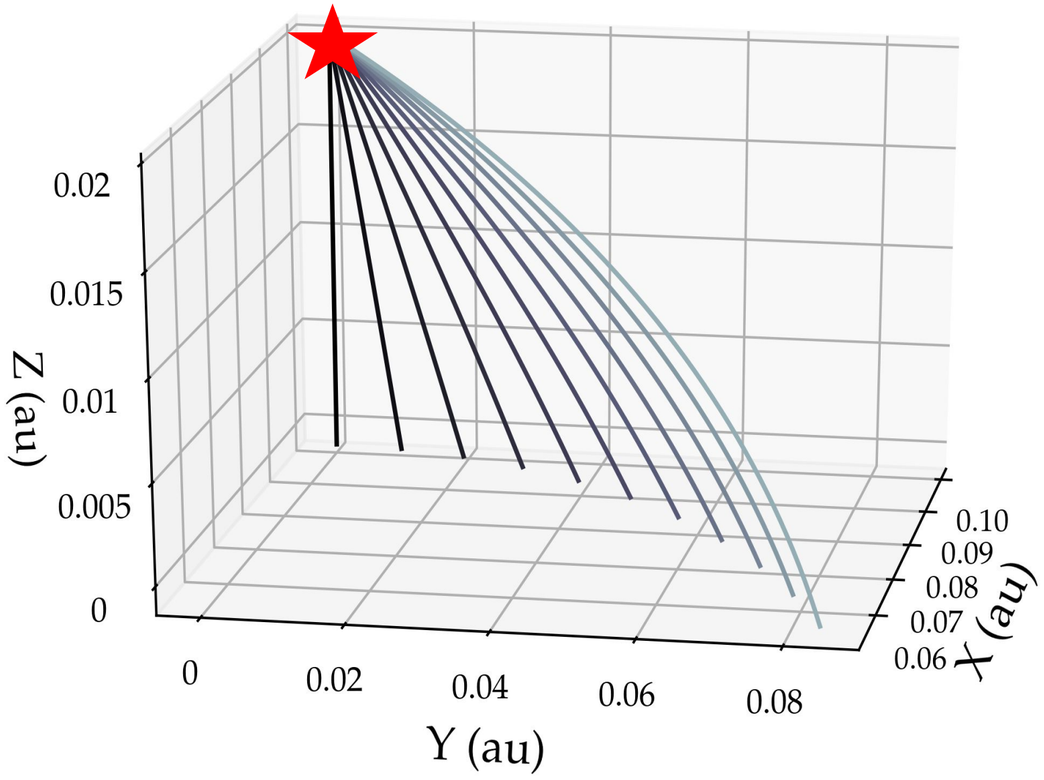

$$b_g = \frac{B_\phi}{B_z}, \qquad 0 < b_g < 1$$

Particles acceleration is reduced by the **toroïdal component** of the reconnecting fields :

$$\delta \approx 2.5 + 4\, b_g^2$$

Arnold et al. 2021

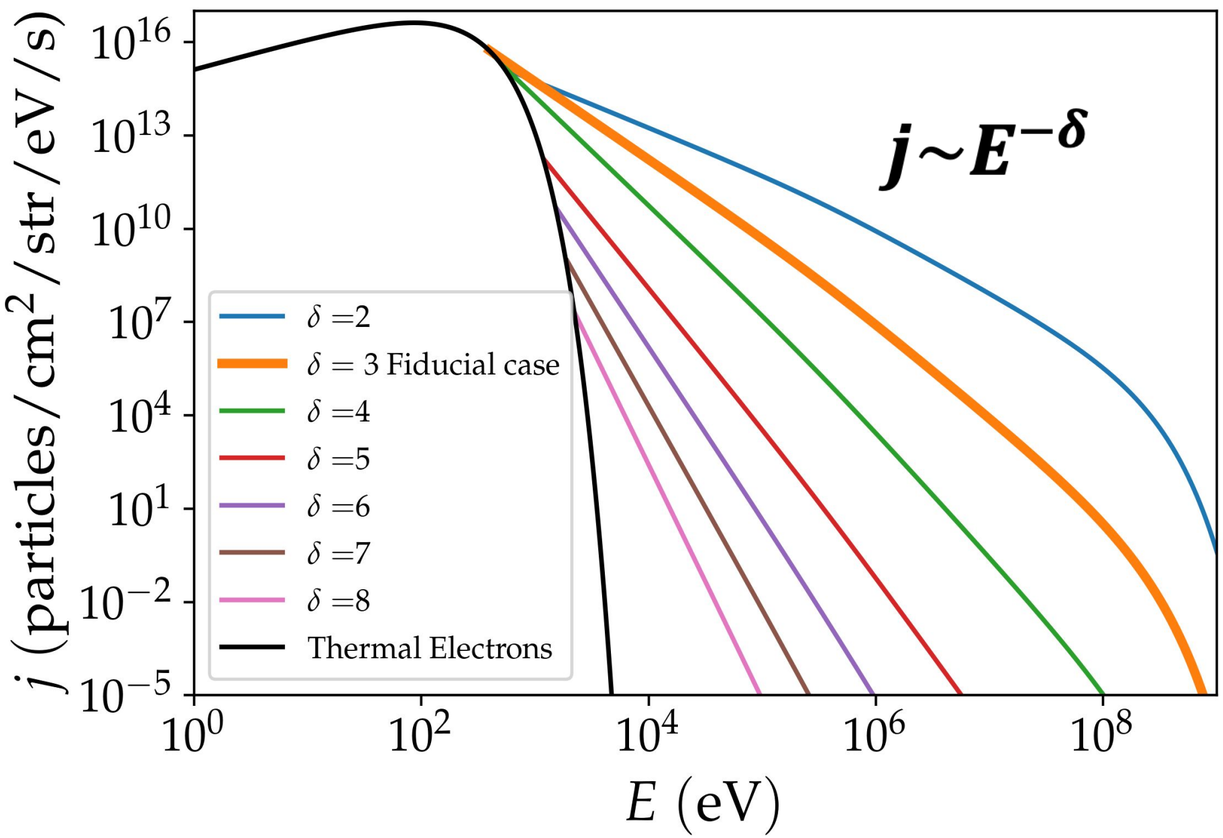

Each spectrum injects the **same amount** of **energy**

The total energy is **regulated** by the **injection energy** of non thermal particles

Mean Loss function

$$\bar{L}(E,s) = \sum_i f_i(s)\, L_i(E) \quad i = H, H_2, He$$

$$f_i = \frac{1}{s}\int_0^s \frac{n_i(s')}{n_{tot}(s')}\, ds'$$

We build a mean loss function at **each position**

Mean Loss function

$$\bar{L}(E,s) = \sum_i f_i(s)\, L_i(E) \quad i = H, H_2, He$$

$$f_i = \frac{1}{s}\int_0^s \frac{dN_i}{dN_{tot}} ds' = \frac{1}{s}\int_0^s \frac{n_i(s')}{n_{tot}(s')} ds'$$

We build a mean loss function at each position

Mean Loss function

$$\bar{L}(E,s) = \sum_i f_i(s)\, L_i(E)$$

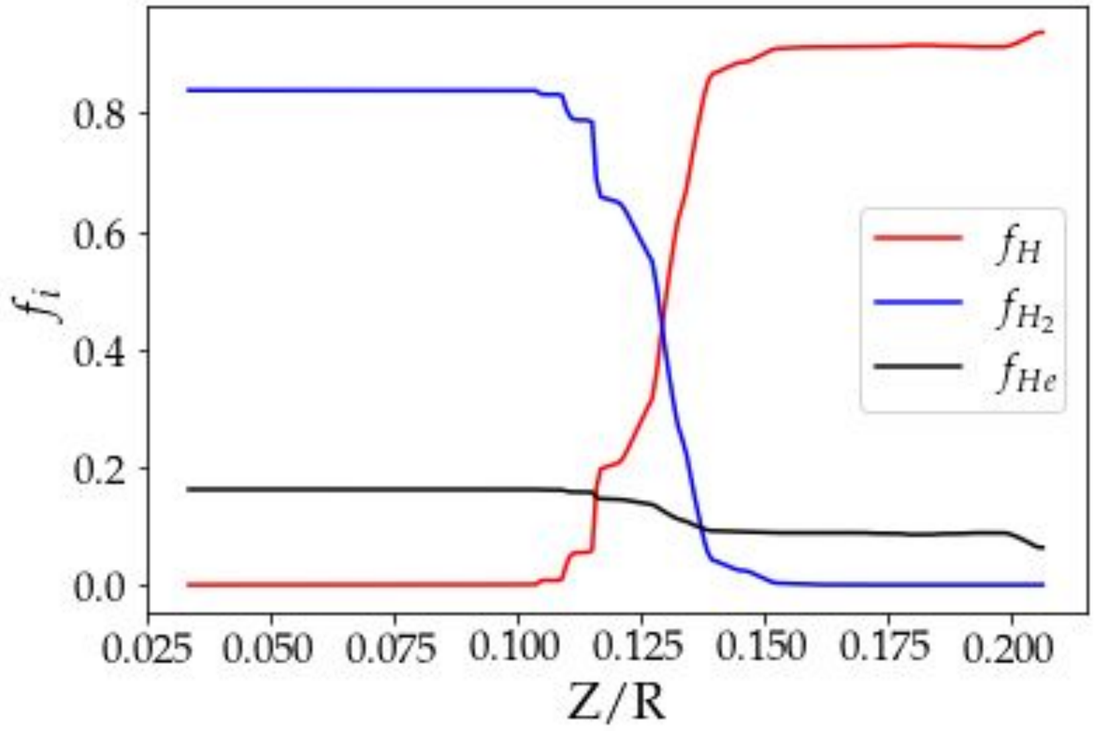

Two regions:

-Atomic hydogen dominated
-Molecular hydogen dominated

Expression of final energy E as a function of initial energy E_0 for a column density $N = 6{\times}10^{23}\ cm^{-2}$.

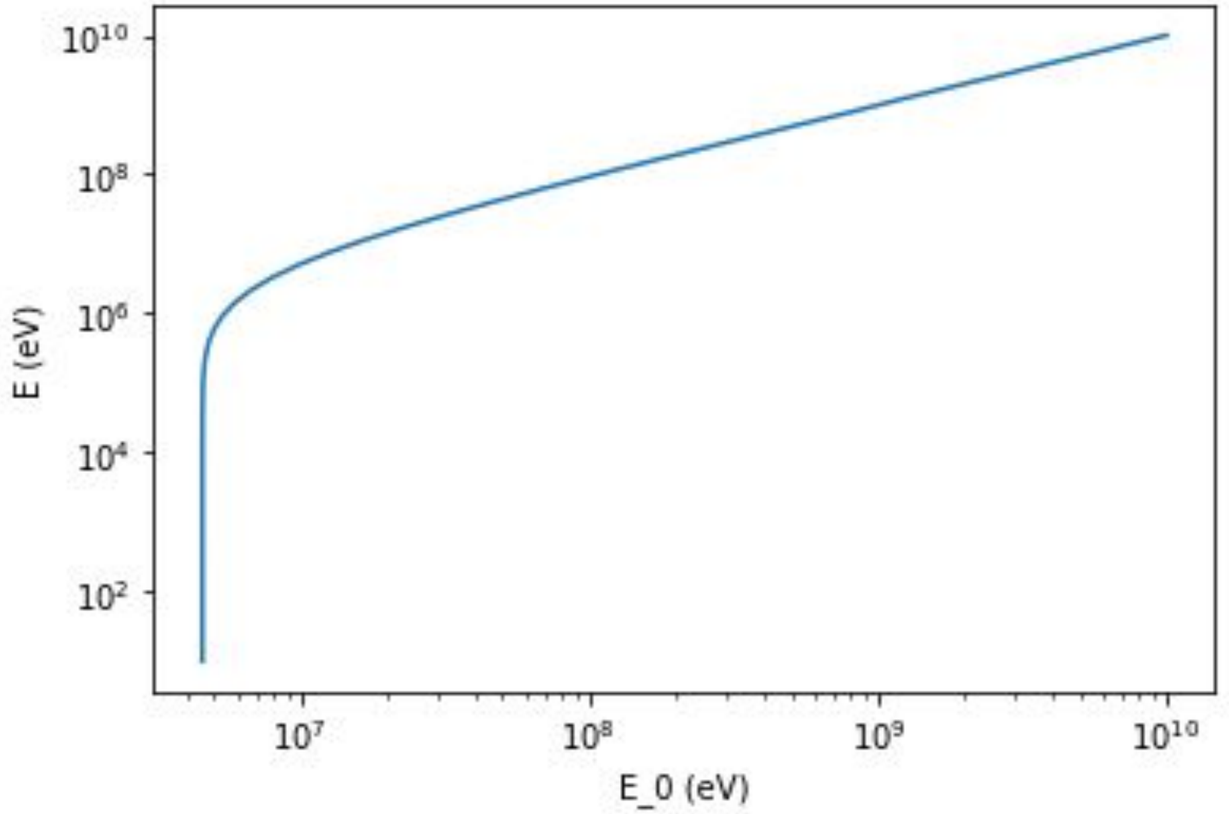

$$j(E,N) = j(E_0)\frac{L(E_0)}{L(E)}$$

Relation between $\boldsymbol{E}$ and $\boldsymbol{E_0}$ is found by solving :

$$\frac{dE}{dN} = -L(E)$$

$$\int_{E}^{E_0} \frac{dE}{L(E)} = \int_{0}^{s} n(s')ds' = N$$

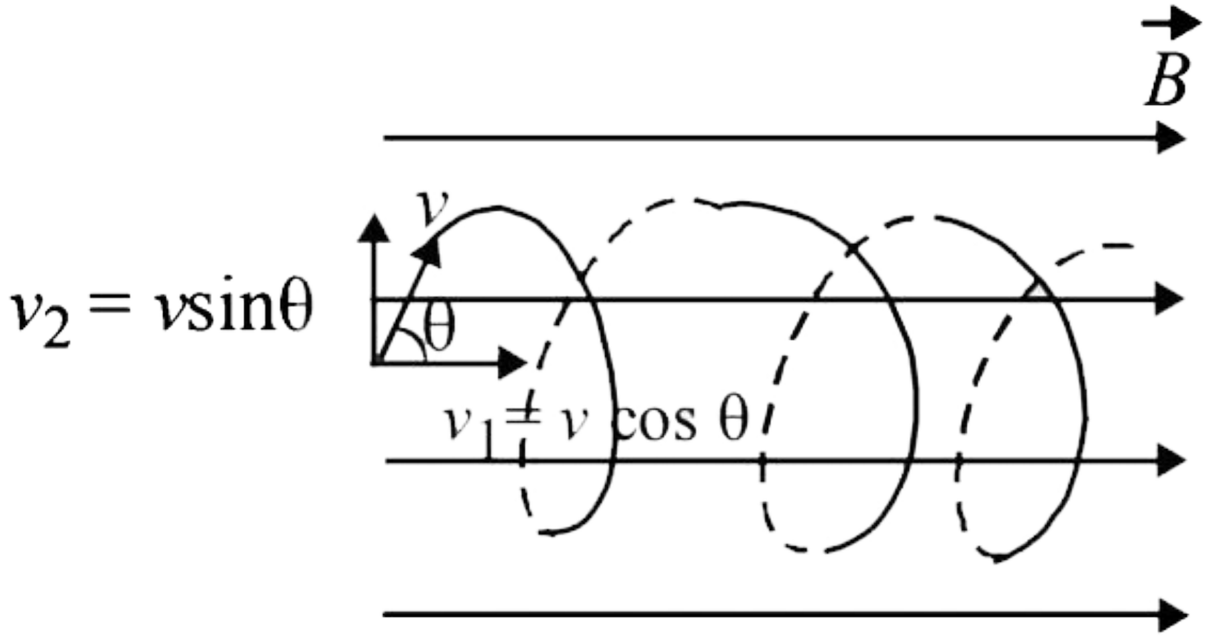

Particle's **trajectory** depends on initial **pitch angle**

$$j(E) = \int_0^{\pi/2} j(E,\theta)\sin(\theta)\,d\theta$$

Spectra have to be **summed** over pitch angles

Ionisation rate

$$\zeta(N) = 2\pi \int \boldsymbol{j(E,N)}\big(1 + \phi(E)\big)\sigma_{ion}(E)dE$$

$j(E,N)$: propagated flux

N: effective column density

σ_{ion}: ionisation cross section

L: loss fuction

ϕ: secondary electrons

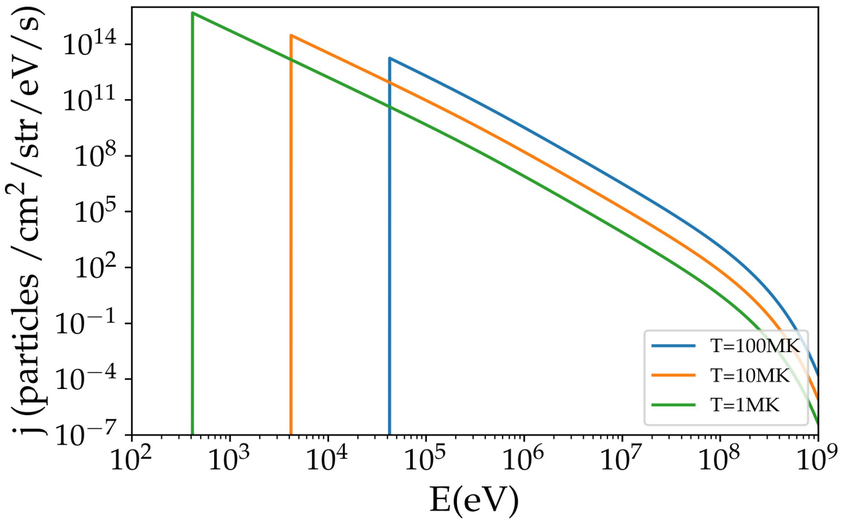

Hotter flare, higher ionisation rate

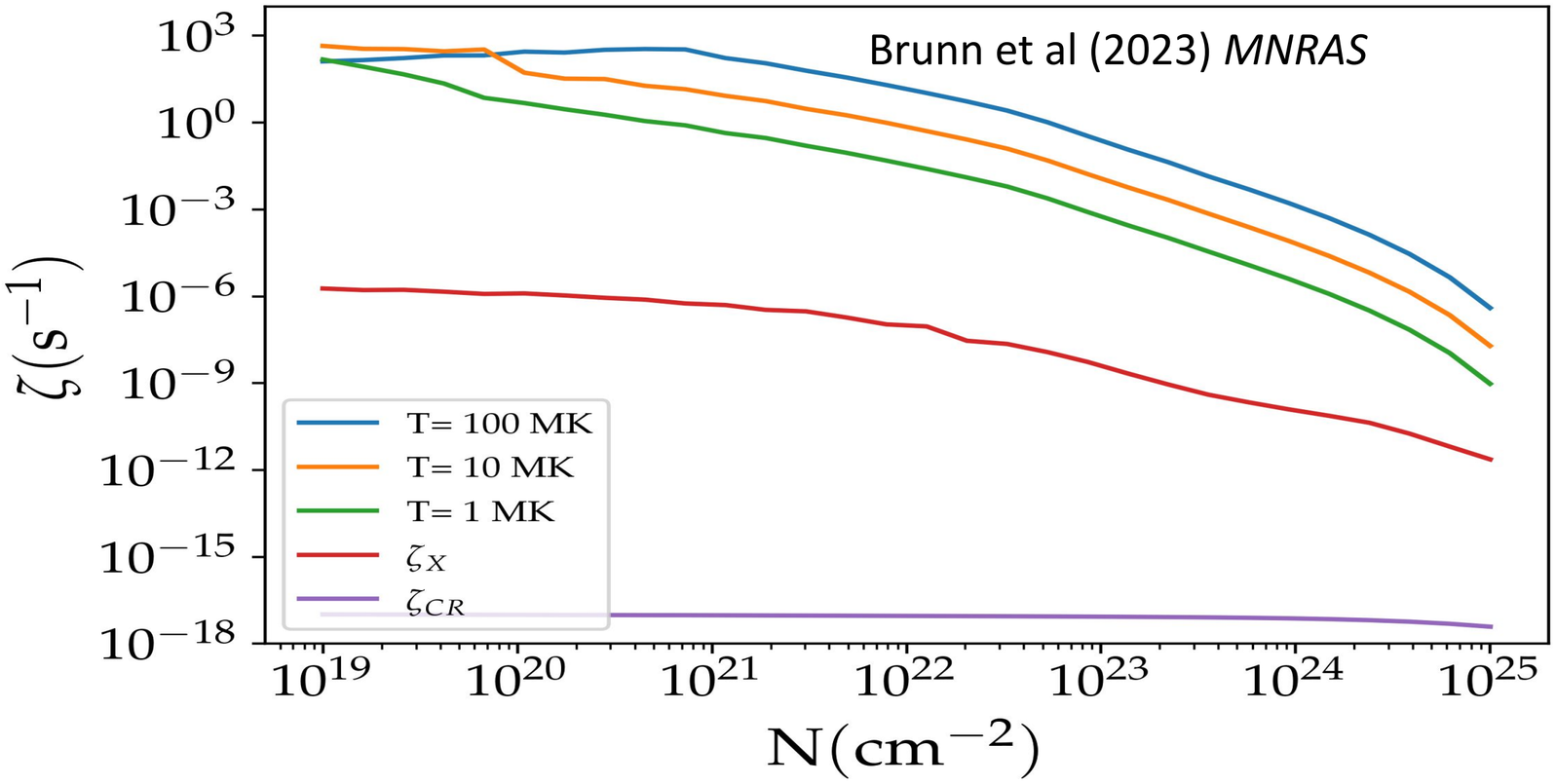

Even **weak flares** are a **dominant** source of **ionisation**

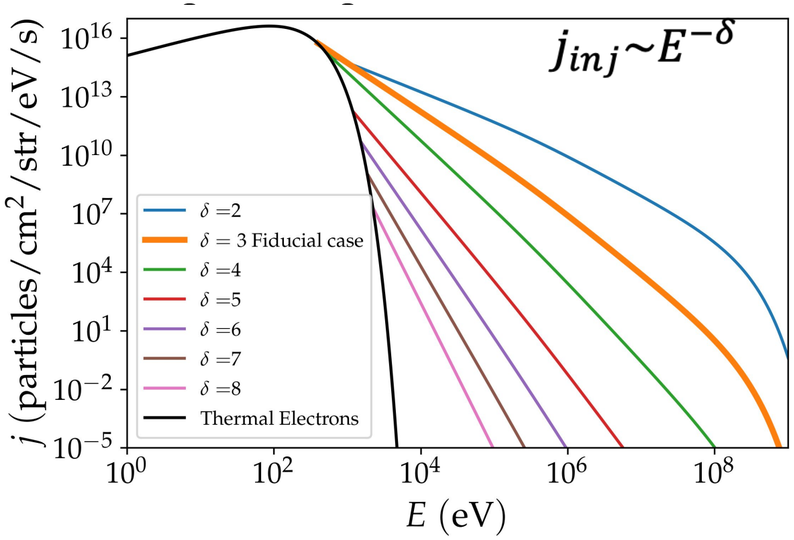

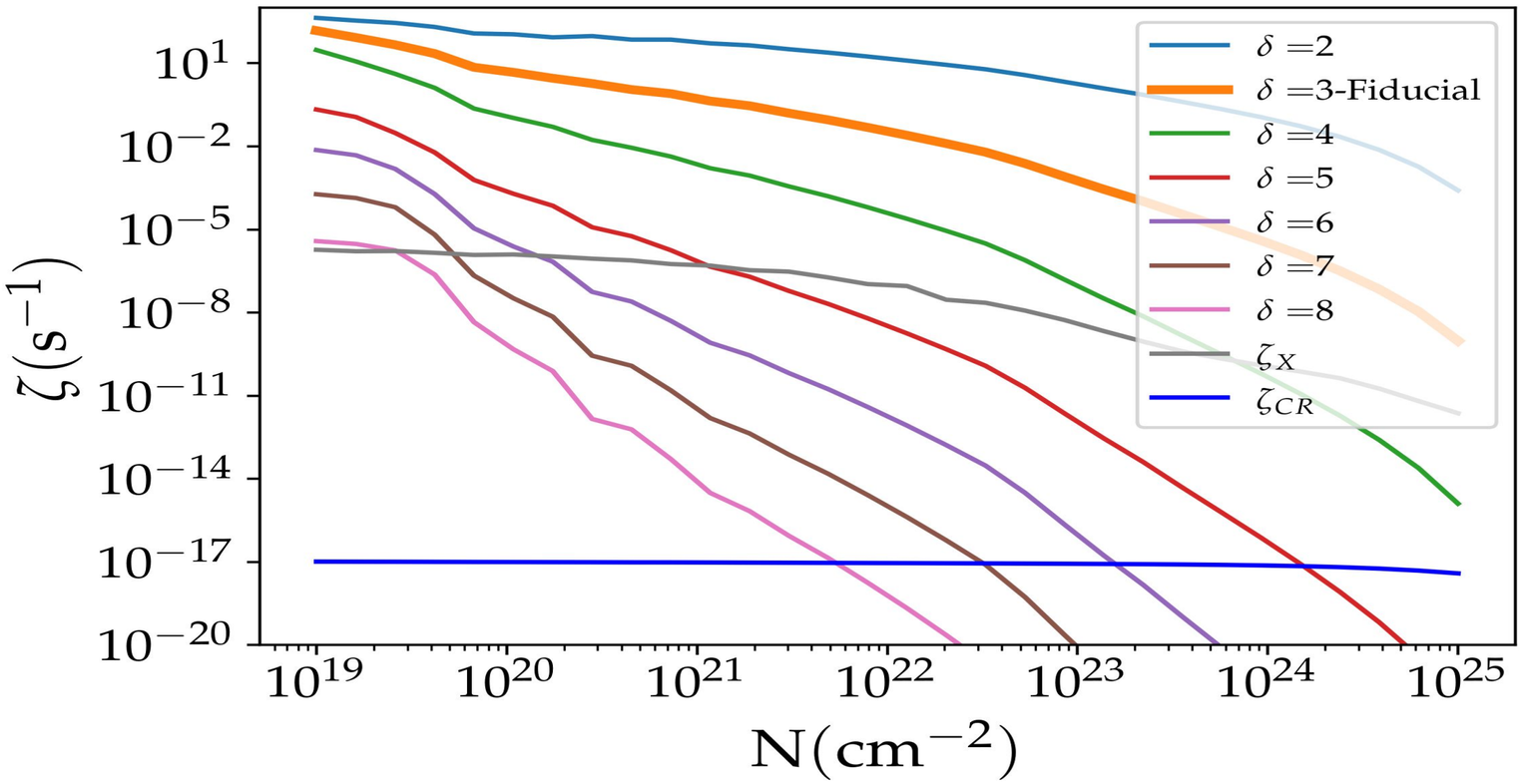

Lower index, higher ionisation rate

Dominant source of ionisation for $\boldsymbol{\delta < 5}$

Monte-Carlo Analysis

Luminosity distribution

Duration distribution

PMS Observations (Getman 2021)

Waiting time distribution

Solar Observations (Aschwanden 2010)

Position of occurence

Based on loop size

Monte-Carlo Analysis

Luminosity distribution → Power-law

Duration distribution → Poissonian

Power-law, Poissonian → PMS Observations

Waiting time distribution → Pareto II → Solar Observations

Position of occurence → Derived from luminosity and duration distribution

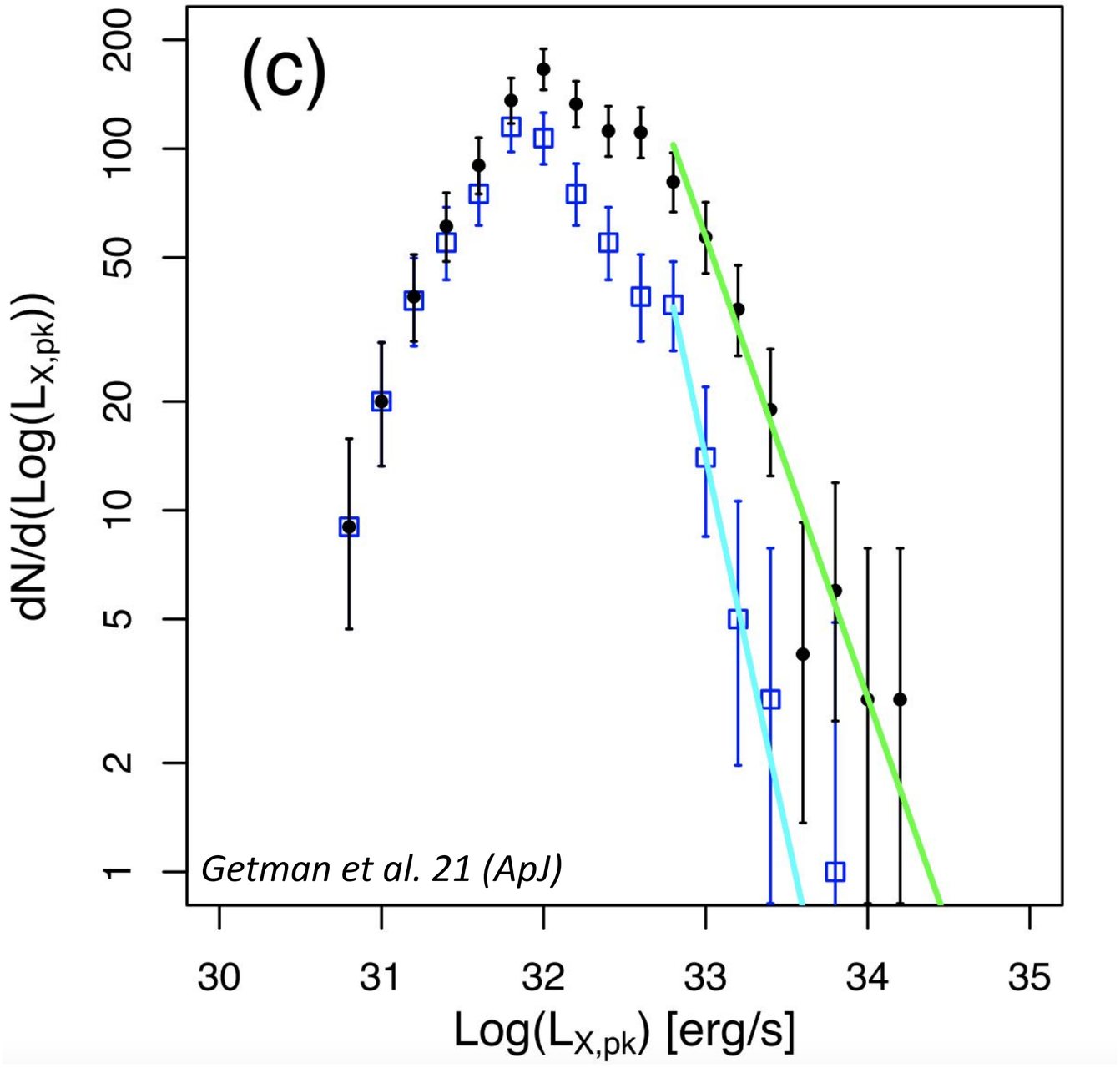

Luminosity distribution

X ray observations from CHANDRA

Sample of more than 20 000 PMS of 40 star forming regions

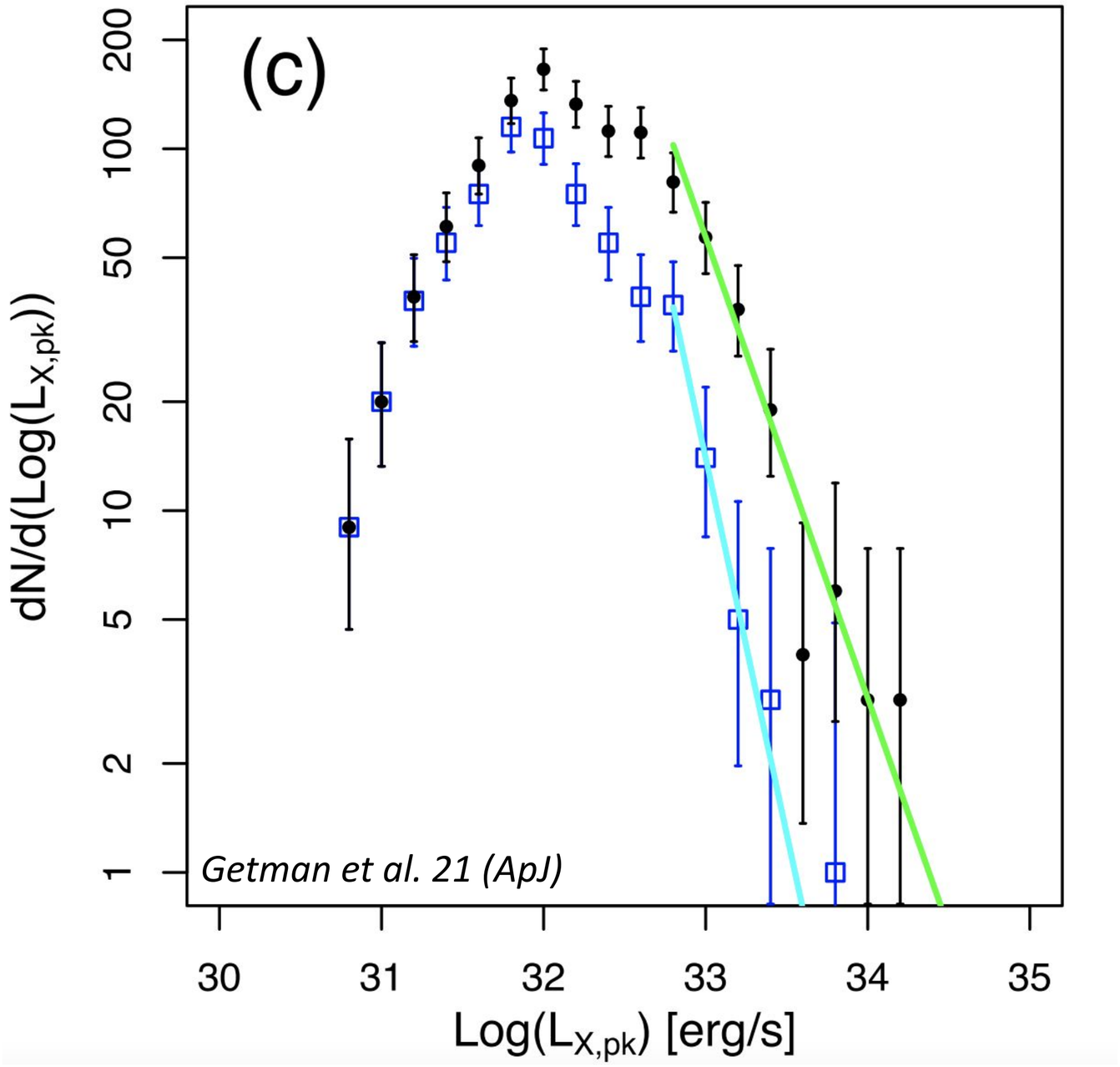

Luminosity Distribution

Power law distribution :

$$\frac{dN}{dL} \propto L^{-2.11}$$

Index consistant with index in the **Sun** at lower luminosity:

$L \sim 10^{24} - 10^{29}\ erg\ s^{-1}$

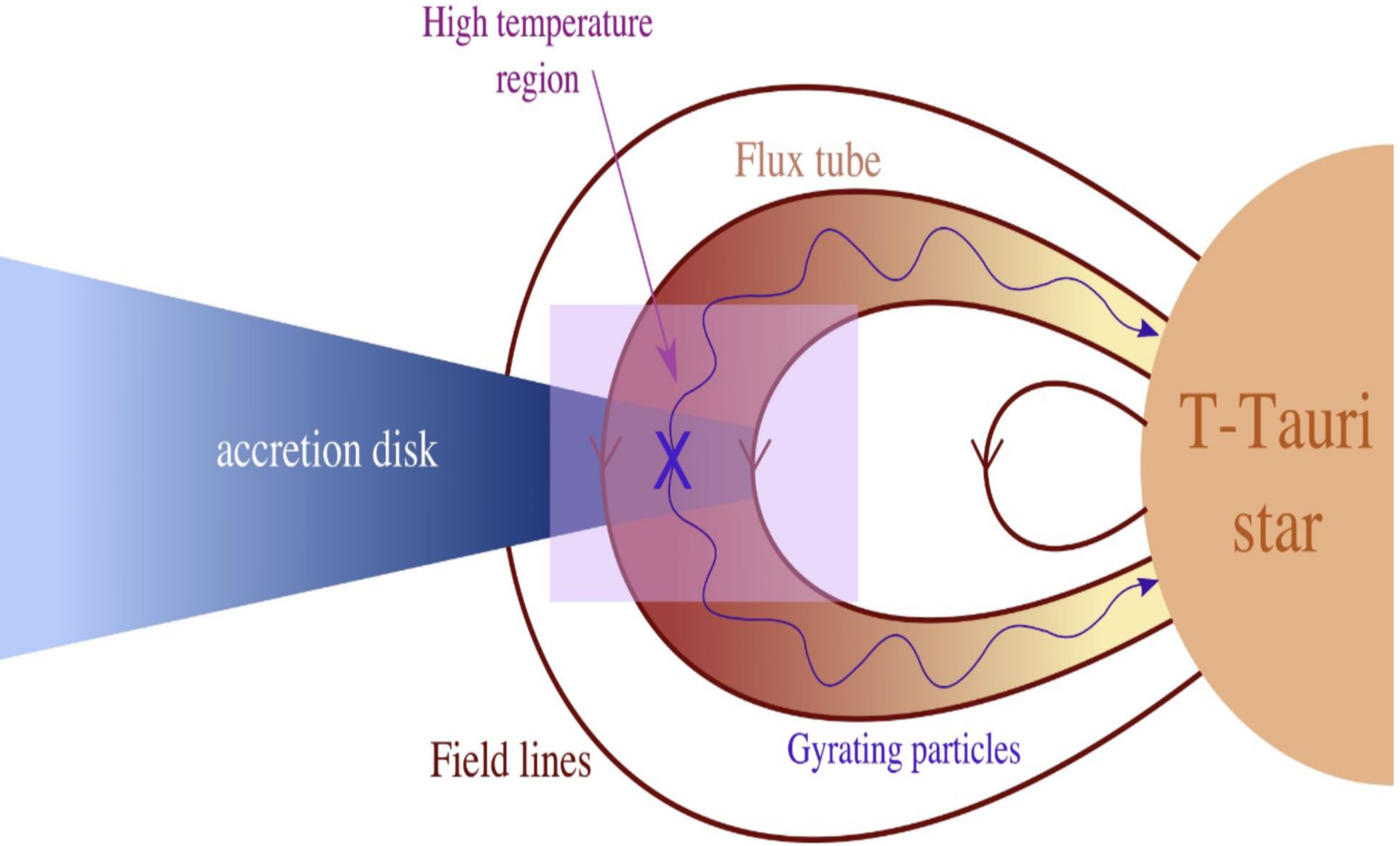

Position of occurrence

$$R_f = \frac{\tau_d T^{1/2}}{\alpha}$$

τ_d: Picked from observed distribution

$T = T(L_X)$ is derived from the luminosity distribution

C. O. G. Waterfall et al. (2020)

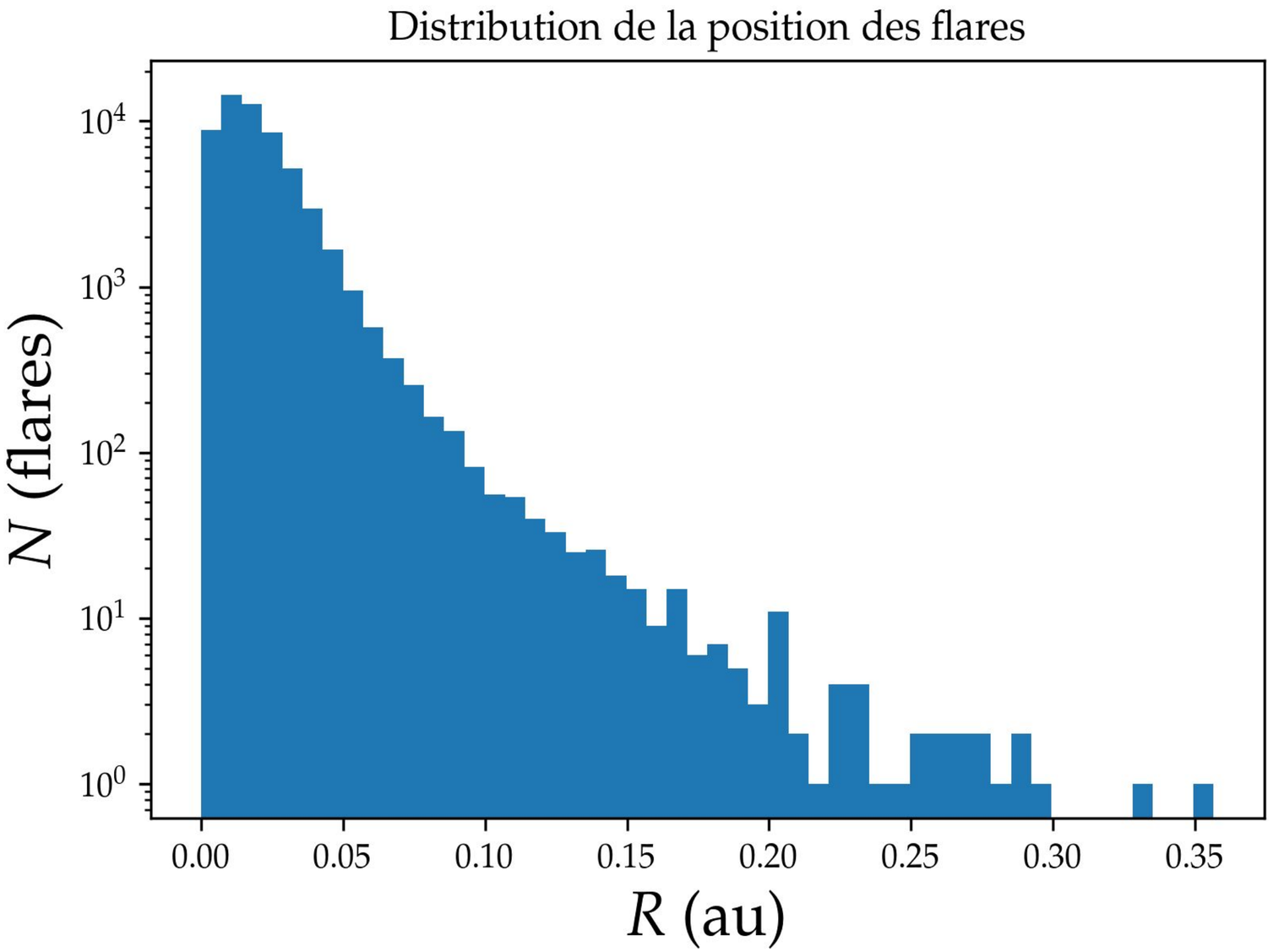

Position of occurrence

$$R_f = \frac{\tau_d T^{1/2}}{\alpha}$$

Less luminous flares are more frequent and doesn't reach the disc

Some very srong flares reach radii $> 0.2\ au$.

Top view of the disc

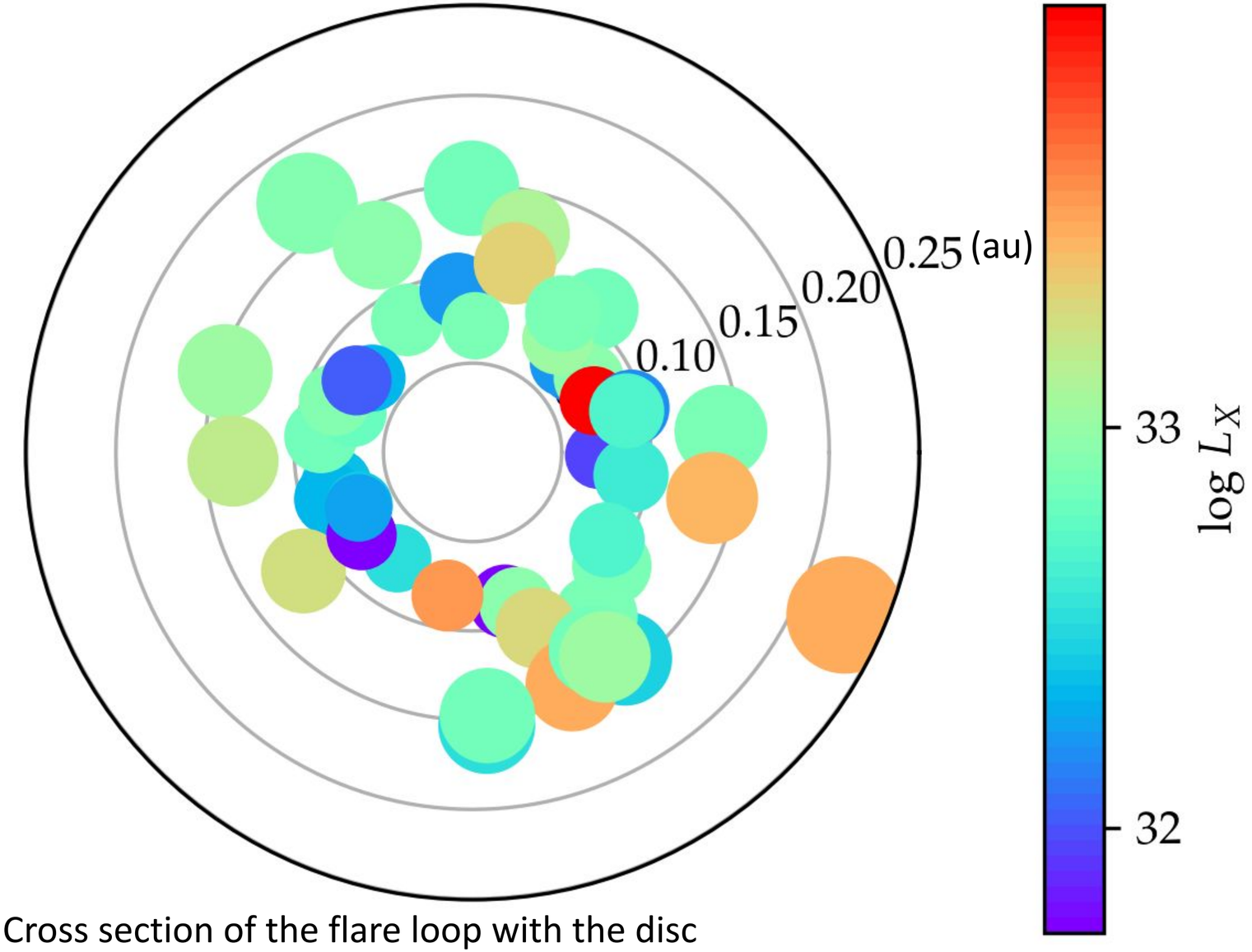

Cross section of the flare loop with the disc

Modelisation of the flaring activity over 10 years :

-position
-luminosity
-area in contact with the disc

$A = \beta^2 L_f^2$ ($\beta \approx 0.1$)

Alternative Position Distribution

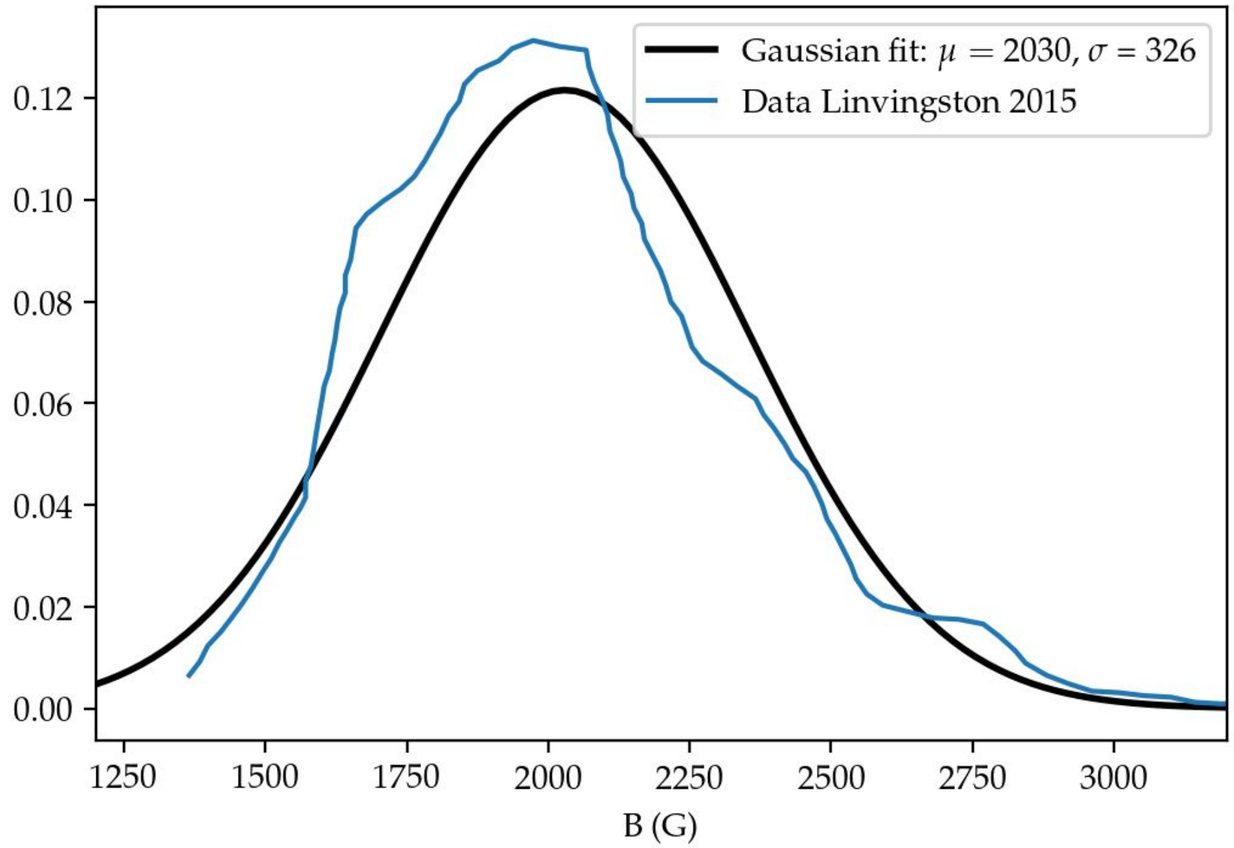

MRI active region

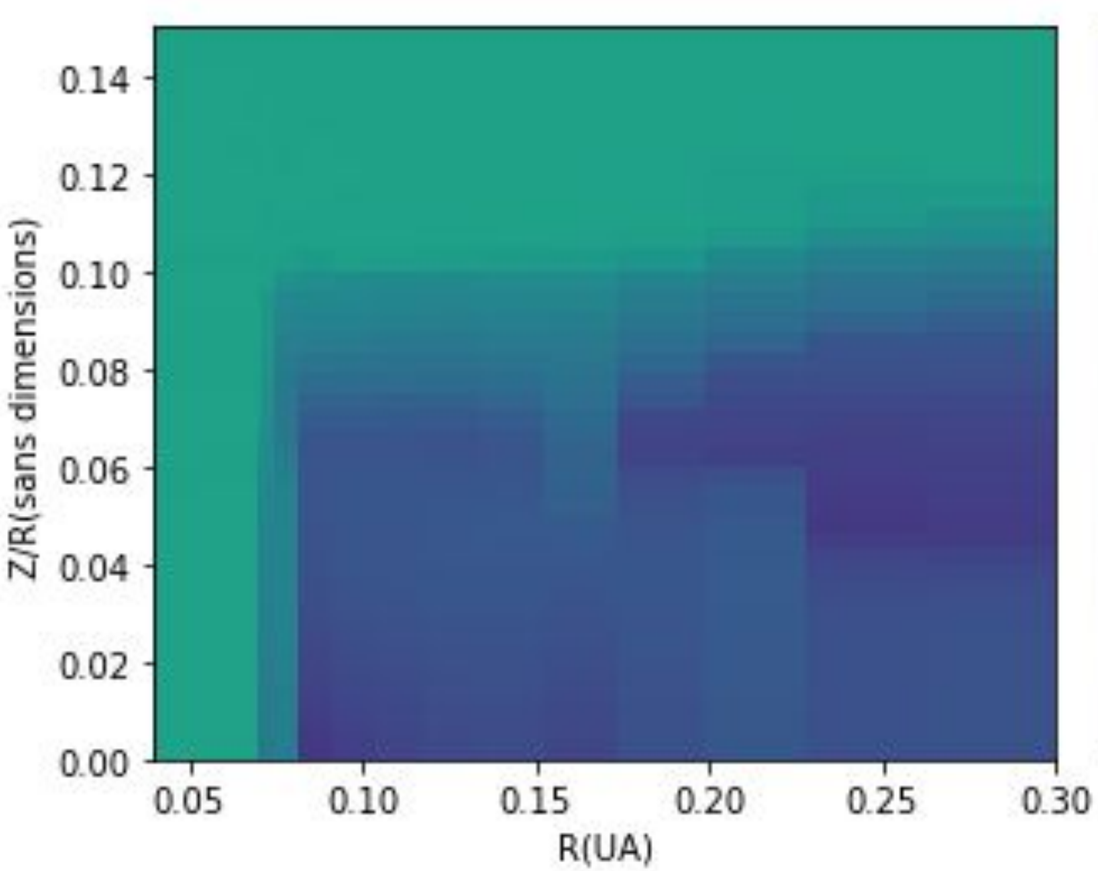

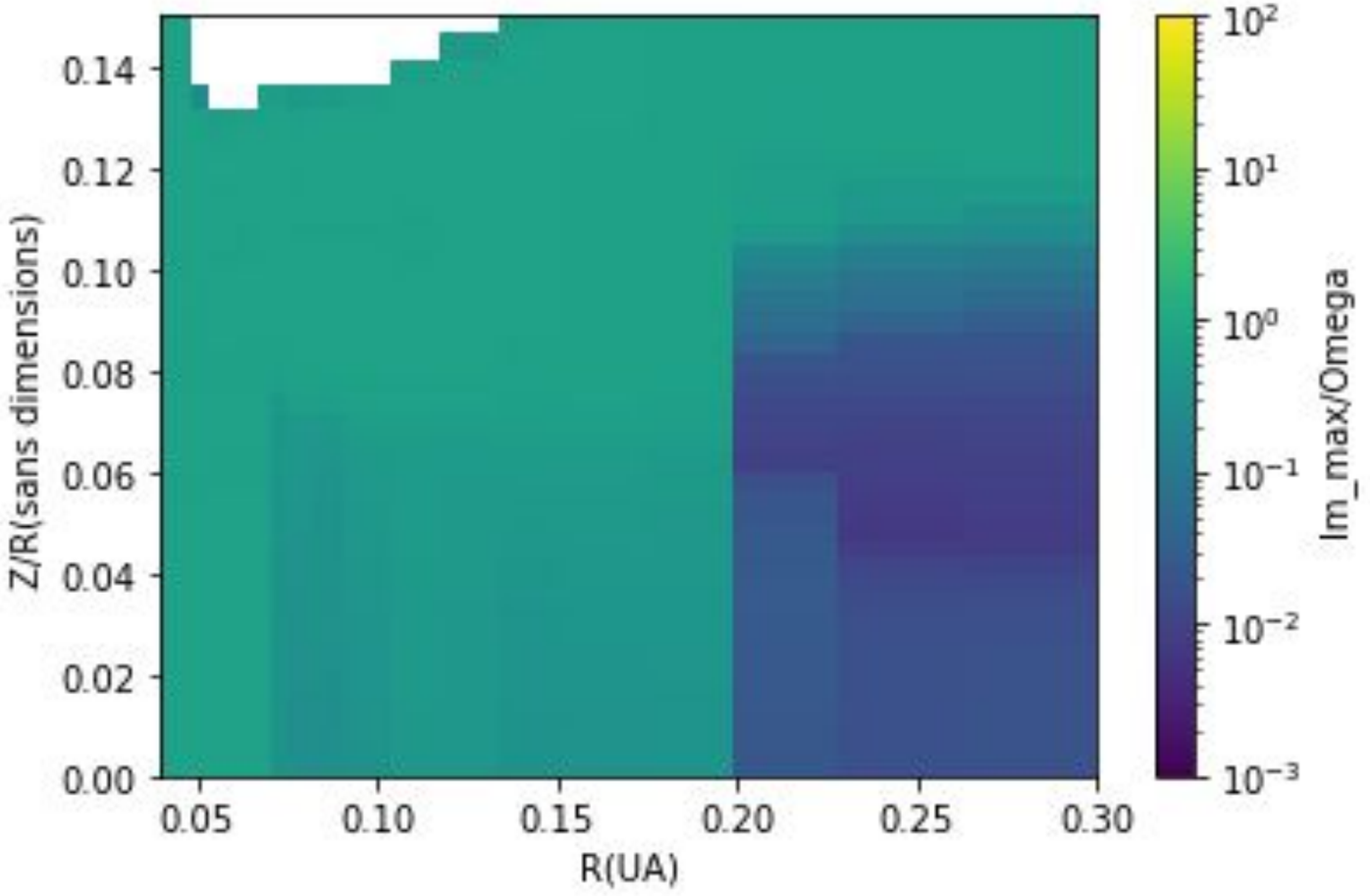

Temporal evolution of the flare luminosity

(Getman 2021)

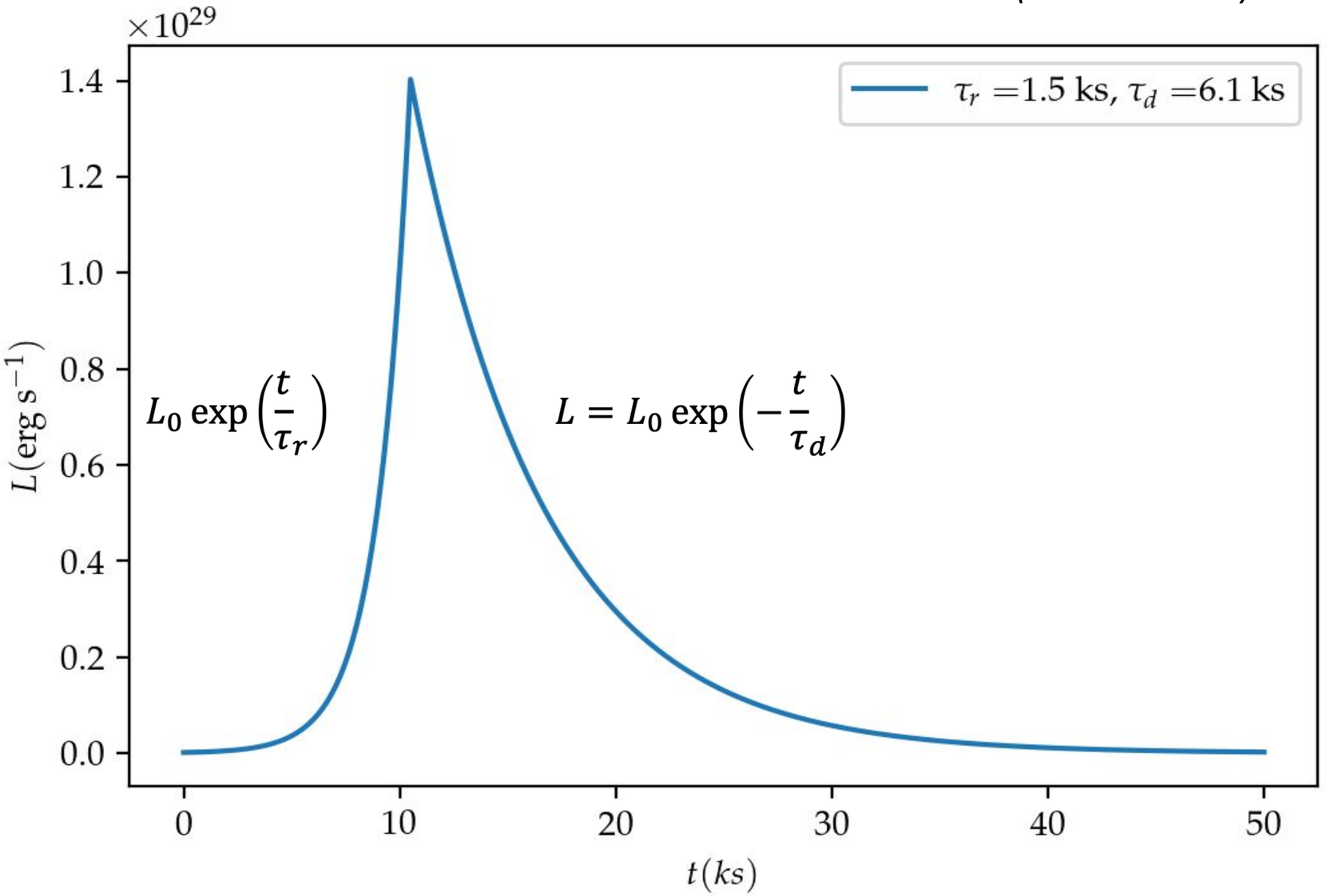

Exponential rise and decay of the luminosity

Poissonian distribution for τ_r with mean value : $\lambda = 26\ ks$

Correlation between rise and decay time:

$$\tau_d \approx 5\,\tau_r^{0.5}$$

Rate equation for electron density

$$\frac{dn_e}{dt} = \zeta(t) n_n - \beta(T) n_e n_{m^+}$$

$\zeta(t)$:ionisation rate

$\beta(T)$: recombination rate

n_e: electron density

n_{m^+}: ion density

Initial conditions are fixed by ProDiMo

Electron density at different deepness as function of time

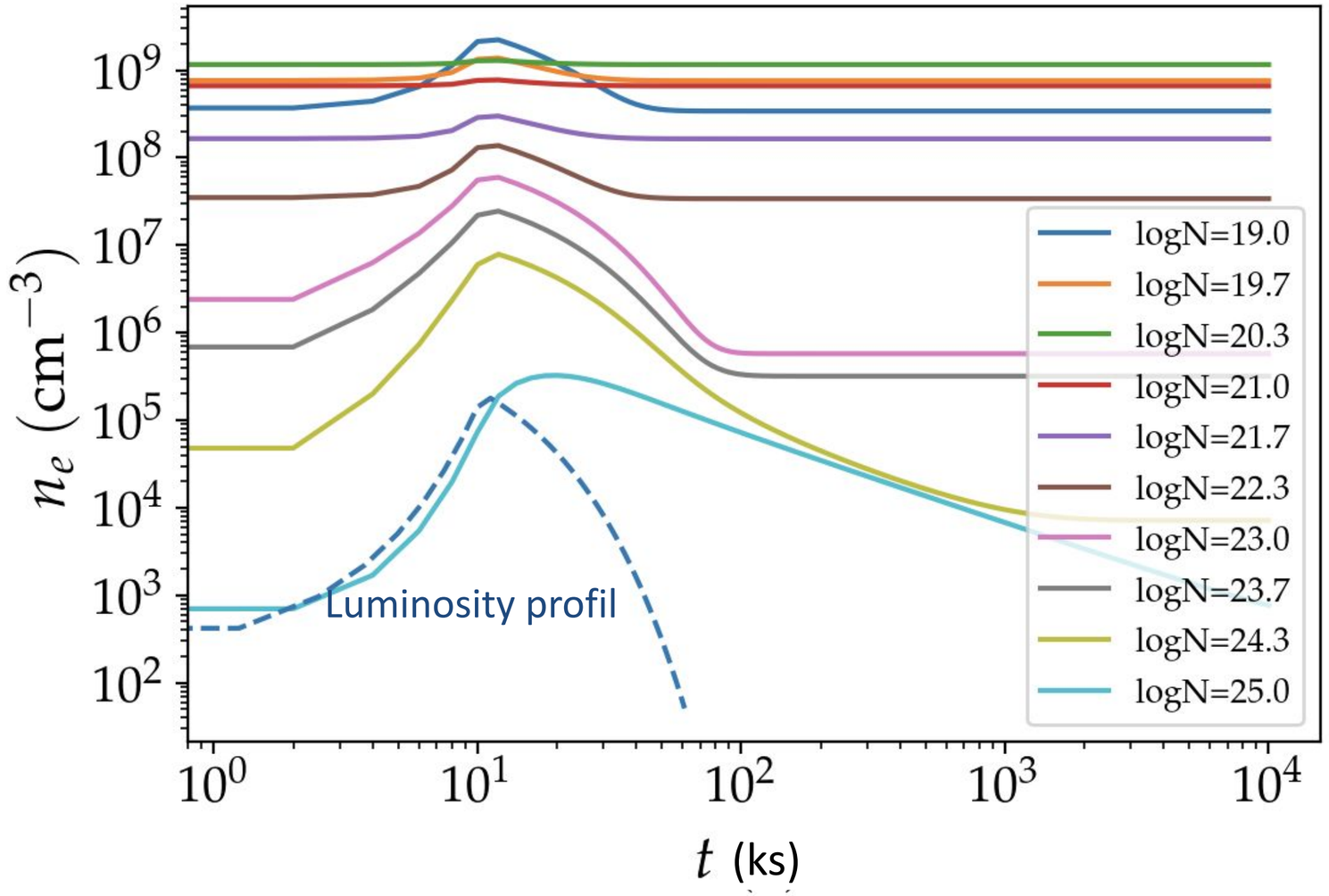

$N < 10^{24} cm^{-2}$:

Electron density profil stick to the luminosity profil

Increase of density of **1 order** of magnitude max

Electron density at different deepness as function of time

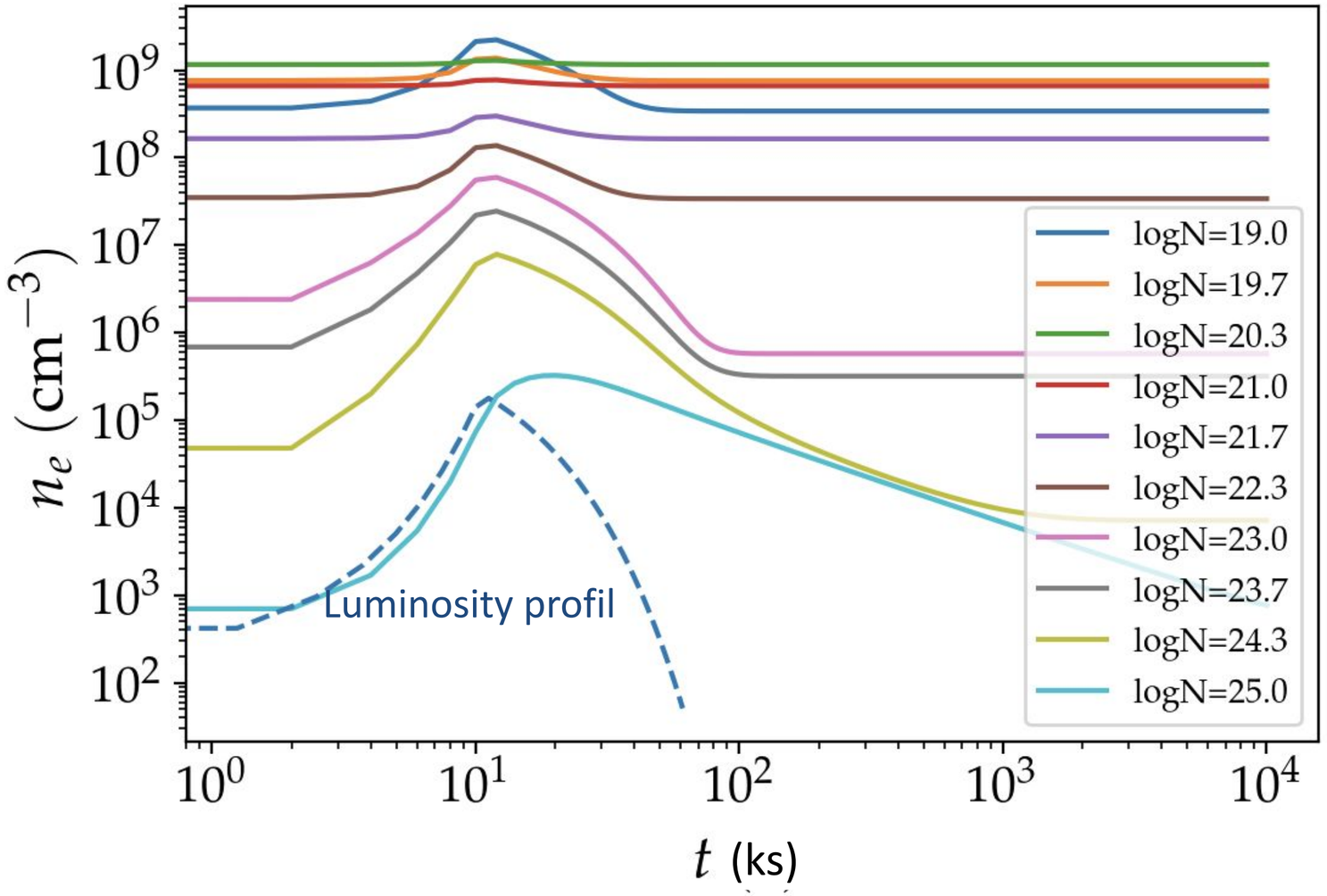

$N > 10^{24} cm^{-2}$:

Recombination time is longer due to low temperature

Increase of density of **3 orders** of magnitude

Waiting time between two solar flares

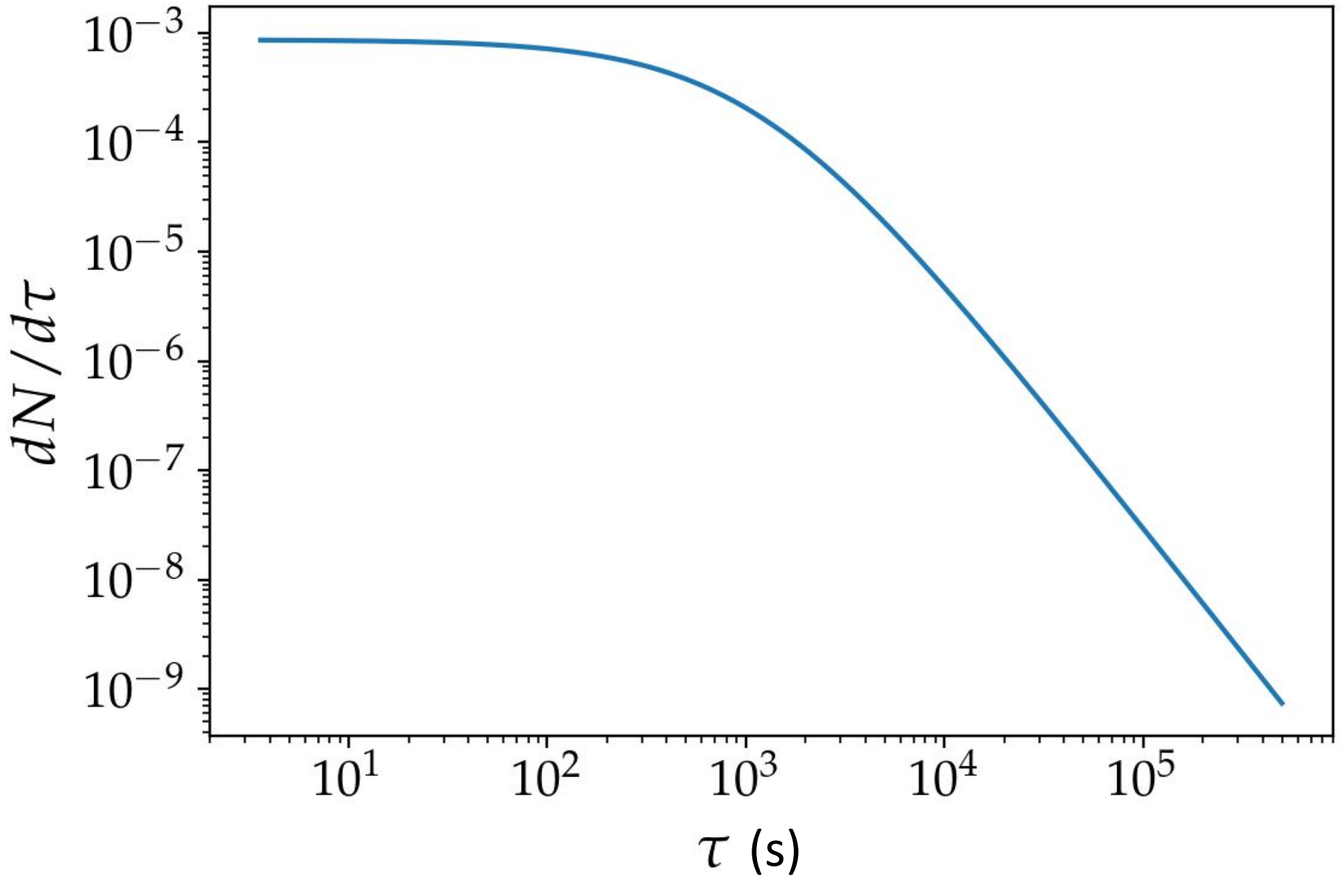

$$\frac{dN}{d\tau} = \lambda_0(1+\lambda_0\tau)^{2.3}, \qquad 1/\lambda_0 = 0.8\ h$$

Aschwanden et al. 2010

Data are from **solar** flares

We assume the **same distribution** for **T Tauri** stars

Luminosity Distribution of Flares from PMS

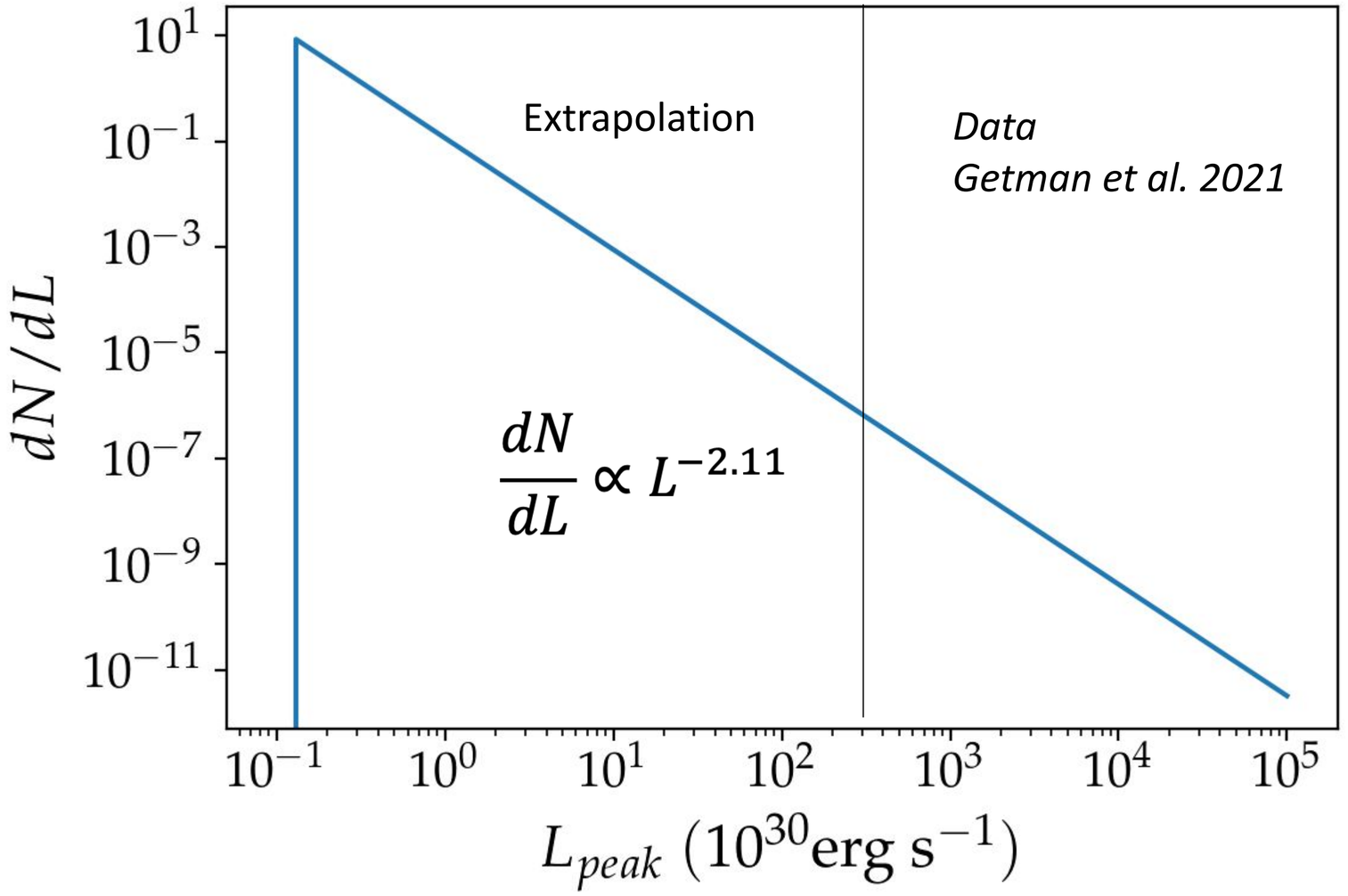

Data for
$L > 10^{32.5}\mathrm{erg\ s^{-1}}$

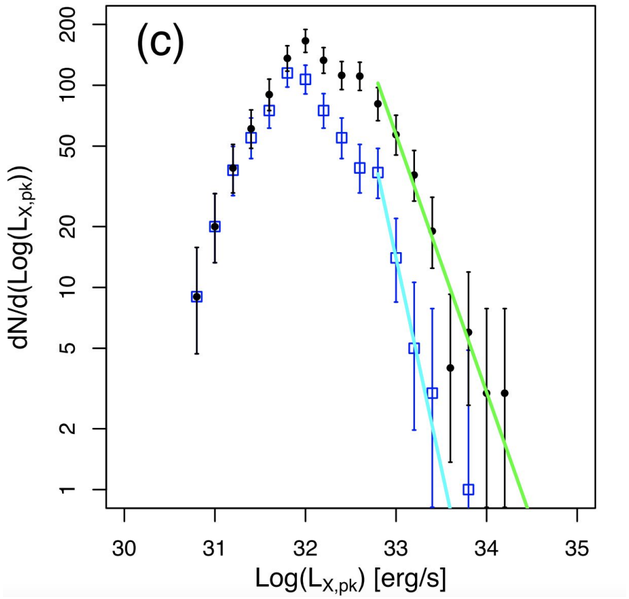

Extrapolation for
$L < 10^{32.5}\mathrm{erg\ s^{-1}}$

Modelisation of the X ray luminosity of the flares of a PMS

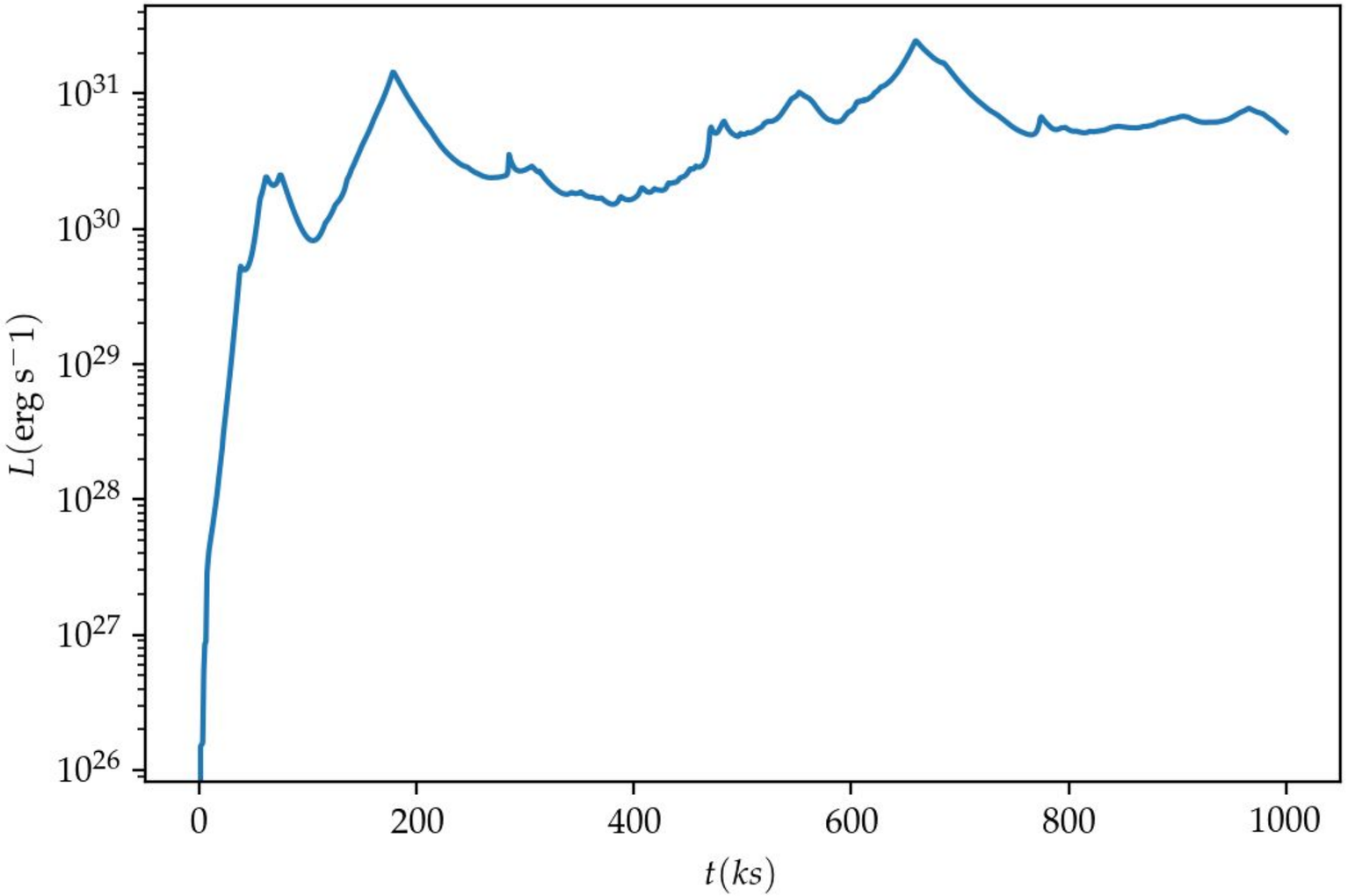

Parameters are chosen randomely according to their **observed distributions**

Energetic particles affect the observational tracers in discs

Synthetic JWST spectra

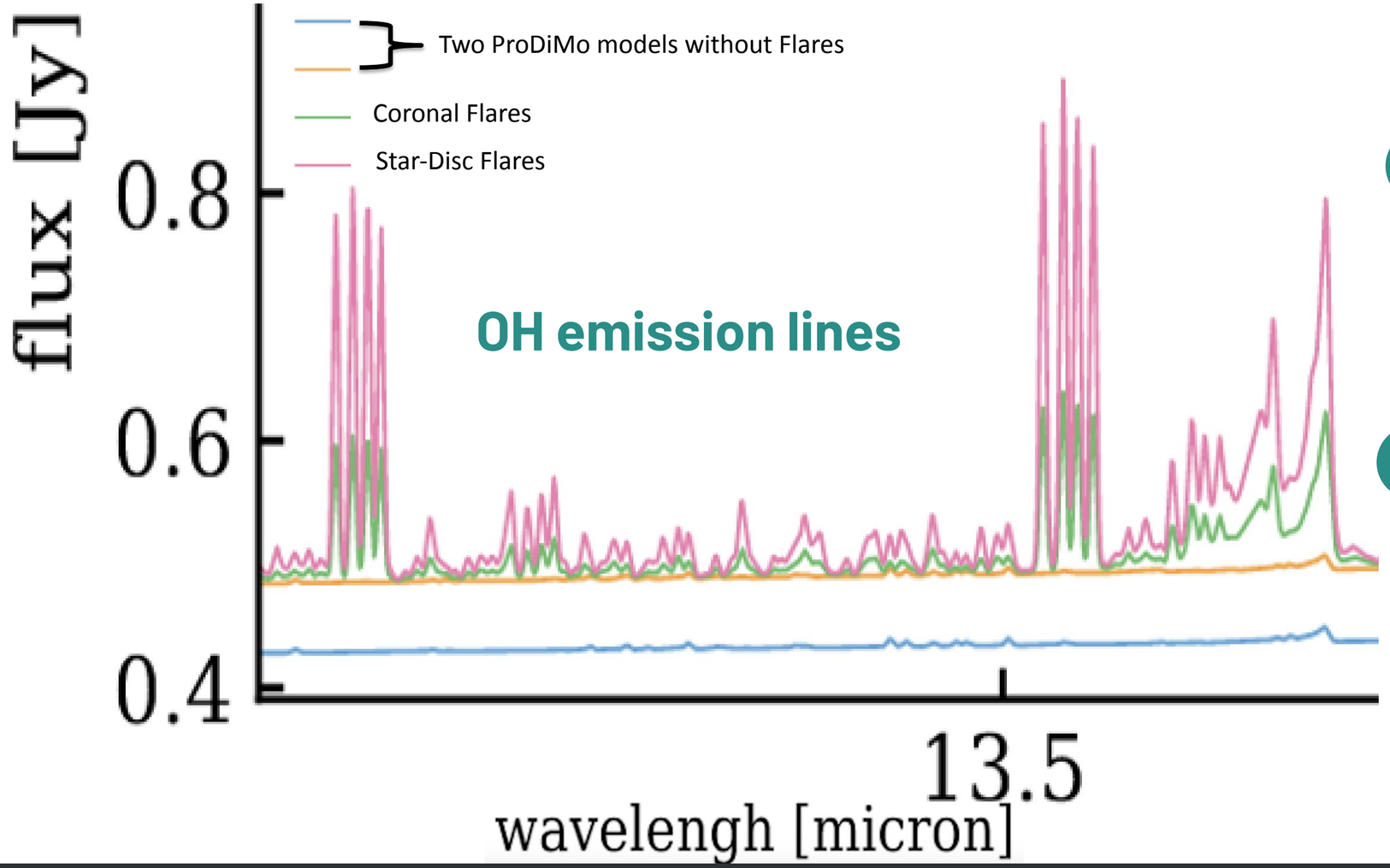

- The CO and OH emission lines are very sensitive to EP
- In the future we will use JWST spectra to constrain our model

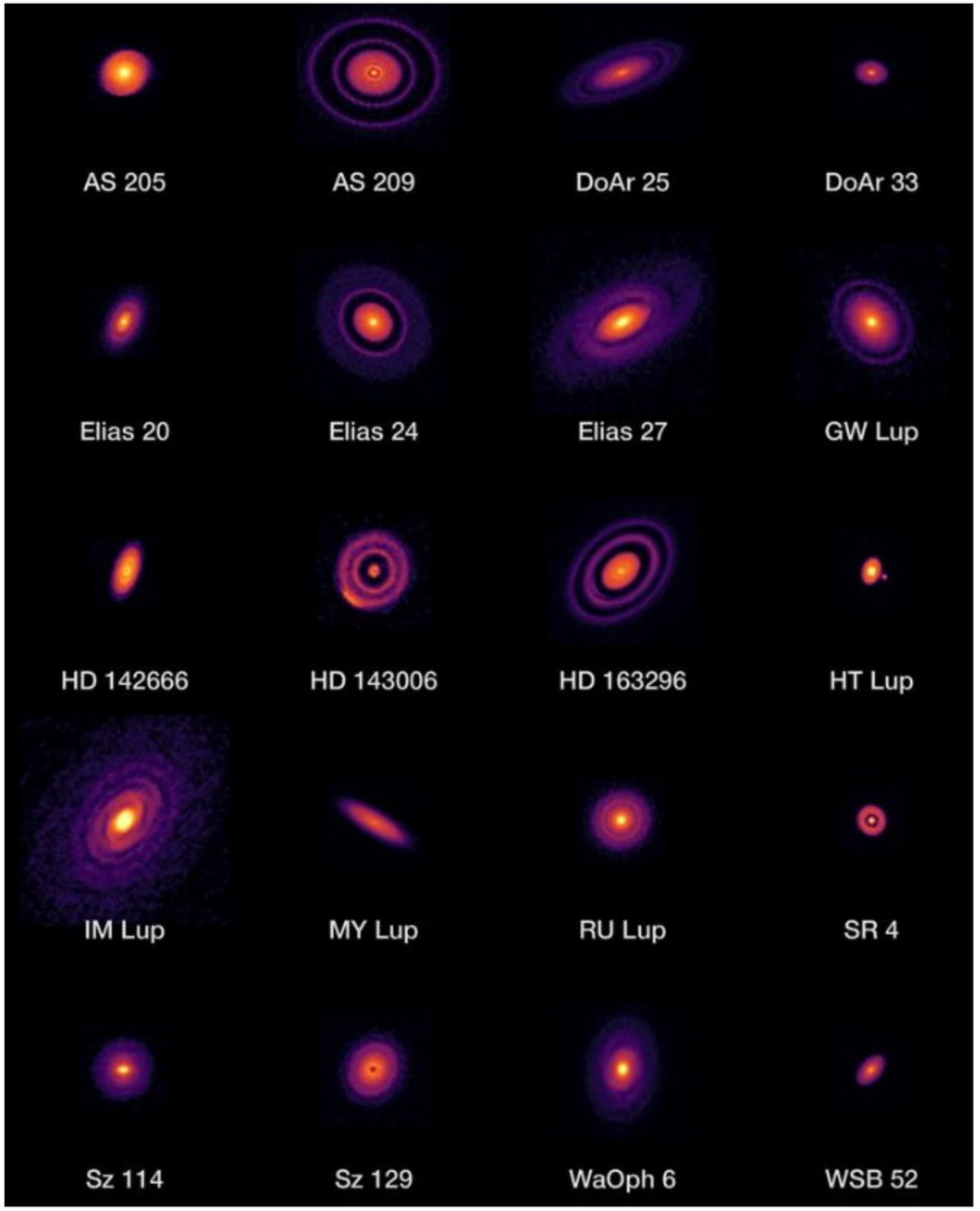
AS 205
AS 209
DoAr 25
DoAr 33
Elias 20
Elias 24
Elias 27
GW Lup
HD 142666
HD 143006
HD 163296
HT Lup
IM Lup
MY Lup
RU Lup
SR 4
Sz 114
Sz 129
WaOph 6
WSB 52

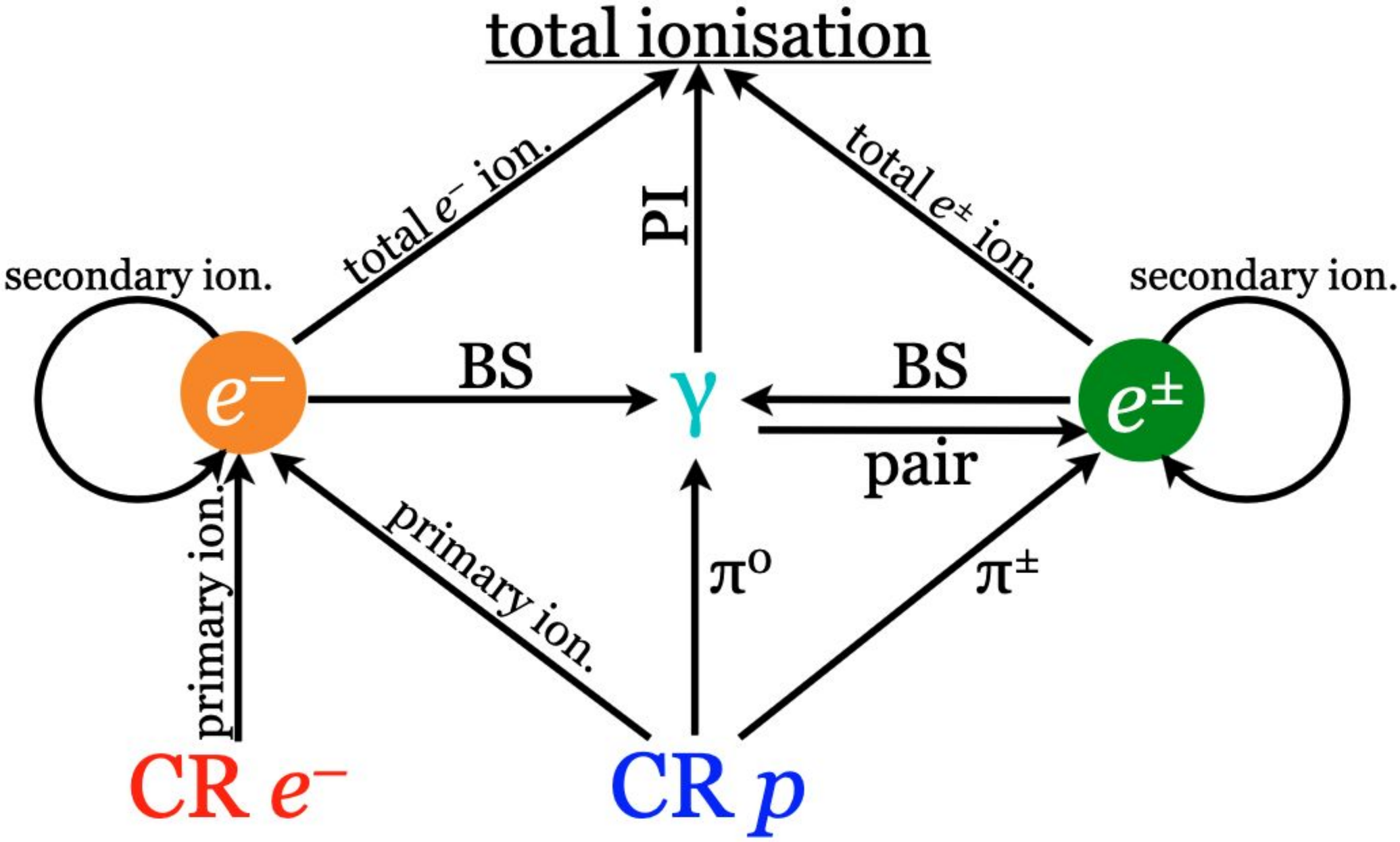
total ionisation
secondary ion.
total e^- ion.
PI
total $e^\pm$ ion.
secondary ion.
e^-
BS
γ
BS
$e^\pm$
pair
primary ion.
primary ion.
π^o
$\pi^\pm$
CR e^-
CR p

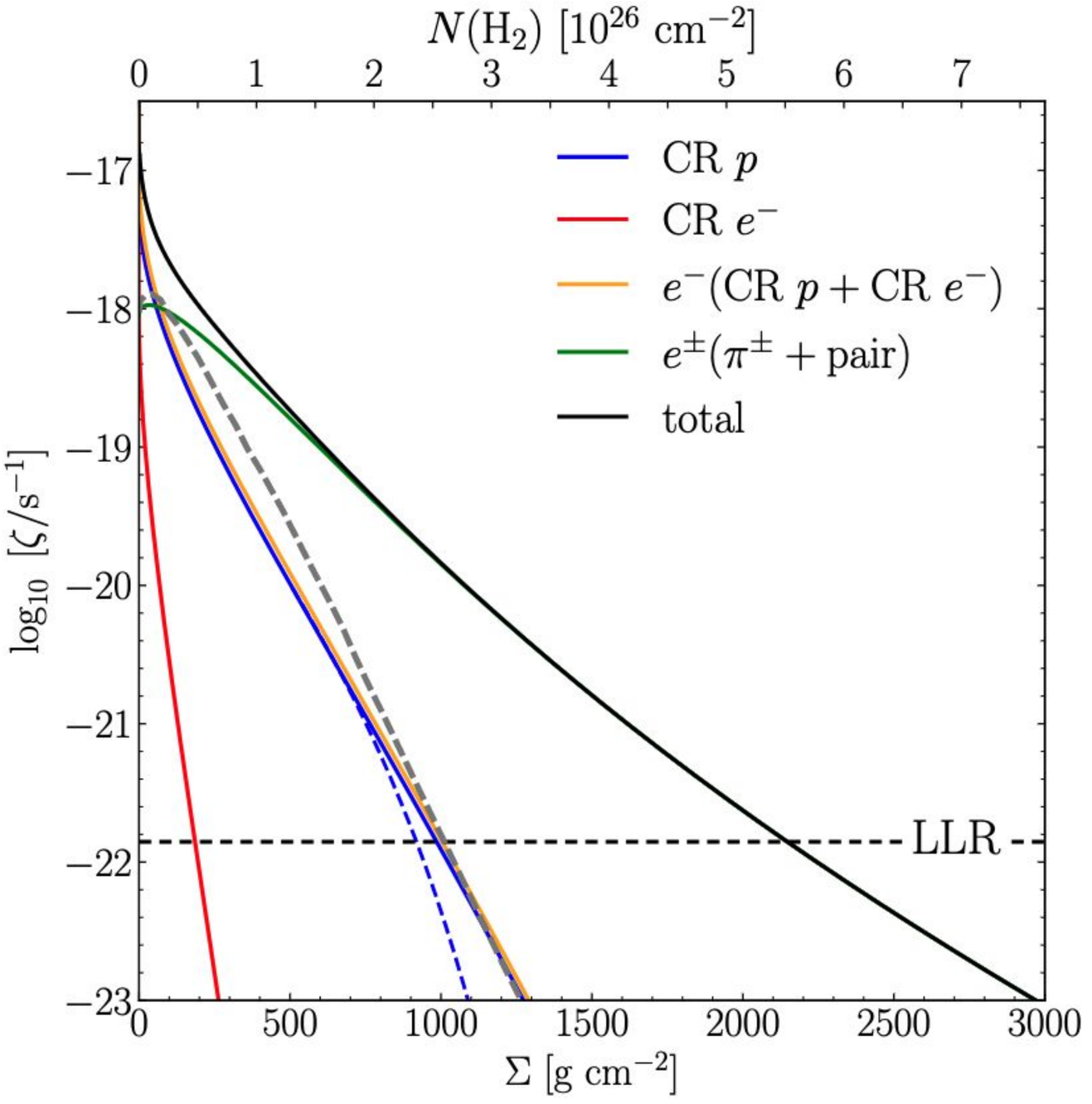
$N(\mathrm{H_2})$ $[10^{26}$ cm$^{-2}]$
0
1
2
3
4
5
6
7
CR p
CR e^-
e^-(CR p + CR e^-)
$e^{\pm}(\pi^{\pm}$ + pair)
total
LLR
$\log_{10}$ $[\zeta/\mathrm{s}^{-1}]$
−17
−18
−19
−20
−21
−22
−23
0
500
1000
1500
2000
2500
3000
Σ [g cm^{-2}]

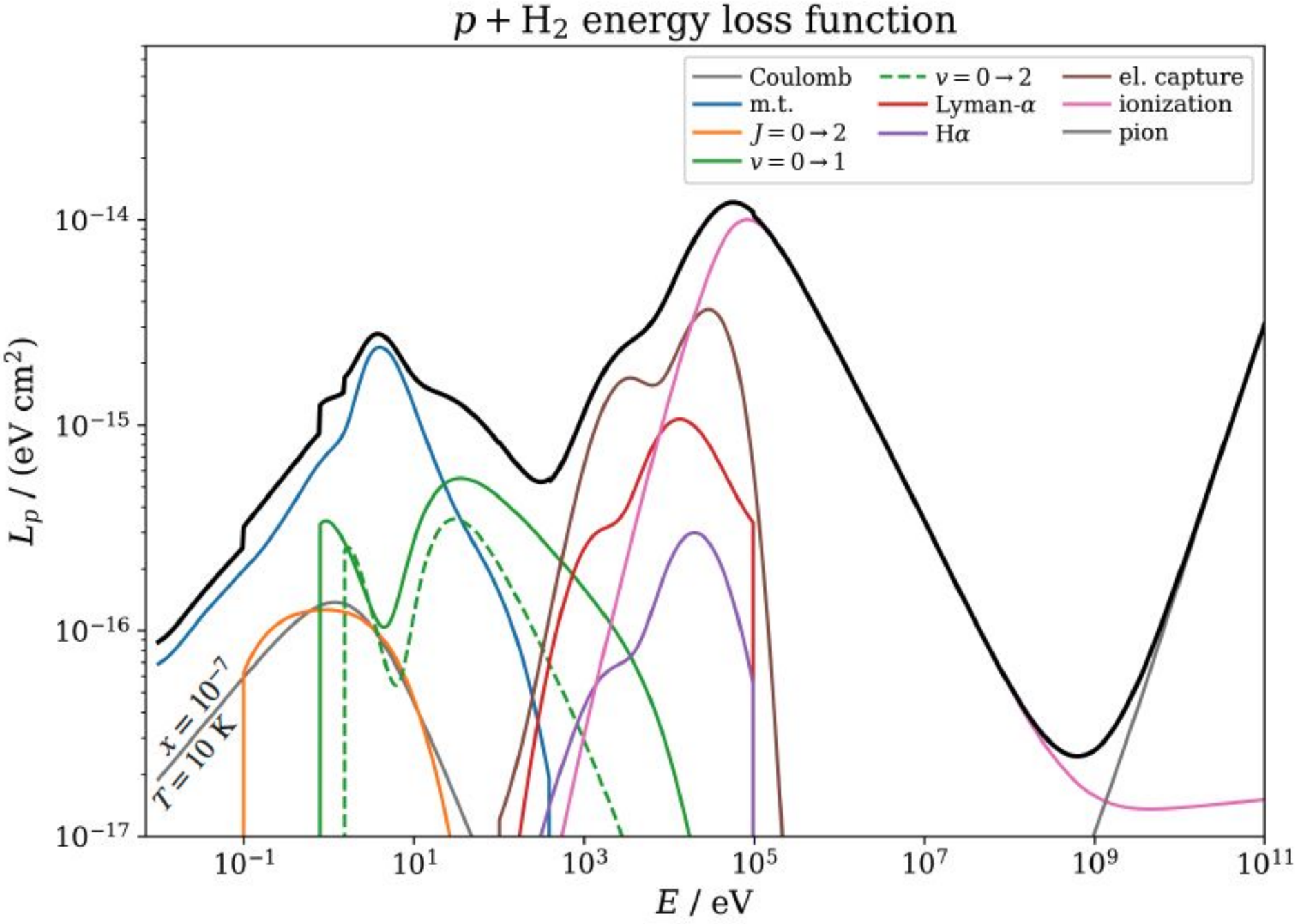
$p + H_2$ energy loss function
Coulomb
m.t.
$J = 0 \to 2$
$v = 0 \to 1$
$v = 0 \to 2$
Lyman-α
Hα
el. capture
ionization
pion
$x = 10^{-7}$
$T = 10$ K
L_p / (eV cm^2)
E / eV
10^{-14}
10^{-15}
10^{-16}
10^{-17}
10^{-1}
10^{1}
10^{3}
10^{5}
10^{7}
10^{9}
10^{11}

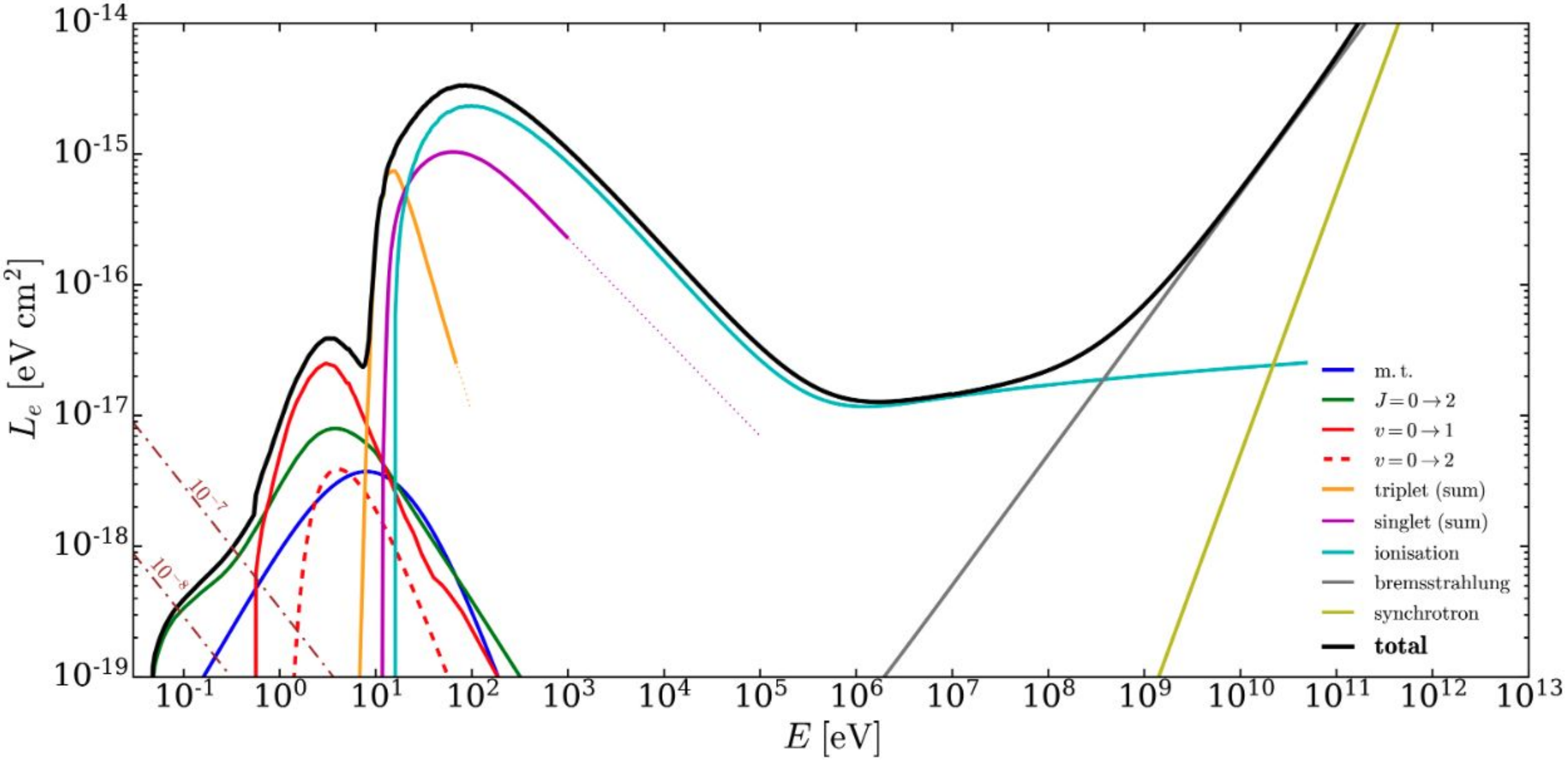
10^{-14}
10^{-15}
10^{-16}
10^{-17}
10^{-18}
10^{-19}
L_e [eV cm^2]
10^{-1} 10^{0} 10^{1} 10^{2} 10^{3} 10^{4} 10^{5} 10^{6} 10^{7} 10^{8} 10^{9} 10^{10} 10^{11} 10^{12} 10^{13}
E [eV]
10^{-7}
10^{-8}
m. t.
$J=0\rightarrow 2$
$v=0\rightarrow 1$
$v=0\rightarrow 2$
triplet (sum)
singlet (sum)
ionisation
bremsstrahlung
synchrotron
total

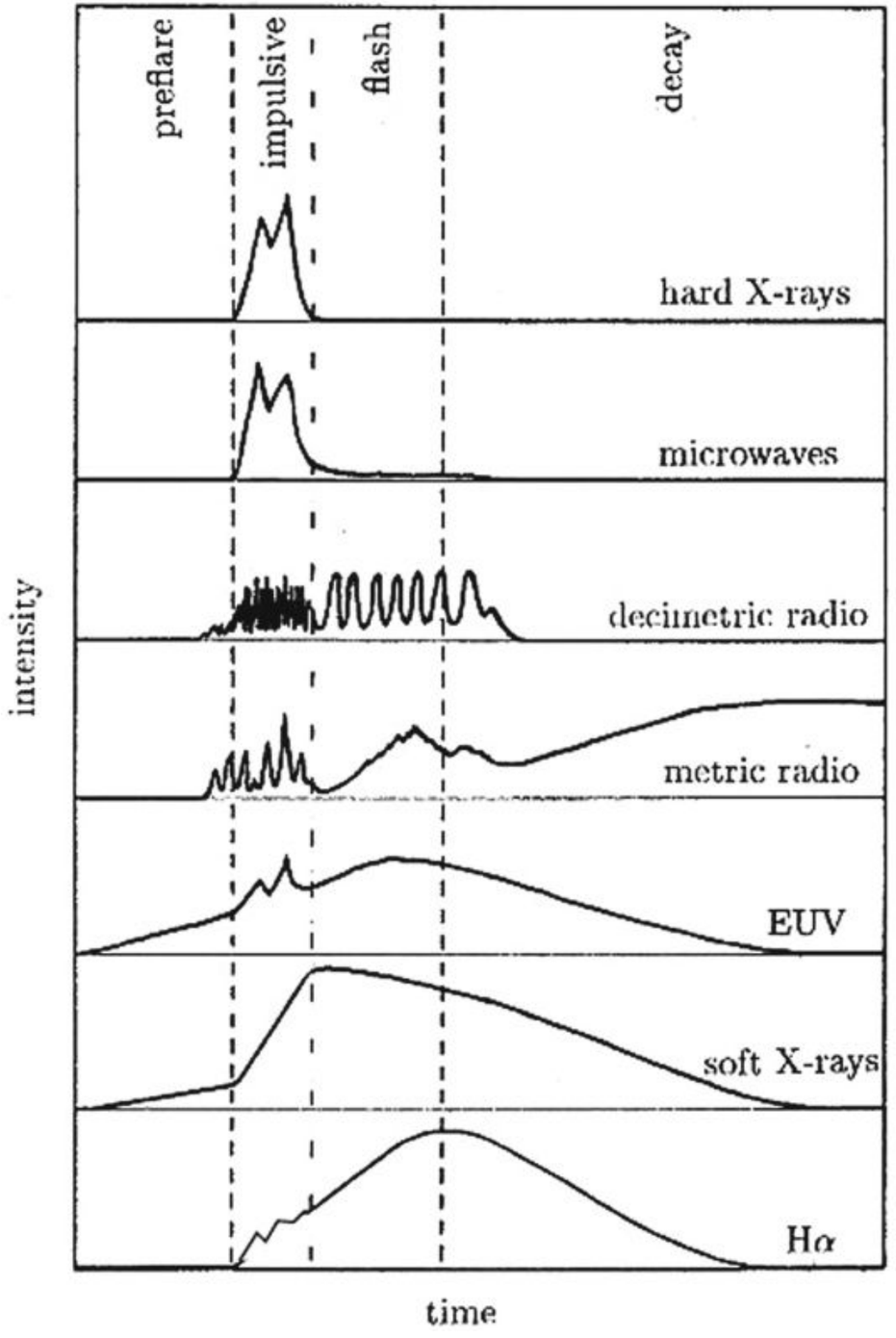
preflare
impulsive
flash
decay
hard X-rays
microwaves
decimetric radio
metric radio
EUV
soft X-rays
Hα
intensity
time

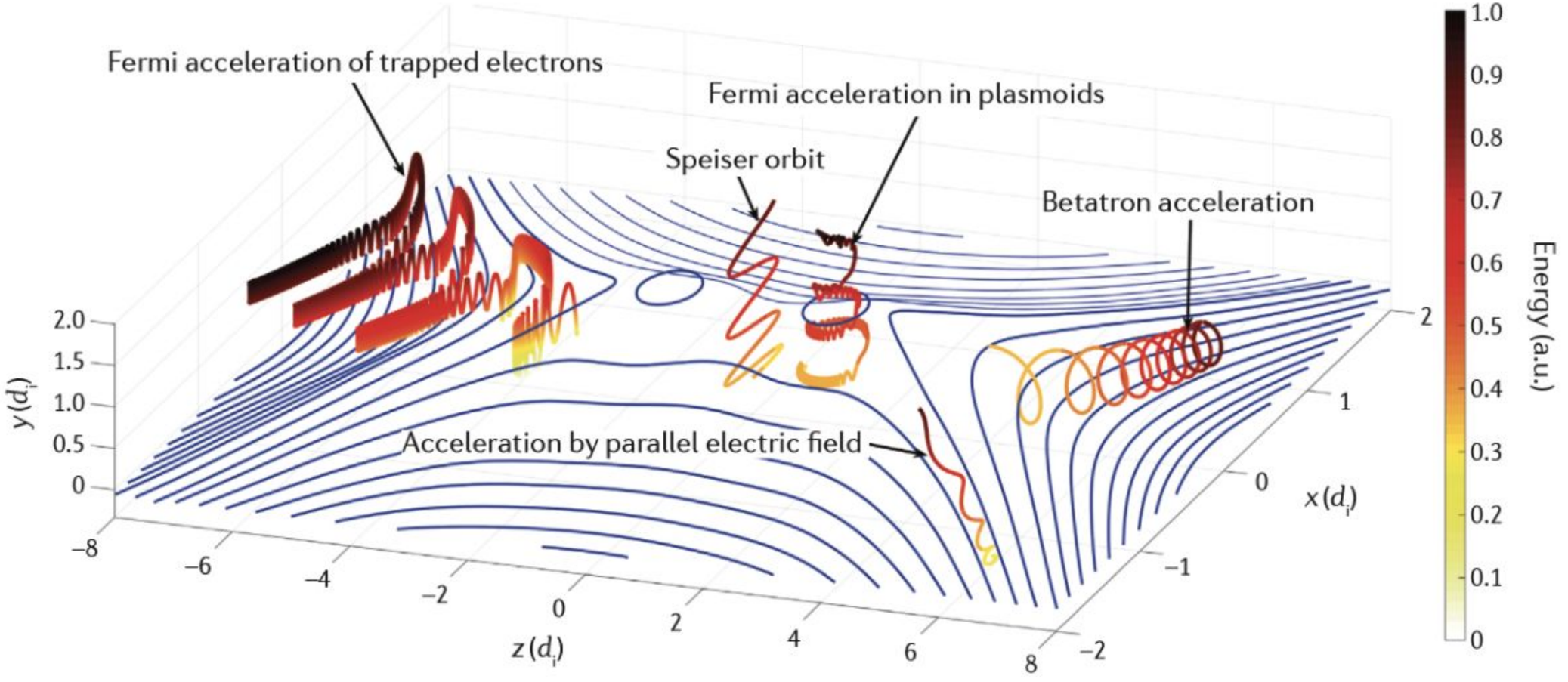
Fermi acceleration of trapped electrons
Fermi acceleration in plasmoids
Speiser orbit
Betatron acceleration
Acceleration by parallel electric field
y (d_i)
z (d_i)
x (d_i)
Energy (a.u.)
2.0
1.5
1.0
0.5
0
−8
−6
−4
−2
0
2
4
6
8
−2
−1
0
1
2
1.0
0.9
0.8
0.7
0.6
0.5
0.4
0.3
0.2
0.1
0

There are many types of magnetic reconnection

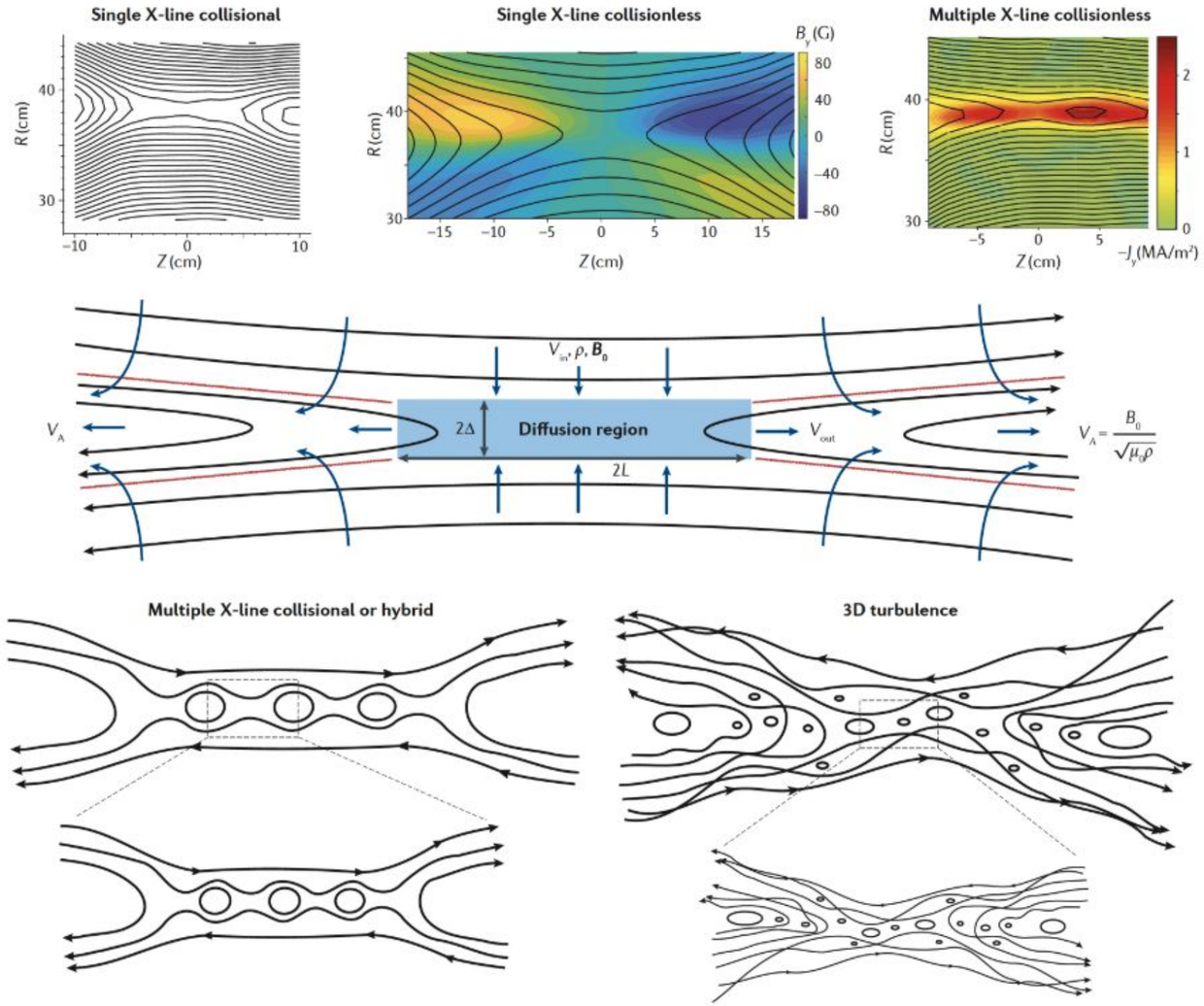

- Reconnection is dominated by collisional or non-collisional processes, with or without plasmoids, turbulent or not, 2D or 3D, etc.
- The type of reconnection determines the acceleration processes and ultimately the particle energy distribution.

Ji et al. 2022

We estimate the reconnection regime in T Tauri flares

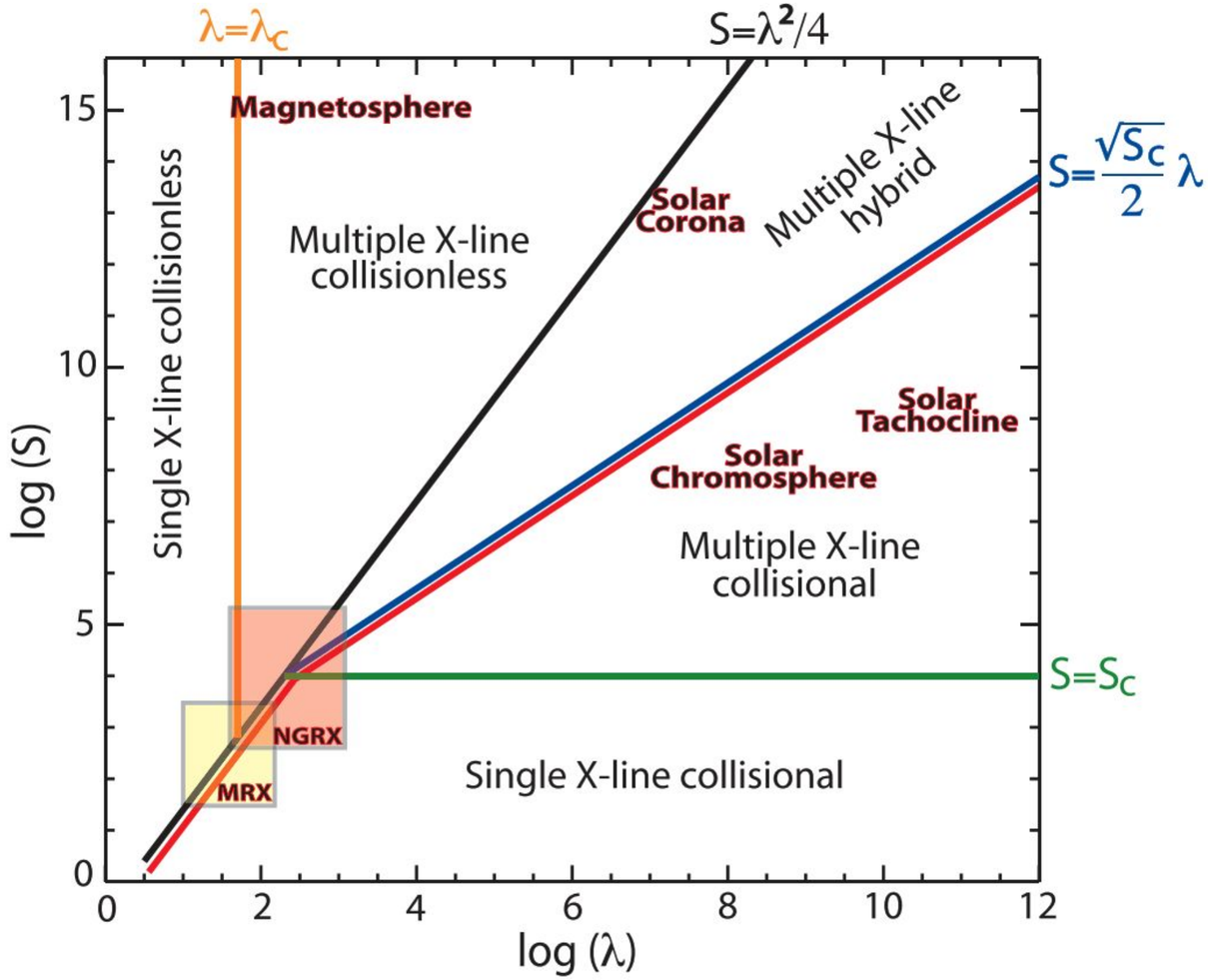

Ji and Daughton (2011)

- $S = L\frac{V_A}{\eta}$, Lundquist number
- $\lambda = \frac{L}{\rho_s}$, Effective plasma size

L: Flare size
$V_A(B,n)$: Alfven speed
$\eta(T,n)$: resistivity
$\rho_s(T,B)$: ion skin depth

B: magnetic field intensity
n: plasma density
T: plasma temperature

We can estimate the reconnection regime

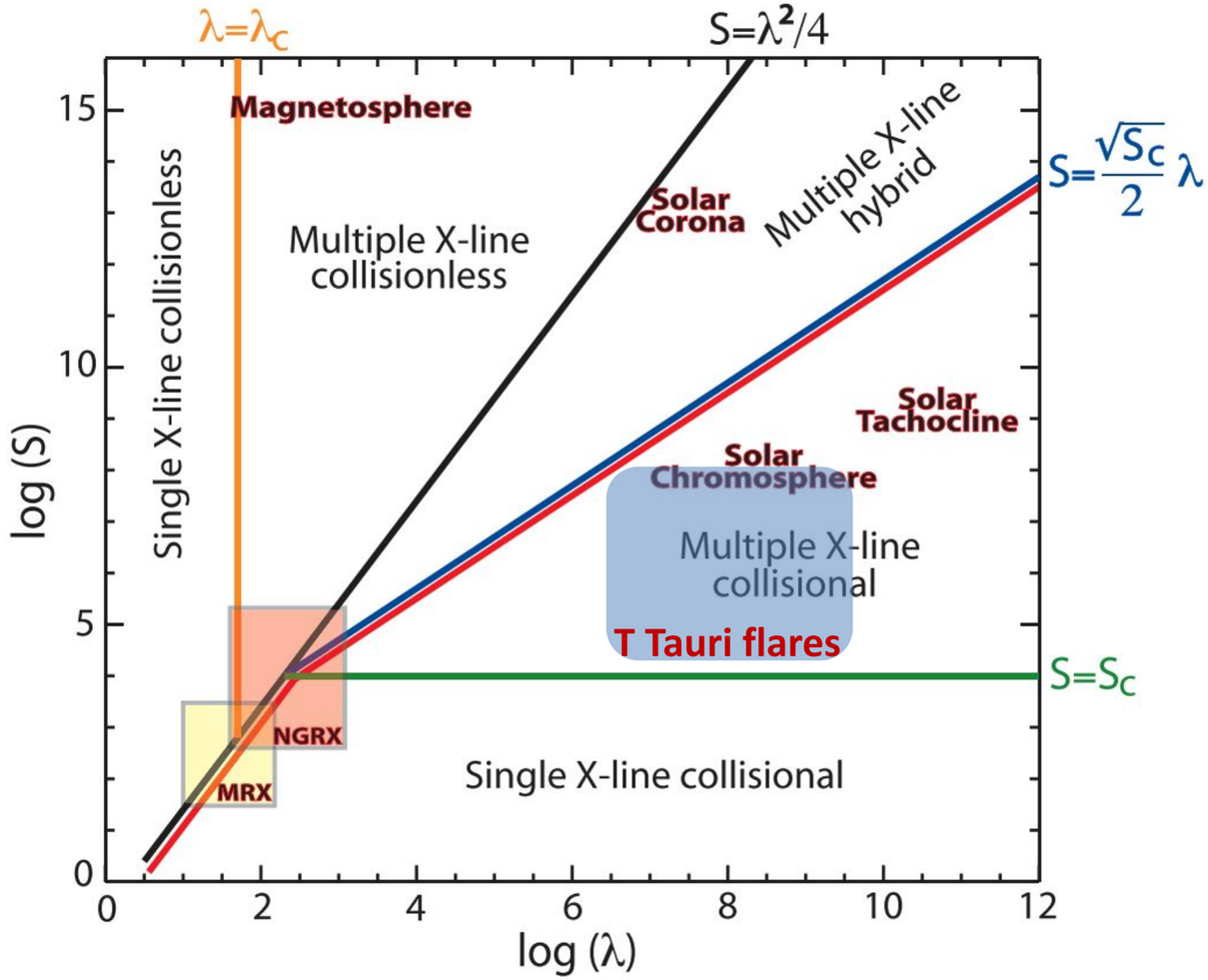

- The reconnection regime can be determined based on temperature, density, magnetic fields intensity and the length of the reconnecting layer.
- The reconnection regime in T Tauri flare is “Multiple X-line collisional”.

Ji and Daughton (2011)

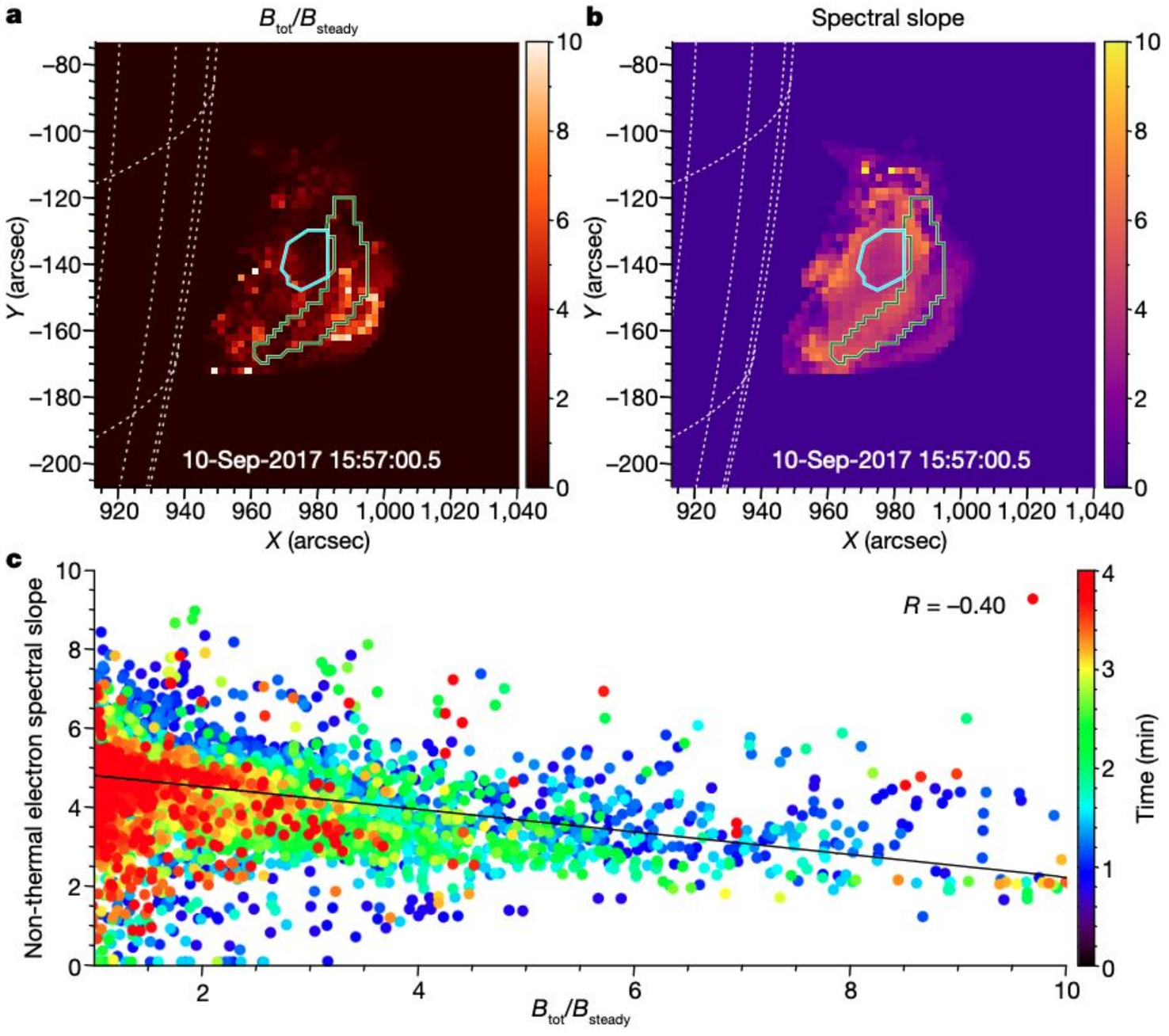
a
B_{tot}/B_{steady}
b
Spectral slope
Y (arcsec)
X (arcsec)
10-Sep-2017 15:57:00.5
c
Non-thermal electron spectral slope
B_{tot}/B_{steady}
R = –0.40
Time (min)

- **Bibliography :**

- Woitke, P., Kamp, I., & Thi, W. F. (2009). Radiation thermo-chemical models of protoplanetary disks-I. Hydrostatic disk structure and inner rim. *Astronomy & Astrophysics*, *501*(1), 383-406.

- Zanni, C., & Ferreira, J. (2013). MHD simulations of accretion onto a dipolar magnetosphere-II. Magnetospheric ejections and stellar spin-down. *Astronomy & Astrophysics*, *550*, A99.

- Orlando, S., Reale, F., Peres, G., & Mignone, A. (2011). Mass accretion to young stars triggered by flaring activity in circumstellar discs. *Monthly Notices of the Royal Astronomical Society*, *415*(4), 3380-3392.

- Getman, K. V., Feigelson, E. D., Micela, G., Jardine, M. M., Gregory, S. G., & Garmire, G. P. (2008). X-ray flares in Orion young stars. II. Flares, magnetospheres, and protoplanetary disks. *The Astrophysical Journal*, *688*(1), 437.

- Padovani, M., Galli, D., & Glassgold, A. E. (2009). Cosmic-ray ionization of molecular clouds. *Astronomy & Astrophysics*, *501*(2), 619-631.

- Padovani, M., Hennebelle, P., & Galli, D. (2013). Cosmic-ray ionisation in collapsing clouds. *Astronomy & Astrophysics*, *560*, A114.

- Ball, D., Sironi, L., & Özel, F. (2018). Electron and proton acceleration in trans-relativistic magnetic reconnection: dependence on plasma beta and magnetization. *The Astrophysical Journal*, *862*(1), 80.

- Oka, M., Birn, J., Battaglia, M., Chaston, C. C., Hatch, S. M., Livadiotis, G., ... & Retinò, A. (2018). Electron power-law spectra in solar and space plasmas. *Space Science Reviews*, *214*(5), 1-66.